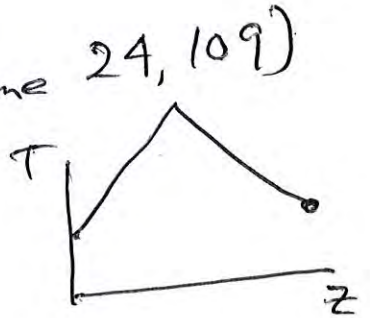


Models of nonpremixed turbulent combustion

- A. Lockwood $k-\epsilon$ fast chemistry (no X_s)
- B. Scaling relations for mixing in jets
- C. SLF = steady laminar flamelet
- Pitsch, Janicka, Fluent
- D. other model = Pope's

(A) Lockwood + Naguib (Comb Flame 24, 109)

fast chemistry \rightarrow single state veln.
no X_s , no strain



$$p = \text{const}$$

jet = two stream mixing

constants in Favre avg. eqns on next page

$$\partial/\partial\theta = 0 \quad \partial/\partial t = 0$$

grad. diff assumption

$P(z)$ = clipped Gaussian with mean + variance
flame cannot extinguish - overpredicts T ,

Favre Averaged Conservation Equations

See Kuo for complex version, see FLUENT, see Lockwood & Naguib CNF 24, 109

Assume: turbulent jet, $p = \text{constant}$, Favre averaged, steady mean, $\frac{\partial}{\partial \theta} = 0$

Seven unknowns: $(\tilde{u}, \tilde{v}, \bar{Z}, k, \epsilon, g, \bar{\rho})$, seven equations

1. Continuity for radial velocity \tilde{v}
$$\frac{\partial}{\partial z} (\bar{\rho} \tilde{u}) + \frac{1}{r} \frac{\partial}{\partial r} (r \bar{\rho} \tilde{v}) = 0$$

2. Axial momentum eqn for \tilde{u}
$$\bar{\rho} \tilde{u} \frac{\partial \tilde{u}}{\partial x} + \bar{\rho} \tilde{v} \frac{\partial \tilde{u}}{\partial r} = \frac{1}{r} \frac{\partial}{\partial r} \left(r \bar{\rho} v_T \frac{\partial \tilde{u}}{\partial r} \right)$$

3. Mixture fraction eqn for \bar{Z}
$$\bar{\rho} \tilde{u} \frac{\partial \bar{Z}}{\partial x} + \bar{\rho} \tilde{v} \frac{\partial \bar{Z}}{\partial r} = \frac{1}{r} \frac{\partial}{\partial r} \left(r \bar{\rho} \frac{v_T}{\sigma_Z} \frac{\partial \bar{Z}}{\partial r} \right)$$

Turbulent kinematic viscosity
$$v_T = C_D \frac{k^2}{\epsilon}$$

4. k equation for k
$$k = \frac{1}{2} (\overline{u'^2} + \overline{v'^2} + \overline{w'^2}) \quad \text{turbulent K.E./mass}$$

$$\bar{\rho} \tilde{u} \frac{\partial k}{\partial x} + \bar{\rho} \tilde{v} \frac{\partial k}{\partial r} = \frac{1}{r} \frac{\partial}{\partial r} \left(r \bar{\rho} \frac{v_T}{\sigma_k} \frac{\partial k}{\partial r} \right) + \bar{\rho} v_T \left(\frac{\partial \tilde{u}}{\partial r} \right)^2 - \bar{\rho} \epsilon$$

epsilon (ϵ) is the sink term in the k-equation

5. epsilon eqn for ϵ

$$\bar{\rho} \tilde{u} \frac{\partial \epsilon}{\partial x} + \bar{\rho} \tilde{v} \frac{\partial \epsilon}{\partial r} = \frac{1}{r} \frac{\partial}{\partial r} \left(r \bar{\rho} \frac{v_T}{\sigma_\epsilon} \frac{\partial \epsilon}{\partial r} \right) + C_{\epsilon 1} C_D \bar{\rho} k \left(\frac{\partial \tilde{u}}{\partial r} \right)^2 - \frac{C_{\epsilon 2}}{C_D} \frac{\bar{\rho} \epsilon^2}{k}$$

6. g equation for scalar fluctuation variance $g = \overline{Z'^2}$

$$\bar{\rho} \tilde{u} \frac{\partial g}{\partial x} + \bar{\rho} \tilde{v} \frac{\partial g}{\partial r} = \frac{1}{r} \frac{\partial}{\partial r} \left(r \bar{\rho} \frac{v_T}{\sigma_g} \frac{\partial g}{\partial r} \right) + C_{g1} \bar{\rho} v_T \left(\frac{\partial \bar{Z}}{\partial r} \right)^2 - \bar{\rho} \bar{\chi}$$

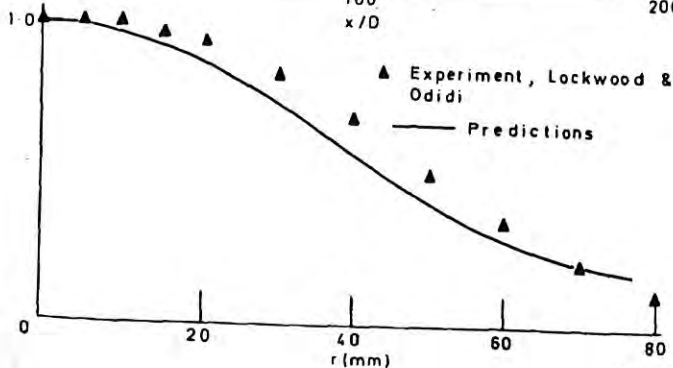
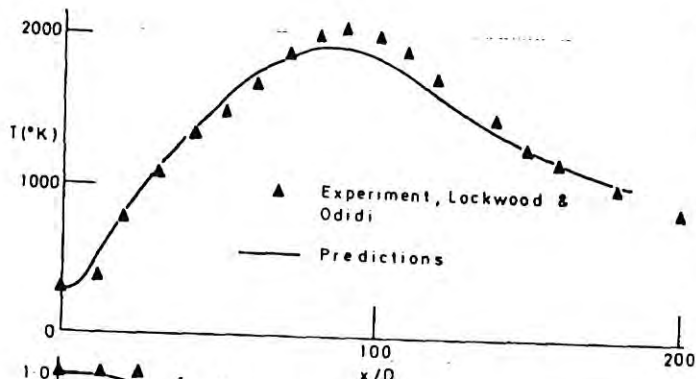
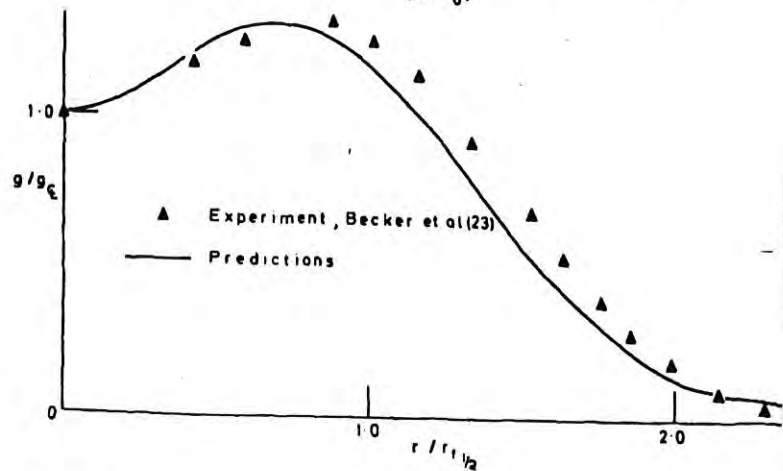
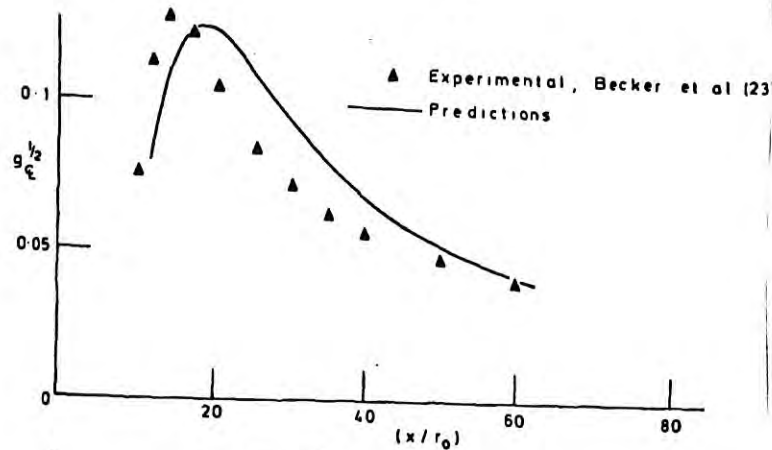
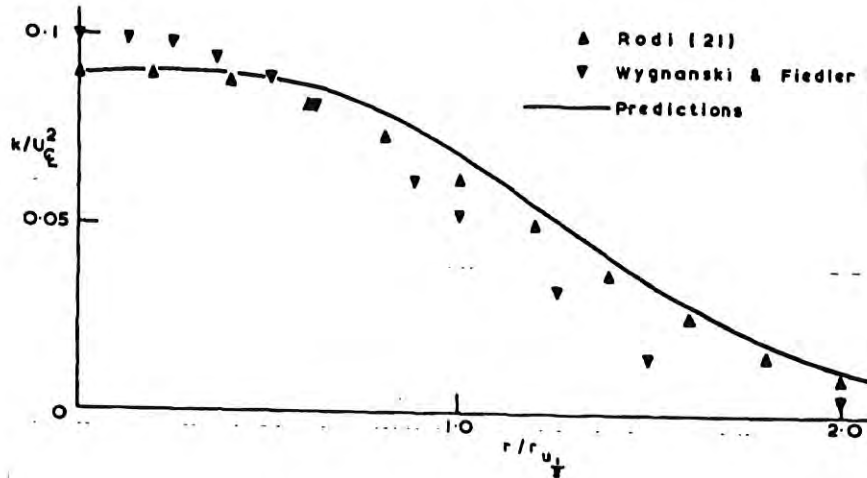
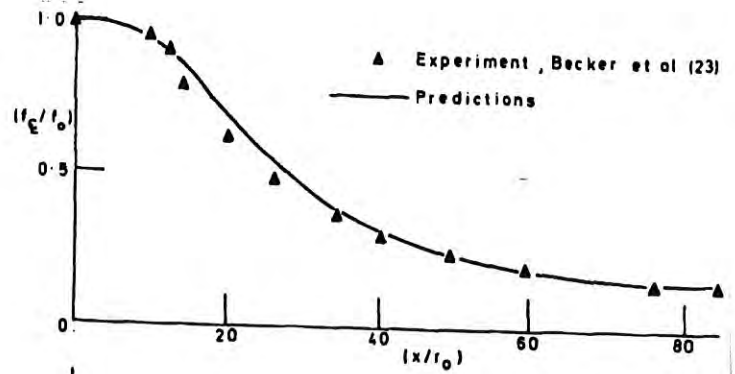
scalar dissipation rate is the sink term in the g-equation: $\bar{\chi} = \frac{C_{g2}}{C_D} \left(\frac{\epsilon}{k} \right)$

7. equation of state for mean density $\bar{\rho}$

$$\bar{\rho} = \int_0^1 \frac{p/R}{T(Z)} P(Z, \bar{Z}, g) dZ$$

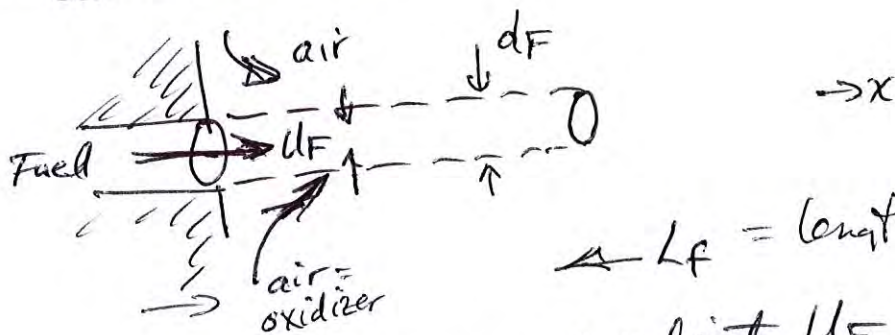
TABLE 1
Values of Adjustable Constants Used

Constant	Present study	Elghobashi et al. [17, 18]	Mason and Spalding [19, 20]
C_D	0.09	0.09	0.09
C_{e1}	1.44	1.45	1.45
C_{e2}	0.170 isothermal inert flow		
	0.166 non-isothermal, inert flow	0.18	0.173
	0.161 reacting flow		
C_{s1}	2.8	2.8	2.7
C_{s2}	0.17 isothermal, inert flow		
	0.166 non-isothermal, inert flow	0.18	0.173
	0.161 reacting flow		
C_p	1.5	-	-
σ_k	1.0	1.0	1.0
σ_e	1.3	1.3	1.3
σ_f	0.7	0.7	0.7
σ_g	0.7	0.7	0.7



(B) Scaling relations for mixing - what does turbulence do?
 Rehal, J. Fluid Mech
 Glassman, Kuo

- imagine a simplified concept of a jet and assume the jet fluid stays in a cylinder of diameter d_F
- air enters in the radial inward direction as shown



$L_f = \text{length to mix} = \text{flame length}$

- fuel enters cylinder at velocity U_F
- after an x -distance of L_f the amount of air entrained is just enough to make the mixture at the end of the cylinder stoichiometric

$$\frac{\dot{m}_F (\text{entering at end})}{\dot{m}_{Ox} (\text{entering on curved wall})} = \left(\frac{\text{grams fuel}}{\text{grams oxidizer}} \right)_{\text{stoich}}$$

show that $\left(\frac{\dot{m}_F}{\dot{m}_{Ox}} \right)_s = \frac{z_s}{1-z_s} = \frac{0.111}{1-0.111} = 0.125$ for H_2 and O_2

now $\dot{m}_F = \rho_F U_F (\pi d_F^2 / 4)$

Fick's Law says $J = \frac{\text{mass oxid.}}{\text{sec. area}} = \frac{\rho}{A} D \frac{dY_A}{dr}$

approximate $\frac{dY_A}{dr} = \frac{+1}{d_F}$ $D = \text{diffusivity}$

$\therefore \dot{m}_A = J \cdot \text{area of curved cylinder} = J (\pi d_F L_f)$

$\dot{m}_A = \rho_A D \frac{1}{d_F} (\pi d_F L_f)$

so $\frac{\dot{m}_F}{\dot{m}_A} = \frac{\rho_F U_F \pi d_F^2 / 4}{\rho_A D \pi L_f} = \frac{z_s}{(1-z_s)}$ assume $z_s \ll 1$
neglect

solve for flame length = mixing length L_f

(a) laminar jet

$$\frac{L_f}{d_F} = \frac{\rho_F}{\rho_A} \left(\frac{1}{z_s} \right) \left(\frac{U_F d_F}{D} \right)$$

if U_F is large, mass/sec of fuel is large, you need more air to mix to stoich, $L_f = \text{long}$

if $z_s = \text{small}$, you need lot of air to get to stoich. so $L_f = \text{long}$

if diffusivity D is large, mix faster, length is short

$z_s \sim \frac{\text{mass fuel}}{\text{mass air}} \Big|_{\text{stoich}}$

(b.) turbulent jet

replace D (molecular diff) with D_T (turb. diff.)

$$D_T = u'_x \cdot L_x$$

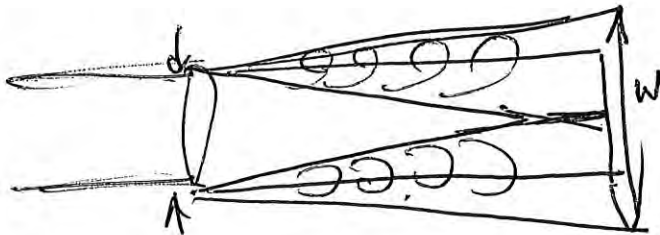
$$u'_x = U_F (x/d_F)^{-1}$$

$$L_x = d_F (x/d_F)^{+1}$$

integral scale

momentum diffusion in radial direction

shear layer growth



where shear layers merge
 the eddy size is about the
 $\frac{1}{2}$ the width of the jet (W)
 larger $d_F =$ larger W

$\therefore D_T = U_F d_F$ plug into last eqn

$$\frac{L_f}{d_F} = \frac{\rho_F}{\rho_A} \frac{1}{Z_s} \left(\frac{U_F d_F}{d_F d_F} \right)^{-1} \text{ constant}$$

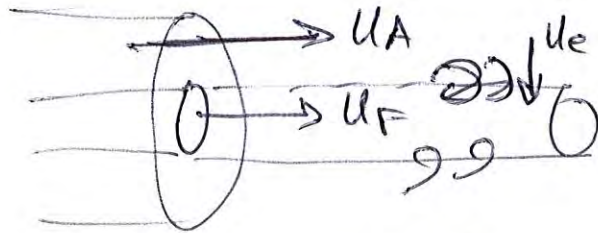
turbulent jet flame

as $U_F \uparrow$ turbulence $u' \uparrow$ mixes faster } turbulence
 as $U_F \uparrow$ more mass/sec fuel to burn } cancel each other out
 turbulence tends to make flames shorter, for same fuel flow

$$D = 0.15 \text{ cm}^2/\text{s}$$

$$D_T = 180 \text{ times larger}$$

Coaxial air



eddies rotate opp. direction
due to large U_A

U_e = entrainment velocity,
radially inward

$$U_e = (\text{const}) \cdot U_A$$

$$u' \sim U_e \quad L_T \sim d_F$$

$$D_T = U_A \cdot d_F \cdot (\text{const})$$

plug in:

$$\frac{L_F}{d_F} = \left(\frac{\rho_F}{\rho_A}\right) \left(\frac{1}{Z_s}\right) \left(\frac{U_F}{U_A}\right)$$

increase $U_A \rightarrow$ shorter, more compact flame - more mixing

increase $U_F \rightarrow$ longer flame, more fuel to burn

gas turbines always use strong coaxial air U_A

Turbulent Non-premixed Flame

- Mixing controlled* D_T important, \bar{w}_i does not appear in cons. eqn
- not a "wave" - is only an interface between fuel + oxidizer only in state relations
- does not "propagate" like premixed flame (at wave speed)
- * mixing rate \ll reaction rate slowest process determines the solution
- easier to model than premixed or PPC
- scalar dissipation rate $\bar{\chi}$ is the mixing rate:

$$\bar{\chi} \approx \bar{u} \frac{\partial g}{\partial x} = - \bar{\chi} \bar{\chi}$$

$$g = \bar{z}^2$$

change in g in time as it convects

- RANS = Reynolds decomposition

$$u = \bar{u} + u' \rightarrow \overline{u'v'} \text{ terms}$$

taking time averages - unsteady "mean" not considered (need LES)
 taking spatial averages u' from large + small eddies not separated - (need LES to separate scales)

FLUENT Non-Premixed Flamelet Model

(RANS)

The laminar flamelet approach models a turbulent flame brush as an ensemble of discrete laminar flames, called flamelets.

The **advantage** of the laminar flamelet approach is that realistic chemical kinetic effects can be incorporated into turbulent flames. The chemistry can then be preprocessed and tabulated, offering tremendous computational savings. It contains full chemistry.

The **disadvantage** is that the laminar flamelet model cannot do slow chemistry associated with deep non-equilibrium effects such as ignition and extinction.

Prior to the computation of flow field, construct "State relations" and a "Lookup Table"

1. **Compute State relations** – these are formulas for instantaneous T , mass fractions Y_i , and reaction rates ω_i , in terms of Z and χ_s , obtained by solving the flamelet equation:

$$\frac{\rho \chi}{2} \frac{d^2 Y_{H2}}{dZ^2} = \dot{\omega}_{H2}$$

2. **Compute a Lookup table -**

The Lookup table is a table of Mean values; $(\bar{T}, \bar{Y}_i, \bar{\omega}_i, \bar{\rho})$ each is a function of four variables: $(\bar{Z}, \bar{Z}'^2, \bar{\chi}_s, \bar{\chi}_s'^2)$. These four numbers are the means and the variances of mixture fraction Z and scalar dissipation rate (stoichiometric) χ_s .

The lookup table values for \bar{T} are computed from:

$$\bar{T}(\bar{Z}, \bar{Z}'^2, \bar{\chi}_s, \bar{\chi}_s'^2) = \int_{10/s}^{1000/s} \int_0^1 T(Z, \chi_s) P_1(Z, \bar{Z}, \bar{Z}'^2) P_2(\chi_s, \bar{\chi}_s, \bar{\chi}_s'^2) dZ d\chi_s$$

$T(Z, \chi_s)$ is the state relation for temperature T , from step 1.

First decide that Z will vary from 0 to 1 and χ_s will vary from $10s^{-1}$ to $1000 s^{-1}$.

P_1 is a beta function, is a function of Z and its mean and its variance.

P_2 is a log normal function of χ_s , its mean and its variance.

Now decide that \bar{Z} and \bar{Z}'^2 also will vary from 0 to 1 and that $\bar{\chi}_s$ varies from 10 to $1000 s^{-1}$ and $\bar{\chi}_s'^2$ varies from 1 to $100 s^{-1}$. Select many values in this range and construct the lookup table, prior to solving any conservation equations.

3. **Write four conservation equations for the four independent variables in the lookup table** $(\bar{Z}, \bar{Z}'^2, \bar{\chi}_s, \bar{\chi}_s'^2)$

These are the \bar{Z} equation and g equation, where $g = \bar{Z}'^2$. FLUENT assumes that the other two equations are

$$\bar{\chi}_s = C_\chi \frac{\epsilon g}{k} \quad \text{and} \quad (\bar{\chi}_s'^2) = 0 \quad \text{See the FLUENT flamelet manual below}$$

4. Solve these conservation equations for $(\bar{Z}, \bar{Z}'^2, \bar{\chi}_s, \bar{\chi}_s'^2)$ at each point (x,y,z)
5. Perform a "mapping" using lookup tables. For the $(\bar{Z}, \bar{Z}'^2, \bar{\chi}_s, \bar{\chi}_s'^2)$ at a point, use lookup table to quickly look up \bar{T} , etc. It is not quite this simple because the conservation equations contain $\bar{\rho}$ etc. that must be determined from the lookup table, so there is a coupling that has to be done in the algorithm.

Favre Averaged Conservation Equations

See Kuo for complex version, see FLUENT, see Lockwood & Naguib CNF 24, 109

Assume: turbulent jet, $p = \text{constant}$, Favre averaged, steady mean, $\frac{\partial}{\partial \theta} = 0$

Seven unknowns: $(\tilde{u}, \tilde{v}, \bar{Z}, k, \epsilon, g, \bar{\rho})$, seven equations

1. Continuity for radial velocity \tilde{v} $\frac{\partial}{\partial z} (\bar{\rho} \tilde{u}) + \frac{1}{r} \frac{\partial}{\partial r} (r \bar{\rho} \tilde{v}) = 0$

2. Axial momentum eqn for \tilde{u} $\bar{\rho} \tilde{u} \frac{\partial \tilde{u}}{\partial x} + \bar{\rho} \tilde{v} \frac{\partial \tilde{u}}{\partial r} = \frac{1}{r} \frac{\partial}{\partial r} \left(r \bar{\rho} v_T \frac{\partial \tilde{u}}{\partial r} \right)$

3. Mixture fraction eqn for \bar{Z} $\bar{\rho} \tilde{u} \frac{\partial \bar{Z}}{\partial x} + \bar{\rho} \tilde{v} \frac{\partial \bar{Z}}{\partial r} = \frac{1}{r} \frac{\partial}{\partial r} \left(r \bar{\rho} \frac{v_T}{\sigma_Z} \frac{\partial \bar{Z}}{\partial r} \right)$

Turbulent kinematic viscosity $v_T = C_D \frac{k^2}{\epsilon}$

4. k equation for k $k = \frac{1}{2} (\overline{u'^2} + \overline{v'^2} + \overline{w'^2})$ turbulent K.E./mass

$$\bar{\rho} \tilde{u} \frac{\partial k}{\partial x} + \bar{\rho} \tilde{v} \frac{\partial k}{\partial r} = \frac{1}{r} \frac{\partial}{\partial r} \left(r \bar{\rho} \frac{v_T}{\sigma_k} \frac{\partial k}{\partial r} \right) + \bar{\rho} v_T \left(\frac{\partial \tilde{u}}{\partial r} \right)^2 - \bar{\rho} \epsilon$$

epsilon (ϵ) is the sink term in the k-equation

5. epsilon eqn for ϵ

$$\bar{\rho} \tilde{u} \frac{\partial \epsilon}{\partial x} + \bar{\rho} \tilde{v} \frac{\partial \epsilon}{\partial r} = \frac{1}{r} \frac{\partial}{\partial r} \left(r \bar{\rho} \frac{v_T}{\sigma_\epsilon} \frac{\partial \epsilon}{\partial r} \right) + C_{\epsilon 1} C_D \bar{\rho} k \left(\frac{\partial \tilde{u}}{\partial r} \right)^2 - \frac{C_{\epsilon 2}}{C_D} \frac{\bar{\rho} \epsilon^2}{k}$$

6. g equation for scalar fluctuation variance $g = \overline{Z'^2}$

$$\bar{\rho} \tilde{u} \frac{\partial g}{\partial x} + \bar{\rho} \tilde{v} \frac{\partial g}{\partial r} = \frac{1}{r} \frac{\partial}{\partial r} \left(r \bar{\rho} \frac{v_T}{\sigma_g} \frac{\partial g}{\partial r} \right) + C_{g1} \bar{\rho} v_T \left(\frac{\partial \bar{Z}}{\partial r} \right)^2 - \bar{\rho} \bar{\chi}$$

scalar dissipation rate is the sink term in the g-equation: $\bar{\chi} = \frac{C_{g2}}{C_D} \left(\frac{\epsilon}{k} \right)$

7. equation of state for mean density $\bar{\rho}$

$$\bar{\rho} = \int_0^1 \frac{p/R}{T(Z)} P(Z, \bar{Z}, g) dZ$$

FLUENT MANUAL 15.3 Laminar Flamelet Model

15.3.1 Introduction

In a diffusion flame, at the molecular level, fuel and oxidizer diffuse into the reaction zone. Here they encounter high temperatures and radical species, and ignite. More heat and radicals are generated in the reaction zone, and some diffuse out. In near-equilibrium flames, the reaction rate is much faster than the diffusion rate. However, as the flame is stretched and strained by the turbulence, species and temperature gradients increase, and radicals and heat diffuse more quickly out of the flame. The species have less time to reach chemical equilibrium, and the degree of local non-equilibrium increases.

The laminar flamelet model is suited to predict moderate chemical non-equilibrium in turbulent flames due to aerodynamic straining by the turbulence. The chemistry, however, is assumed to respond rapidly to this strain, so as the strain relaxes, the chemistry relaxes to equilibrium. When the chemical time-scale is comparable to the fluid convection time-scale, the species can be considered to be in global chemical non-equilibrium. Such cases include NO_x formation and low-temperature CO oxidation. The laminar flamelet model is not suitable for such slow-chemistry flames. Instead, you can model slow chemistry using the trace species assumption in the NO_x model.

The Flamelet Concept

The flamelet concept views the turbulent flame as an ensemble of thin, laminar, locally one-dimensional flamelet structures embedded within the turbulent flow field. A common laminar flame used to represent a flamelet in a turbulent flow is the counterflow diffusion flame. This geometry consists of opposed, axisymmetric fuel and oxidizer jets. As the distance between the jets is decreased and/or the velocity of the jets increased, the flame is strained and increasingly departs from chemical equilibrium until it is eventually extinguished. The species mass fraction and temperature fields can be measured in laminar counterflow diffusion flame experiments, or, most commonly, calculated. For the latter, a self-similar solution exists, and the governing equations can be simplified to one dimension along the axis of the fuel and oxidizer jets, where complex chemistry calculations can be affordably performed. In the laminar counterflow flame, the mixture fraction, f , decreases monotonically from unity at the fuel jet to zero at the oxidizer jet. If the species mass fraction and temperature along the axis are mapped from physical space to mixture fraction space, they can be uniquely described by two parameters: the mixture

fraction and the strain rate (or, equivalently, the scalar dissipation). Hence, the chemistry is reduced and completely described by the two quantities, f and χ . This reduction of the complex chemistry to two variables allows the flamelet calculations to be preprocessed, and stored in look-up tables. By preprocessing the chemistry, computational costs are reduced considerably.

Strain Rate and Scalar Dissipation

Instead of using the strain rate to quantify the departure from equilibrium, it is expedient to use the scalar dissipation. The scalar dissipation is defined as

$$\chi = 2D|\nabla f|^2 \quad (15.3-1)$$

Note that the scalar dissipation, varies along the axis of the flamelet. For the counterflow geometry, the flamelet strain rate a_s can be related to the scalar dissipation at the position where f is stoichiometric by:

$$\chi_{st} = \frac{a_s \exp\left(-2[\text{erfc}^{-1}(2f_{st})]^2\right)}{\pi} \quad (15.3-2)$$

Physically, as the flame is strained, the width of the reaction zone diminishes, and the gradient of f at the stoichiometric position $f = f_{st}$ increases. The instantaneous stoichiometric scalar dissipation, χ_{st} , is used as the essential non-equilibrium parameter. It has the dimensions s^{-1} and may be interpreted as the inverse of a characteristic diffusion time. In the limit $\chi_{st} \rightarrow 0$ the chemistry tends to equilibrium, and as χ_{st} increases due to aerodynamic straining, the non-equilibrium increases. Local quenching of the flamelet occurs when χ_{st} exceeds a critical value.

f same as z = mixture fraction

Embedding Laminar Flamelets in Turbulent Flames

A turbulent flame brush is modeled as an ensemble of discrete laminar flamelets. Since, for adiabatic systems, the species mass fraction and temperature in the laminar flamelets are completely parameterized by f and χ_{st} , density-weighted mean species mass fractions and temperature can be determined from the PDF of f and χ_{st} as

$$\bar{\phi} = \int \int \phi(f, \chi_{st}) p(f, \chi_{st}) df d\chi_{st} \quad (15.3-3)$$

where ϕ represents species mass fractions and temperature. In FLUENT, f and χ_{st} are assumed to be statistically independent, so the joint PDF $p(f, \chi_{st})$ can be simplified as

$p_f(f)p_{\chi}(\chi_{st})$. A β PDF shape is assumed for p_f , and transport equations for f and f'^2

are solved in FLUENT to specify p_f . Fluctuations in χ_{st} are ignored so that the

PDF of χ_{st} is a delta function, $p_{\chi} = \delta(\chi - \bar{\chi})$. The first moment, namely the mean

scalar dissipation, $\bar{\chi}_{st}$, is modeled in FLUENT as

$$\bar{\chi}_{st} = \frac{C_{\chi} \epsilon \bar{f}'^2}{k}$$

mean scalar
dissip. rate
(15.3-4)

where C_{χ} is a constant with a default value of 2. For LES, the mean scalar dissipation is

$$\bar{\chi}_{st} = C_{\chi} \frac{(\mu_t + \mu)}{\rho \sigma_t} |\nabla f|^2 \quad (15.3-5)$$

To avoid the PDF convolutions at FLUENT run-time, the integrations in Equation 15.3-3 are preprocessed and stored in look-up tables. For adiabatic flows, single-flamelet

tables have two dimensions: f and f'^2 . The multiple-flamelet tables have the additional

dimension $\bar{\chi}_{st}$. In FLUENT, you can either generate your own flamelets, or import them as flamelet files calculated with other stand-alone packages. Such stand-alone codes include OPPDIF [208], RIF [18, 19, 262] and RUN-1DL [260]. FLUENT can import flamelet files in OPPDIF format or standard flamelet file format.

Instructions for generating and importing flamelets are provided in Section 15.3.4 and Section 15.3.5.

15.3.4 Flamelet Generation

3-17

$\bar{f}'^2 = g$
we have
equations
for
(k, ε, g)
do not
need
conservative
eqn for
 $\bar{\chi}_{st} =$
mean of the

PDF
 $P(\chi_s)$

The laminar counterflow diffusion flame equations can be transformed from physical space (with x as the independent variable) to mixture fraction space (with f as the independent variable) [263]. In FLUENT, a simplified set of the mixture fraction space equations are solved [262]. Here, N equations are solved for the mass fractions, Y_i ,

$$\rho \frac{\partial Y_i}{\partial t} = \frac{1}{2} \rho \chi \frac{\partial^2 Y_i}{\partial f^2} + S_i \quad (15.3-6)$$

flamelet eqn is in FLUENT

$$\rho \frac{\partial T}{\partial t} = \frac{1}{2} \rho \chi \frac{\partial^2 T}{\partial f^2} - \frac{1}{c_p} \sum_i H_i S_i + \frac{1}{2c_p} \rho \chi \left[\frac{\partial c_p}{\partial f} + \sum_i c_{p,i} \frac{\partial Y_i}{\partial f} \right] \frac{\partial T}{\partial f} \quad (15.3-7)$$

energy eqn for $T(f)$
~~state~~
~~eqn~~
state relation

The notation in Equations 15.3-6 and 15.3-7 is as follows: Y_i , T , ρ , and f are the i th species mass fraction, temperature, density, and mixture fraction, respectively. $c_{p,i}$ and c_p are the i th species specific heat and mixture-averaged specific heat, respectively. S_i is the i th species reaction rate, and H_i is the specific enthalpy of the i th species.

The scalar dissipation, χ , must be modeled across the flamelet. An extension of Equation 15.3-2 to variable density is used [168]:

$$\chi(f) = \frac{a_s}{4\pi} \frac{3(\sqrt{\rho_{\infty}/\rho} + 1)^2}{2\sqrt{\rho_{\infty}/\rho} + 1} \exp(-2[\text{erfc}^{-1}(2f)]^2) \quad (15.3-8)$$

goes into flamelet eqn above

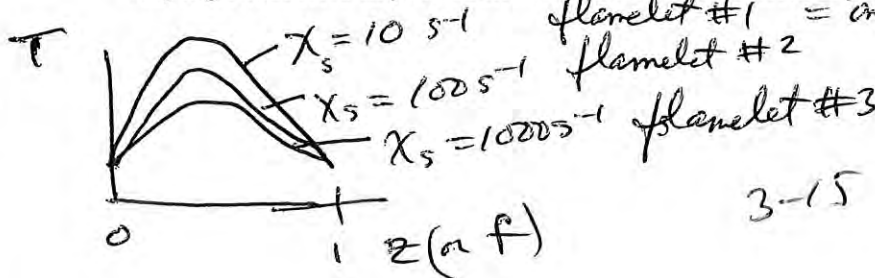
where ρ_{∞} is the density of the oxidizer stream.

Multiple Flamelet Libraries

One flamelet = solution to flamelet equation for one counterflow velocity, i.e., one scalar dissipation rate at stoichiometric contour χ_s

Multiple flamelets = pick many different strain rates, each one gives one scalar dissipation rate at stoch contour

FLUENT can generate multiple flamelets over a range of strain rates to account for the varying strain field in your multi-dimensional simulation. If you specify the number of



flamelets to be greater than one, flamelets are generated at scalar dissipation values as determined by Equation 15.3-9.

$$\chi_i = \begin{cases} 10\chi_{i-1} & \text{for } \chi_{i-1} < 1 \text{ s}^{-1} \\ \chi_{i-1} + \Delta\chi & \text{for } \chi_{i-1} \geq 1 \text{ s}^{-1} \end{cases} \quad (15.3-9)$$

where i ranges from 1 up to the specified maximum number of flamelets, χ_0 is the initial scalar dissipation, and $\Delta\chi$ is the scalar dissipation step. Flamelets are generated until either the maximum number of flamelets is reached, or the flamelet extinguishes. Extinguished flamelets are excluded from the flamelet library. Additionally, you can specify that an equilibrium flamelet be generated, in which an equilibrium calculation is performed to represent the $\chi_0 = 0$ slice, and appended to the flamelet library.

15.3.5 Flamelet Import Overview of the Problem Setup Procedure

For a single-mixture-fraction problem, you will perform the following steps:

(laminar flamelet model only) Import a flamelet file or appropriate CHEMKIN mechanism file if generating flamelets.

(laminar flamelet model only) If you are generating flamelets, compute the flamelet state relationships of species mass fractions, density, and temperature as a function of mixture fraction and scalar dissipation.

Compute the final chemistry look-up table, containing mean values of species fractions, density, and temperature as a function of mean mixture fraction, mixture fraction variance, and possibly enthalpy and scalar dissipation. The contents of this look-up table will reflect your preceding inputs describing the turbulent reacting system.

The look-up table is the stored result of the integration of Equations 15.2-16 (or 15.2-24) and 15.2-18. The look-up table will be used in **FLUENT** to determine mean species mass

fractions, density, and temperature from the values of mixture fraction (\bar{f}), mixture

fraction variance ($\overline{f'^2}$), and possibly enthalpy (\bar{H}) and scalar dissipation ($\bar{\chi}$) as they are computed during the **FLUENT** calculation of the reacting flow. See Section 15.2.4 and Figures 15.2.8 and 15.2.10.

For a problem that includes a secondary stream (and, therefore, a second mixture fraction), you will perform the first two steps listed above for the single-mixture-fraction

approach and then prepare a look-up table of instantaneous properties using Equation 15.2-12 or 15.2-14.

15.4.2 Problem Definition Using the Equilibrium Chemistry Model

In the equilibrium chemistry model, the concentrations of species of interest are determined from the mixture fraction using the assumption of chemical equilibrium (see Section 15.2.1). With this model, you can include the effects of intermediate species and dissociation reactions, producing more realistic predictions of flame temperatures than the Eddy-Dissipation model. When you choose the equilibrium chemistry option, you

To enable the laminar flamelet model, select **Non-Premixed Combustion** in the **Species Model** panel and enable **Create Table** under **PDF Options**. Select **Laminar Flamelet** in the **Chemistry** tab of the **Species Model** panel.

Importing a Flamelet

To import an existing flamelet file, select the **Import Flamelet** option in the **Chemistry** tab of the **Species Model** panel. Select either **Standard** or **Oppdif** format under **File Type** and click the **Import Flamelet File...** button. In the resulting **Select File** dialog box, select the file (for a single flamelet) or files (for multiple flamelets) to be read in to **FLUENT**.

After you have completed this step, you can skip ahead to the **Table** tab of the **Species Model** panel (see Section 15.4.9). The **Flamelet Parameters** are as follows:

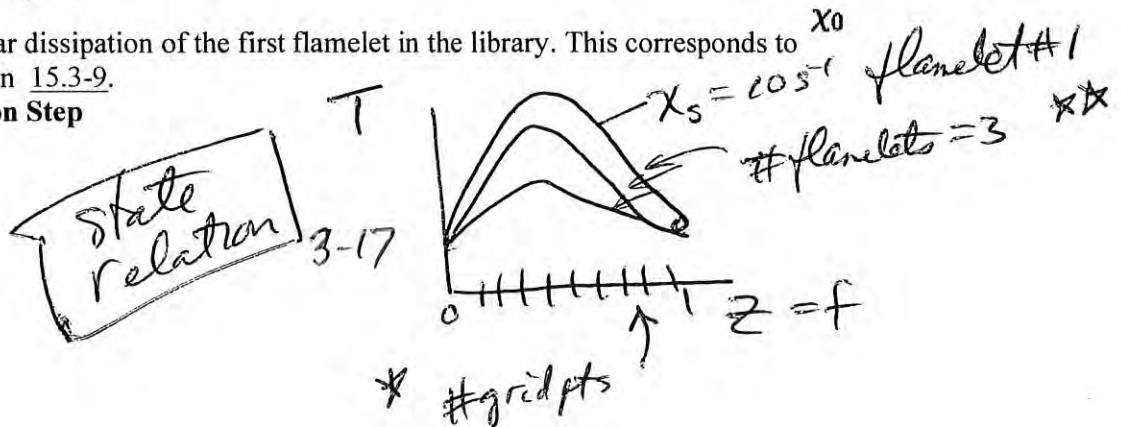
★ **Number of Grid Points in Flamelet** *from $z=0$ to $z=1$*
 specifies the number of mixture fraction grid points distributed between the oxidizer ($f=0$) and the fuel ($f=1$). Increased resolution will provide greater accuracy, but since the flamelet species and temperature are solved coupled and implicit in f space, the solution time and memory requirements increase greatly with the number of f grid points.

★ **Maximum Number of Flamelets**
 specifies the maximum number of laminar flamelet profiles to be calculated. If the flamelet extinguishes before this number is reached, flamelet generation is halted and the actual number of flamelets in the flamelet library will be less than this value.

Initial Scalar Dissipation

is the scalar dissipation of the first flamelet in the library. This corresponds to X_0 in Equation 15.3-9.

Scalar Dissipation Step



specifies the interval between scalar dissipation values (in s^{-1}) for which multiple flamelets will be calculated.

Click **Calculate Flamelets** to begin the laminar flamelet calculation. Sample output for a flamelet calculation is shown below.

$\chi_s =$

Generating flamelet 1 at scalar dissipation 0.01 /s

Time (s)	Temp (K)	Residual
1.679e-05	2233.7	3.779e+00
5.038e-05	2233.0	7.734e-02
1.175e-04	2231.5	1.648e-01
2.519e-04	2228.6	3.652e-01
5.206e-04	2223.6	8.295e-01
1.058e-03	2215.7	2.100e+00
2.133e-03	2205.5	3.540e+00
4.282e-03	2197.0	4.607e+00
8.581e-03	2193.6	6.639e+00
1.718e-02	2193.1	4.905e+00
3.437e-02	2193.4	5.792e+00
6.877e-02	2194.3	4.659e+00
1.375e-01	2195.3	3.922e+00
2.751e-01	2192.2	3.181e+00
5.502e-01	2188.6	2.549e+00
1.100e+00	2184.8	1.639e+00
2.201e+00	2182.9	4.604e+00
4.402e+00	2186.8	1.307e+00
8.804e+00	2189.6	4.420e-01
1.761e+01	2190.0	8.581e-02
3.522e+01	2190.0	1.199e-02
7.043e+01	2190.0	1.735e-03
1.409e+02	2190.0	4.217e-04
2.817e+02	2190.0	6.892e-05
5.635e+02	2190.0	6.777e-06

Flamelet successfully generated

15.4.8 Postprocessing the Flamelet Data

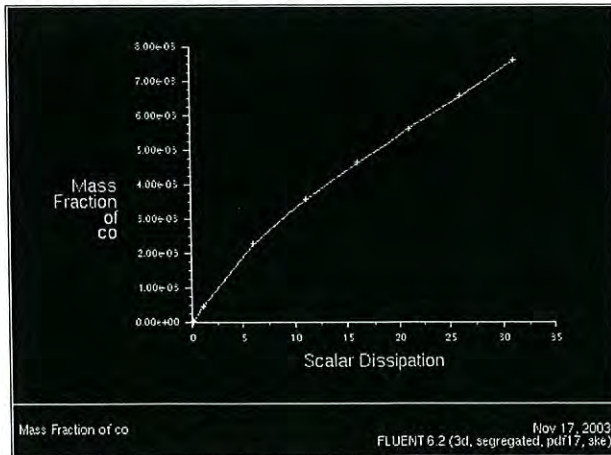


Figure 15.4.8: Example 2D Plot of Flamelet Table Data

3-18

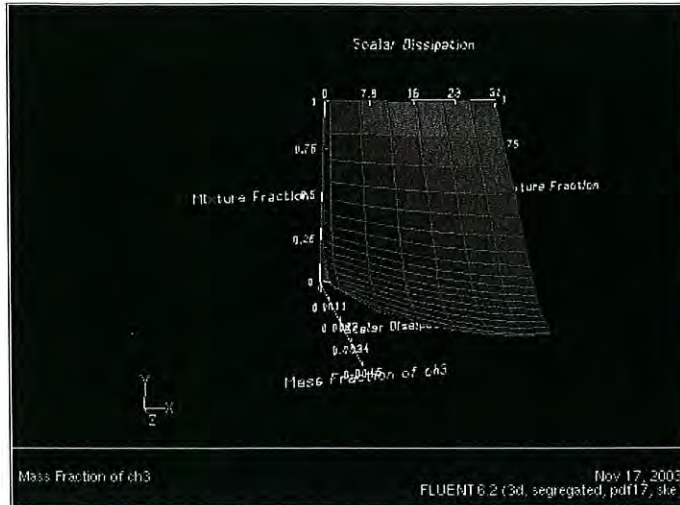


Figure 15.4.9: Example 3D Plot of Flamelet Table Data

Lookup table
 $\bar{T} = f(\bar{z}, g, \bar{\chi}_s)$
 after integrating the state relations

15.4.9 Calculating the Look-Up Tables

FLUENT requires additional inputs that are used in the creation of the look-up tables. Several of these inputs control the number of discrete values for which the look-up tables will be computed.

The look-up table parameters are as follows:

Number of Mean Mixture Fraction Points

\bar{f} is the number of discrete values of \bar{f} at which the look-up tables will be computed. For a two-mixture-fraction model, this value will also be the number of points used by FLUENT to compute the PDF if you choose the β model (see Section 15.8.4). Increasing the number of points will yield a more accurate PDF shape, but the calculation will take longer. The mean mixture fraction points will be clustered around the stoichiometric mixture fraction value.

Number of Mixture Fraction Variance Points

\bar{f}'^2 is the number of discrete values of \bar{f}'^2 at which the look-up tables will be computed. Lower resolution is acceptable because the variation along the \bar{f} axis is, in general, slower than the variation along the \bar{f}'^2 axis of the look-up tables. This option is available only when no secondary stream has been defined.

1. compute state relns
 $T = T(\bar{z}, \chi_s)$
 2. integrate using PDFs
 of \bar{z} with variance
 $\bar{z}, g, \bar{\chi}_s$
 \uparrow
 $\bar{f}'^2 = \bar{z}'^2$
 set $\bar{\chi}_s'^2 = 0$

GT2013-94282

CO PREDICTION FOR AIRCRAFT GAS TURBINE COMBUSTORS

F. Xu¹

Honeywell Aerospace
Phoenix, AZ 85034, USA

V. Nori, J. Basani

Honeywell Technology Solutions
Bangalore, India

ABSTRACT

The predictive capabilities of two candidate approaches for CO predictions were assessed for a series of aircraft gas turbine combustors. The first approach involved constructing a large reduced order reactor network coupled with a detailed, 500 species n-dodecane mechanism to simulate the combustion process. The second approach was the traditional RANS based CFD using two finite rate based combustion models in FLUENT. A four step Jet-A global mechanism was developed in-house and was used in the CFD simulations. The global mechanism was validated against the detailed Jet-A mechanism published by Dagaut in 2006 and was able to reproduce the flame speed and species profiles satisfactorily over the range of relevant operating temperatures and pressures. The calibration combustors comprised seven configurations with identical fuel nozzles but different wirlers, dome effusion, liner and quench jet air flow splits. It was found that the CFD approach was better at capturing the trend of rig data than the reactor network approach and was able to capture most of the variations seen in the measurement. The improvement in prediction was attributed mainly to the more accurate global mechanism which results in more accurate kinetic calculation in CFD.

INTRODUCTION

Modern aircraft gas turbine engines are subject to increasingly stringent emission requirements to meet FAA certification, CAEP regulation and customer requirement. Historically, successful combustor design that met the design target often requires a significant number of rig and engine tests which were very expensive. The increasingly faster computers and sophisticated CFD modeling techniques have been proven to be invaluable in reducing the number of rig tests, usually by indicating a correct trend and sometimes even predicting the correct measurement values. This has been observed for certain emission parameters, such as NOx. Unfortunately, significant obstacles still remain for CO and UHC predictions. In a recent assessment of the current status of modeling techniques pertinent to gas turbine combustors, the applied research team in the Multi-Agency Coordination Committee for Combustion Research

¹Corresponding Author

(MACCCR) workshop in 2011 rated the current modeling capability to capture the CO trend as inadequate [1].

The fundamental reason that CO prediction is more difficult than NOx prediction is because of the difference in reaction chemistry. For traditional Rich-Quench-Lean (RQL) type aircraft gas turbine combustors, NOx formation is dominated by high temperature oxidation of molecular nitrogen through the Zel'dovich thermal mechanism, while other modes of NOx formation can often be neglected. Typically such high temperature regions consist of a narrow, near stoichiometric shear layer where intense fuel and air mixing takes place. Even for military engines that burn very rich and have very high combustor exit temperatures, the small residence time, typically just a few milliseconds, ensures that only a trace amount of NOx will form, and NOx concentration remains far below the equilibrium value. A significant advantage for NOx prediction is that NOx is not consumed once it is formed. This greatly simplifies the modeling. On the other hand, all carbon based jet fuel will be converted into numerous intermediate hydrocarbons starting at low temperature. Most of these hydrocarbons are then further oxidized into significant amount of CO over a very wide range of temperature, typically resulting in peak molar concentrations in excess of 10% before nearly all CO is eventually oxidized into CO₂. Even for idle engine conditions, the concentration of CO at the combustor exit is typically well below 0.1%. This means one must capture more than 99% of the CO oxidation process in order to predict the right amount of CO at the combustor exit, certainly a very challenging task.

The second reason that CO prediction is difficult is that numerous reactions are involved in CO formation and oxidation, whereas only three principal elementary reactions are sufficient to capture the thermal NOx formation. Therefore accurate CO prediction in principle requires a large, accurate kinetic mechanism, which unfortunately, remains under-developed for aviation fuel that consists of numerous fuel components and exhibits significant variation in its composition depending on the vendor [2]. A detailed mechanism for aviation fuel, or Jet-A is typically very large, consisting of hundreds to thousands of species and

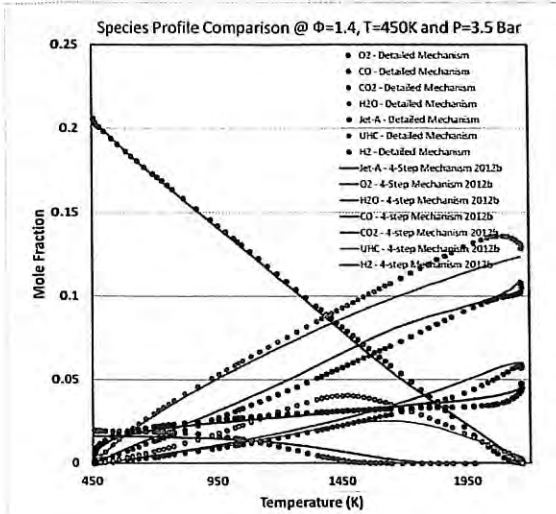


FIGURE 10. PREDICTED SPECIES CONCENTRATIONS OF FOUR STEP JET-A GLOBAL MECHANISM 2012b AND THE DETAILED MECHANISM FOR A FUEL EQUIVALENCE RATIO OF 1.4.

Since the detailed Jet-A mechanism [13] contains three Jet-A surrogate components (74% n-decane, 15% propylbenzene and 11% cyclohexane), as well as numerous intermediate hydrocarbons, in all figures shown above, the Jet-A fuel composition was computed as the sum of all three surrogate components, while the total UHC was computed by summing all intermediate hydrocarbons. In contrast, the UHC in the global mechanism is represented solely by C_2H_4 . Note that the initial Jet-A fuel concentrations in two mechanisms are slightly different. This results in the average Jet-A composition in the detailed mechanism being equal to $C_{9.74}H_{20.1}$ instead of $C_{12}H_{23}$.

The ability to predict the formation and oxidation characteristics of CO over a wide range of fuel equivalence ratios is believed to be very important to successfully predict CO emission in traditional, rich-quench-lean (RQL) aircraft gas turbine combustors. RQL combustors typically use a rich primary zone, followed by intensive, sudden quenching of combustion to transition the combustion mixture into a final lean burn state. The concept was developed to reduce the NOx production by reducing the residence time of the combustion mixture in high temperature, near stoichiometric burning region. Since the fuel rich and fuel lean zones are many times larger than the stoichiometric zone in volume, it is necessary to correctly simulate the formation and oxidation of CO for both rich and lean conditions. Figure 11 shows the predicted CO mole fraction as a function of distance for five different fuel equivalence ratios using the detailed mechanism. It shows that as the amount of fuel increases, CO formation gradually dominates over its oxidation due to decreasing amount of available oxidizer, and an inflection point is reached somewhere between $\phi=1.2$ and $\phi=1.4$. This behavior is captured quite well by the four step mechanism shown in Figure 12. As a comparison, the modified two step mechanism does not capture the formation and oxidation of CO correctly,

as shown in Figure 13. The performance of the original two step mechanism [12] was a little worse than the modified two step mechanism.

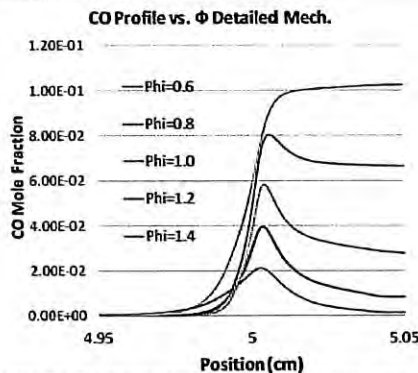


FIGURE 11. PREDICTED CO CONCENTRATIONS OF THE DETAILED MECHANISM FOR A FUEL EQUIVALENCE RATIO RANGE BETWEEN 0.6 AND 1.4.

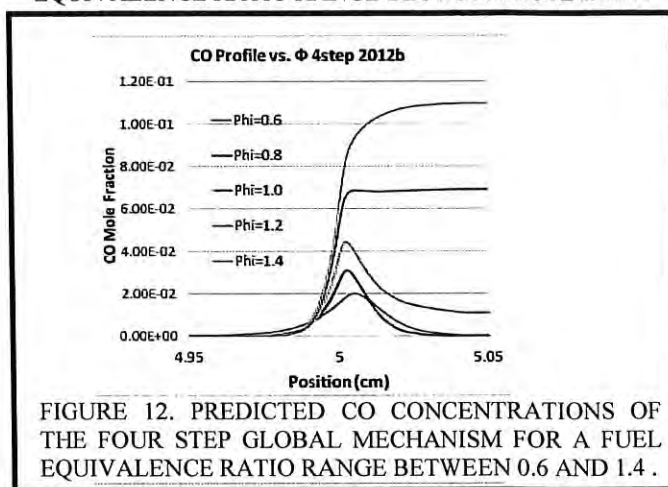


FIGURE 12. PREDICTED CO CONCENTRATIONS OF THE FOUR STEP GLOBAL MECHANISM FOR A FUEL EQUIVALENCE RATIO RANGE BETWEEN 0.6 AND 1.4.

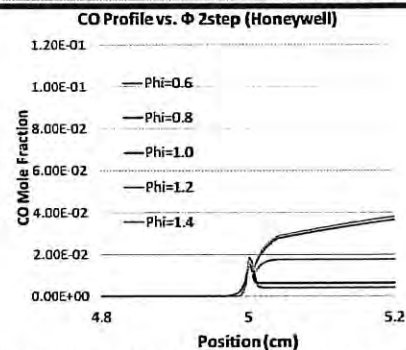


FIGURE 13. PREDICTED CO CONCENTRATIONS OF THE TWO STEP GLOBAL MECHANISM FOR A FUEL EQUIVALENCE RATIO RANGE BETWEEN 0.6 AND 1.4.

The accuracy of the four step mechanism extends beyond the three fuel equivalence ratios considered in Figure 5 through Figure 13. In Figure 14, the predicted CO and CO_2 by the four step and two step mechanisms are compared with the detailed mechanisms for a much wider range of fuel equivalence from 0.5 to 2.8 using three dimensional surface plots. This range covers virtually all flammable conditions of

interest since the flame speeds have fallen to nearly zero and very little changes in species concentrations occur. The four step global mechanism over-predicts CO by approximately 20% and under-predicts CO₂ slightly in ultra-rich conditions, but its predicted CO surface contour is reasonably close to that of the detailed mechanism, and is vastly superior to the two step mechanism. The accuracy of the rest of the species is similar.

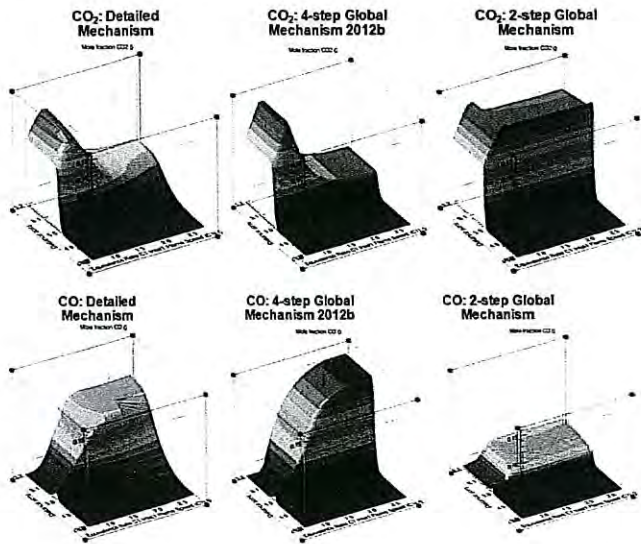


FIGURE 14. PREDICTED CO and CO₂ CONCENTRATIONS OF THE DETAILED MECHANISM (LEFT), 4-STEP (MIDDLE) AND 2-STEP (RIGHT) GLOBAL MECHANISMS AS A FUNCTION OF AXIAL DISTANCE FOR A FUEL EQUIVALENCE RATIO RANGE BETWEEN 0.5 AND 2.8.

A known past issue of CFD using the two step mechanism was that incorrect amount of major species such as CO and CO₂ were predicted in the primary zone of the combustor. This adversely impacted the temperature distributions in the primary zone due to incorrect enthalpy distribution among species. Figure 15 shows the typical contour plot of CO and CO₂ at a plane of symmetry for a calibration combustor using the two step mechanism. The peak concentrations of CO and CO₂ seen in CFD are determined by the peak concentrations shown in Figure 14 for the two step mechanism, which is markedly different from the prediction by the detailed mechanism. On the other hand, CFD using the four step mechanism predicted much more realistic distribution of CO and CO₂ that agreed well with the detailed mechanism, as shown in Figure 16. We believe the results shown in Figures 15 and 16 represent a more accurate description of the combustion process and found it also better agreed with the flamelet solution that used the same detailed mechanism [13].

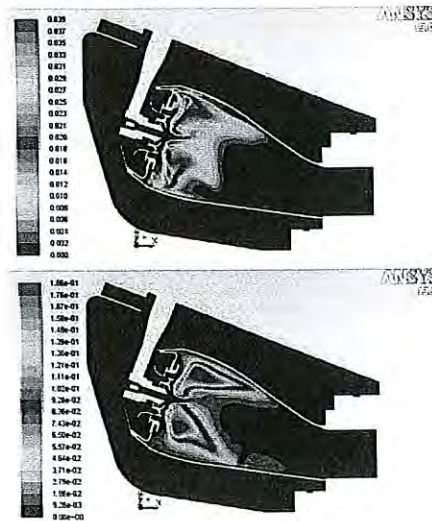


FIGURE 15. CALCULATED CO (TOP) AND CO₂ (BOTTOM) CONCENTRATIONS FOR A CALIBRATION COMBUSTOR USING THE TWO STEP GLOBAL MECHANISM.

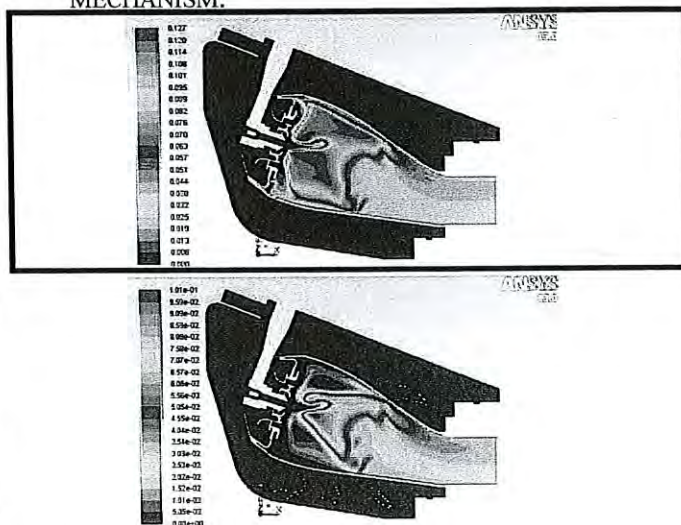
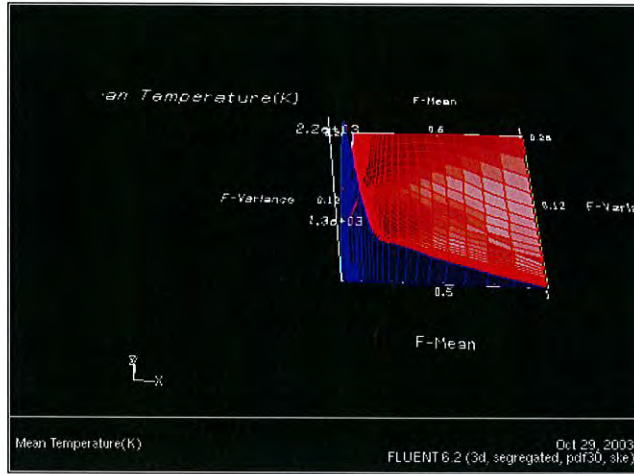


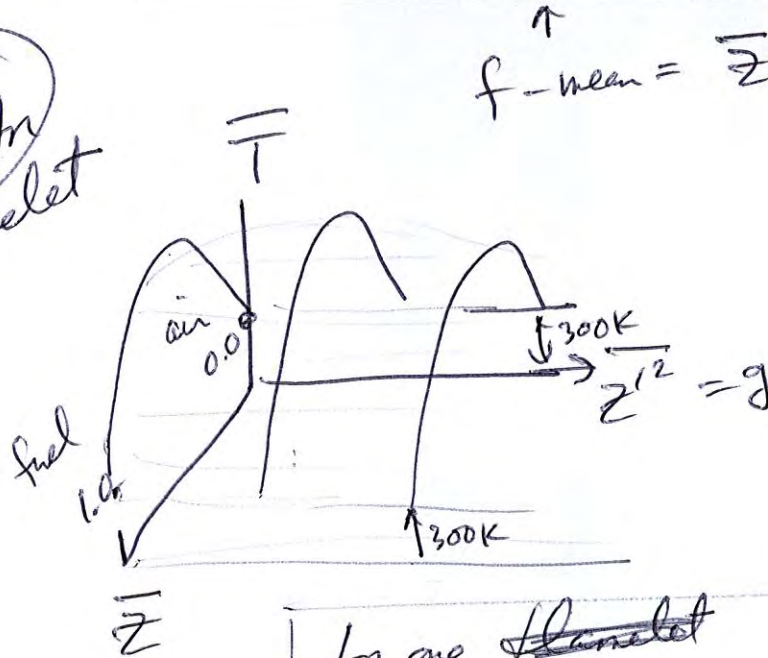
FIGURE 16. CALCULATED CO (TOP) AND CO₂ (BOTTOM) CONCENTRATIONS FOR A CALIBRATION COMBUSTOR USING THE FOUR STEP GLOBAL MECHANISM.

Figure 15.4.14 shows an example of a 3D surface derived for the same system.



$$f_{\text{variance}} = \frac{z^2}{z^2} = f^2 = g$$

Look up Table for one flamelet



$$f_{\text{-mean}} = \bar{z}$$

lookup table

for one flamelet value of $\bar{\chi}_s = 105^{-1}$

$$\bar{T} = f(\bar{z}, \bar{z}^2, \bar{\chi}_s)$$

\uparrow from \bar{z} Cons. eqn 14
 \uparrow from g Cons. eqn
 \uparrow from p. 4 eqn

Fluent : inlet boundary conditions

The K-Epsilon Model in the FLUENT code (taken from Fluent Users Manual, 3-19-2010)

FLUENT provides the following choices of turbulence models:

- Spalart-Allmaras model
- k - ϵ models
 - Standard k - ϵ model
 - Renormalization-group (RNG) k - ϵ model
 - Realizable k - ϵ model
- k - ω models
 - Standard k - ω model
 - Shear-stress transport (SST) k - ω model
- v^2 - f model (addon)
- Reynolds stress model (RSM)
 - Linear pressure-strain RSM model
 - Quadratic pressure-strain RSM model
 - Low-Re stress-omega RSM model
- Detached eddy simulation (DES) model
 - Spalart-Allmaras RANS model
 - Realizable k - ϵ RANS model
 - SST k - ω RANS model
- Large eddy simulation (LES) model
 - Smagorinsky-Lilly subgrid-scale model
 - WALE subgrid-scale model
 - Kinetic-energy transport subgrid-scale model

equations FLUENT
same as on handout

$$\nu_T = C_\mu k^2 / \epsilon \quad (p. 5)$$

$$C_\mu = 0.09$$

k_0 = value of k on inflow boundary

$$k_0 = \frac{1}{2} (\overline{u^2} + \overline{v^2} + \overline{w^2})$$

$$k_0 = \frac{3}{2} \overline{u^2} \quad \text{if isotropic}$$

$$\frac{\sqrt{\overline{u^2}}}{\overline{u}} = 0.16 \quad (Re_0) \quad p. 8$$

inlet integral length scale l

$$l_0 = 0.07 L \quad p. 9$$

L = inlet duct hydraulic diameter

* if $Re_0 = 50,000$, $\frac{\sqrt{\overline{u^2}}}{\overline{u}} = 0.04$

3-24

$$\epsilon_0 = C_\mu^{3/4} \frac{k_0^{3/2}}{l_0}$$

wall functions - p. 13

9.2 Continuity and Momentum Equations

For all flows, FLUENT solves conservation equations for mass and momentum. For flows involving heat transfer or compressibility, an additional equation for energy conservation is solved. For flows involving species mixing or reactions, a species conservation equation is solved or, if the non-premixed combustion model is used, conservation equations for the mixture fraction and its variance are solved. Additional transport equations are also solved when the flow is turbulent.

In this section, the conservation equations for laminar flow in an inertial (non-accelerating) reference frame are presented. The equations that are applicable to rotating reference frames are presented in Chapter 10. The conservation equations relevant to heat transfer, turbulence modeling, and species transport will be discussed in the chapters where those models are described.

The Euler equations solved for inviscid flow are presented in Section 9.7.

The Mass Conservation Equation

The equation for conservation of mass, or continuity equation, can be written as follows:

$$\frac{\partial \rho}{\partial t} + \nabla \cdot (\rho \vec{v}) = S_m = 0 \quad (9.2-1)$$

Equation 9.2-1 is the general form of the mass conservation equation and is valid for incompressible as well as compressible flows. The source S_m is the mass added to the continuous phase from the dispersed second phase (e.g., due to vaporization of liquid droplets) and any user-defined sources.

For 2D axisymmetric geometries, the continuity equation is given by

$$\frac{\partial \rho}{\partial t} + \frac{\partial}{\partial x}(\rho v_x) + \frac{\partial}{\partial r}(\rho v_r) + \frac{\rho v_r}{r} = S_m \quad (9.2-2)$$

where x is the axial coordinate, r is the radial coordinate, v_x is the axial velocity, and v_r is the radial velocity.

325

Conservation of momentum in an inertial (non-accelerating) reference frame is described by [24]

$$\boxed{\frac{\partial}{\partial t}(\rho \vec{v}) + \nabla \cdot (\rho \vec{v} \vec{v}) = -\nabla p + \nabla \cdot (\bar{\tau}) + \rho \vec{g} + \vec{F}} \quad (9.2-3)$$

where p is the static pressure, $\bar{\tau}$ is the stress tensor (described below), and $\rho \vec{g}$ and \vec{F} are the gravitational body force and external body forces (e.g., that arise from interaction with the dispersed phase), respectively. \vec{F} also contains other model-dependent source terms such as porous-media and user-defined sources.

The stress tensor $\bar{\tau}$ is given by

$$\bar{\tau} = \mu \left[(\nabla \vec{v} + \nabla \vec{v}^T) - \frac{2}{3} \nabla \cdot \vec{v} I \right] \quad (9.2-4)$$

where μ is the molecular viscosity, I is the unit tensor, and the second term on the right hand side is the effect of volume dilation.

For 2D axisymmetric geometries, the axial and radial momentum conservation equations are given by

$$\begin{aligned} \frac{\partial}{\partial t}(\rho v_x) + \frac{1}{r} \frac{\partial}{\partial x}(r \rho v_x v_x) + \frac{1}{r} \frac{\partial}{\partial r}(r \rho v_r v_x) = -\frac{\partial p}{\partial x} + \frac{1}{r} \frac{\partial}{\partial x} \left[r \mu \left(2 \frac{\partial v_x}{\partial x} - \frac{2}{3} (\nabla \cdot \vec{v}) \right) \right] \\ + \frac{1}{r} \frac{\partial}{\partial r} \left[r \mu \left(\frac{\partial v_x}{\partial r} + \frac{\partial v_r}{\partial x} \right) \right] + F_x \end{aligned} \quad (9.2-5)$$

and

$$\frac{\partial}{\partial t}(\rho v_r) + \frac{1}{r} \frac{\partial}{\partial x}(r \rho v_x v_r) + \frac{1}{r} \frac{\partial}{\partial r}(r \rho v_r v_r) = -\frac{\partial p}{\partial r} + \frac{1}{r} \frac{\partial}{\partial x} \left[r \mu \left(\frac{\partial v_r}{\partial x} + \frac{\partial v_x}{\partial r} \right) \right]$$

12.4.1 Standard k - ϵ Model

Overview

The simplest "complete models" of turbulence are two-equation models in which the solution of two separate transport equations allows the turbulent velocity and length scales to be independently determined. The standard k - ϵ model in FLUENT falls within this class of turbulence model and has become the workhorse of practical engineering flow calculations in the time since it was proposed by Launder and Spalding [196]. Robustness, economy, and reasonable accuracy for a wide range of turbulent flows explain its popularity in industrial flow and heat transfer simulations. It is a semi-empirical model, and the derivation of the model equations relies on phenomenological considerations and empiricism.

As the strengths and weaknesses of the standard k - ϵ model have become known, improvements have been made to the model to improve its performance. Two of these variants are available in FLUENT: the RNG k - ϵ model [408] and the realizable k - ϵ model [330].

The standard k - ϵ model [196] is a semi-empirical model based on model transport equations for the turbulence kinetic energy (k) and its dissipation rate (ϵ). The model transport equation for k is derived from the exact equation, while the model transport equation for ϵ was obtained using physical reasoning and bears little resemblance to its mathematically exact counterpart.

In the derivation of the k - ϵ model, the assumption is that the flow is fully turbulent, and the effects of molecular viscosity are negligible. The standard k - ϵ model is therefore valid only for fully turbulent flows.

Transport Equations for the Standard k - ϵ Model

The turbulence kinetic energy, k , and its rate of dissipation, ϵ , are obtained from the following transport equations:

$$\frac{\partial}{\partial t}(\rho k) + \frac{\partial}{\partial x_i}(\rho k u_i) = \frac{\partial}{\partial x_j} \left[\left(\mu + \frac{\mu_t}{\sigma_k} \right) \frac{\partial k}{\partial x_j} \right] + G_k + G_b - \rho \epsilon - Y_M + S_k \quad (12.4-1)$$

and

$$\frac{\partial}{\partial t}(\rho \epsilon) + \frac{\partial}{\partial x_i}(\rho \epsilon u_i) = \frac{\partial}{\partial x_j} \left[\left(\mu + \frac{\mu_t}{\sigma_\epsilon} \right) \frac{\partial \epsilon}{\partial x_j} \right] + C_{1\epsilon} \frac{\epsilon}{k} (G_k + C_{3\epsilon} G_b) - C_{2\epsilon} \rho \frac{\epsilon^2}{k} + S_\epsilon \quad (12.4-2)$$

3-27

In these equations, G_k represents the generation of turbulence kinetic energy due to the mean velocity gradients, calculated as described in Section 12.4.4. G_b is the generation of turbulence kinetic energy due to buoyancy, calculated as described in Section 12.4.5. Y_M represents the contribution of the fluctuating dilatation in compressible turbulence to the overall dissipation rate, calculated as described in Section 12.4.6. $C_{1\epsilon}$, $C_{2\epsilon}$, and $C_{3\epsilon}$ are constants. σ_k and σ_ϵ are the turbulent Prandtl numbers for k and ϵ , respectively. S_k and S_ϵ are user-defined source terms.

Modeling the Turbulent Viscosity

The turbulent (or eddy) viscosity, μ_t , is computed by combining k and ϵ as follows:

$$\mu_t = \rho C_\mu \frac{k^2}{\epsilon} \quad (12.4-3)$$

where C_μ is a constant.

Model Constants

The model constants $C_{1\epsilon}$, $C_{2\epsilon}$, C_μ , σ_k , and σ_ϵ have the following default values [196]:

$$C_{1\epsilon} = 1.44, \quad C_{2\epsilon} = 1.92, \quad C_\mu = 0.09, \quad \sigma_k = 1.0, \quad \sigma_\epsilon = 1.3$$

These default values have been determined from experiments with air and water for fundamental turbulent shear flows including homogeneous shear flows and decaying isotropic grid turbulence. They have been found to work fairly well for a wide range of wall-bounded and free shear flows.

Although the default values of the model constants are the standard ones most widely accepted, you can change them (if needed) in the **Viscous Model** panel.

12.2.3 Boussinesq Approach vs. Reynolds Stress Transport Models

The Reynolds-averaged approach to turbulence modeling requires that the Reynolds stresses in Equation 12.2-4 be appropriately modeled. A common method employs the Boussinesq hypothesis [142] to relate the Reynolds stresses to the mean velocity gradients:

$$-\overline{\rho u_i' u_j'} = \mu_t \left(\frac{\partial u_i}{\partial x_j} + \frac{\partial u_j}{\partial x_i} \right) - \frac{2}{3} \left(\rho k + \mu_t \frac{\partial u_k}{\partial x_k} \right) \delta_{ij} \quad (12.2-5)$$

The Boussinesq hypothesis is used in the Spalart-Allmaras model, the k - ϵ models, and the k - ω models. The

12.4.4 Modeling Turbulent Production in the k - ϵ Models

The term G_k , representing the production of turbulence kinetic energy, is modeled identically for the standard, RNG, and realizable k - ϵ models. From the exact equation for the transport of k , this term may be defined as

$$G_k = -\rho \overline{u'_i u'_j} \frac{\partial u_j}{\partial x_i} \quad (12.4-20)$$

To evaluate G_k in a manner consistent with the Boussinesq hypothesis,

$$G_k = \mu_t S^2 \quad (12.4-21)$$

where S is the modulus of the mean rate-of-strain tensor, defined as

$$S \equiv \sqrt{2S_{ij}S_{ij}} \quad (12.4-22)$$

i When using the high-Reynolds number k - ϵ versions, μ_{eff} is used in lieu of μ_t in Equation 12.4-21.

12.14.1 Setting Up the Standard or Realizable k - ϵ Model

If you choose the standard k - ϵ model or the realizable k - ϵ model, the following options are available:

- viscous heating (always activated for the density-based solvers) (Section 12.19.1)
- inclusion of buoyancy effects on ϵ (Section 12.4.5)

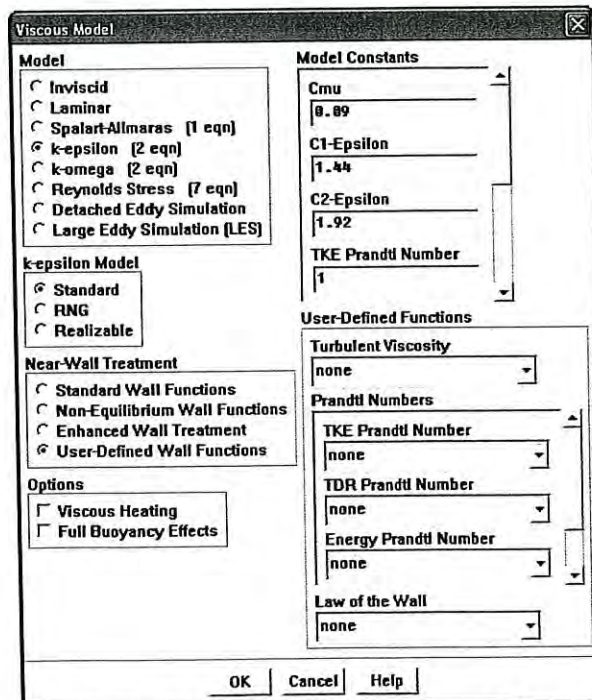


Figure 12.14.1: The Viscous Model Panel Displaying the Standard k - ϵ Model

7.2.2 Determining Turbulence Parameters

When the flow enters the domain at an inlet, outlet, or far-field boundary, **FLUENT** requires specification of transported turbulence quantities. This section describes which quantities are needed for specific turbulence models and how they must be specified. It also provides guidelines for the most appropriate way of determining the inflow boundary values.

Specification of Turbulence Quantities Using Profiles

If it is important to accurately represent a boundary layer or fully-developed turbulent flow at the inlet, you should ideally set the turbulence quantities by creating a boundary profile file (see Section 7.2.6) from experimental data or empirical formulas. If you have an analytical description of the profile, rather than data points, you can either use this analytical description to create a boundary profile file, or create a user-defined function to provide the inlet boundary information. (See the separate **UDF Manual** for information on user-defined functions.)

Once you have created the profile function, you can use it as described below:

- k - ϵ models: Choose **K** and **Epsilon** in the **Turbulence Specification Method** drop-down list and select the appropriate profile names in the drop-down lists next to **Turb. Kinetic Energy** and **Turb. Dissipation Rate**.
- **Outflow boundaries where normal gradients are negligible:** Figure 7.10.1 shows a simple two-dimensional flow problem and several possible outflow boundary location choices. Location C shows the outflow boundary located upstream of the plenum exit but in a region of the duct where the flow is fully-developed. At this location, the outflow boundary condition is exactly obeyed.

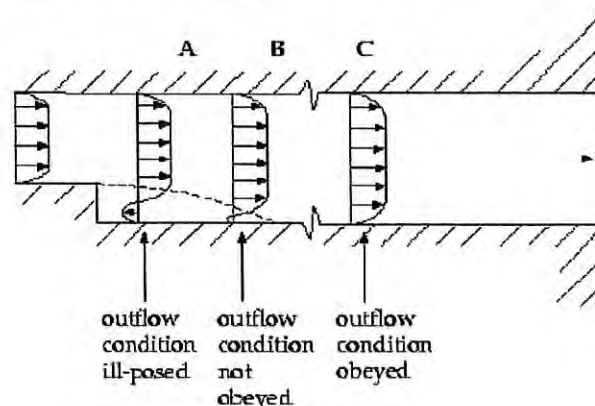


Figure 7.10.1: Choice of the Outflow Boundary Condition Location

- **Ill-posed outflow boundaries:** Location B in Figure 7.10.1 shows the outflow boundary near the reattachment point of the recirculation in the wake of the backward-facing step. This choice of outflow boundary condition is ill-posed as the gradients normal to the exit plane are quite large at this point and can be expected to have a significant impact on the flow field upstream. Because the outflow boundary condition ignores these axial gradients in the flow, location B is a poor choice for an outflow boundary. The exit location should be moved downstream from the reattachment point.

Figure 7.10.1 shows a second ill-posed outflow boundary at location A. Here, the outflow is located where flow is pulled into the **FLUENT** domain through the outflow boundary. In situations like this the **FLUENT** calculation typically does not converge and the results of the calculation have no validity. This is because when flow is pulled into the domain through an outflow, the mass flow rate through the domain is "floating" or undefined. In addition, when flow enters the domain through an outflow boundary, the scalar properties of the flow are not defined. For example, the temperature of the flow pulled in through the outflow is not defined. (**FLUENT** chooses the temperature using the temperature of the fluid adjacent to the outflow, inside the domain.)

- Reynolds stress model: Choose **K and Epsilon** in the **Turbulence Specification Method** drop-down list and select the appropriate profile names in the drop-down lists next to **Turb. Kinetic Energy** and **Turb. Dissipation Rate**. Choose **Reynolds-Stress Components** in the **Reynolds-Stress Specification Method** drop-down list and select the appropriate profile name in the drop-down list next to each of the individual Reynolds-stress components.

In most turbulent flows, higher levels of turbulence are generated within shear layers than enter the domain at flow boundaries, making the result of the calculation relatively insensitive to the inflow boundary values. Nevertheless, caution must be used to ensure that boundary values are not so unphysical as to contaminate your solution or impede convergence. This is particularly true of external flows where unphysically large values of effective viscosity in the free stream can "swamp" the boundary layers.

You can use the turbulence specification methods described above to enter uniform constant values instead of profiles. Alternatively, you can specify the turbulence quantities in terms of more convenient quantities such as turbulence intensity, turbulent viscosity ratio, hydraulic diameter, and turbulence length scale. These quantities are discussed further in the following sections.

Turbulence Intensity

The turbulence intensity, I , is defined as the ratio of the root-mean-square of the velocity fluctuations, u' , to the mean flow velocity, u_{avg} .

A turbulence intensity of 1% or less is generally considered low and turbulence intensities greater than 10% are considered high. Ideally, you will have a good estimate of the turbulence intensity at the inlet boundary from external, measured data. For example, if you are simulating a wind-tunnel experiment, the turbulence intensity in the free stream is usually available from the tunnel characteristics. In modern low-turbulence wind tunnels, the free-stream turbulence intensity may be as low as 0.05%.

For internal flows, the turbulence intensity at the inlets is totally dependent on the upstream history of the flow. If the flow upstream is under-developed and undisturbed, you can use a low turbulence intensity. If the flow is fully developed, the turbulence intensity may be as high as a few percent. The turbulence intensity at the core of a fully-developed duct flow can be estimated from the following formula derived from an empirical correlation for pipe flows:

$$I \equiv \frac{u'}{u_{avg}} = 0.16(Re_{DH})^{-1/8} \quad (7.2-1)$$

At a Reynolds number of 50,000, for example, the turbulence intensity will be 4%, according to this formula.

Turbulence Length Scale and Hydraulic Diameter

The turbulence length scale, ℓ , is a physical quantity related to the size of the large eddies that contain the energy in turbulent flows.

In fully-developed duct flows, ℓ is restricted by the size of the duct, since the turbulent eddies cannot be larger than the duct. An approximate relationship between ℓ and the physical size of the duct is

$$\ell = 0.07L \quad (7.2-2)$$

where L is the relevant dimension of the duct. The factor of 0.07 is based on the maximum value of the mixing length in fully-developed turbulent pipe flow, where L is the diameter of the pipe. In a channel of non-circular cross-section,

you can base L on the hydraulic diameter.

If the turbulence derives its characteristic length from an obstacle in the flow, such as a perforated plate, it is more appropriate to base the turbulence length scale on the characteristic length of the obstacle rather than on the duct size.

It should be noted that the relationship of Equation 7.2-2, which relates a physical dimension (L) to the turbulence length scale (ℓ), is not necessarily applicable to all situations. For most cases, however, it is a suitable approximation.

Guidelines for choosing the characteristic length L or the turbulence length scale ℓ for selected flow types are listed below:

- For fully-developed internal flows, choose the **Intensity and Hydraulic Diameter** specification method and specify the hydraulic diameter $L = D_H$ in the **Hydraulic Diameter** field.
- For flows downstream of turning vanes, perforated plates, etc., choose the **Intensity and Hydraulic Diameter** method and specify the characteristic length of the flow opening for L in the **Hydraulic Diameter** field.
- For wall-bounded flows in which the inlets involve a turbulent boundary layer, choose the **Intensity and Length Scale** method and use the boundary-layer thickness, δ_{99} , to compute the turbulence length scale, ℓ , from $\ell = 0.4\delta_{99}$. Enter this value for ℓ in the **Turbulence Length Scale** field.

Turbulent Viscosity Ratio

The turbulent viscosity ratio, μ_t/μ , is directly proportional to the turbulent Reynolds number ($Re_t \equiv k^2/(\epsilon\nu)$).

Re_t is large (on the order of 100 to 1000) in high-Reynolds-number boundary layers, shear layers, and fully-developed duct flows. However, at the free-stream boundaries of most external flows, μ_t/μ is fairly small. Typically, the turbulence parameters are set so that $1 < \mu_t/\mu < 10$.

To specify quantities in terms of the turbulent viscosity ratio, you can choose **Turbulent Viscosity Ratio** (for the Spalart-Allmaras model) or **Intensity and Viscosity Ratio** (for the k - ϵ models, the k - ω models, or the RSM).

Relationships for Deriving Turbulence Quantities

To obtain the values of transported turbulence quantities from more convenient quantities such as I , L , or μ_t/μ , you must typically resort to an empirical relation. Several useful relations, most of which are used within FLUENT, are presented below.

Estimating Modified Turbulent Viscosity from Turbulence Intensity and Length Scale

To obtain the modified turbulent viscosity, $\tilde{\nu}$, for the Spalart-Allmaras model from the turbulence intensity, I , and length scale, ℓ , the following equation can be used:

This formula is used in FLUENT if you select the **Intensity and Hydraulic Diameter** specification method with the Spalart-Allmaras model. ℓ is obtained from Equation 7.2-2.

Estimating Turbulent Kinetic Energy from Turbulence Intensity

The relationship between the turbulent kinetic energy, k , and turbulence intensity, I , is

$$k = \frac{3}{2}(u_{\text{avg}}I)^2 \quad (7.2-4)$$

where u_{avg} is the mean flow velocity.

This relationship is used in FLUENT whenever the **Intensity and Hydraulic Diameter**, **Intensity and Length Scale**, or **Intensity and Viscosity Ratio** method is used instead of specifying explicit values for k and ϵ .

Estimating Turbulent Dissipation Rate from a Length Scale

If you know the turbulence length scale, ℓ , you can determine ϵ from the relationship

$$\epsilon = C_{\mu}^{3/4} \frac{k^{3/2}}{\ell} \quad (7.2-5)$$

where C_{μ} is an empirical constant specified in the turbulence model (approximately 0.09). The determination of ℓ was discussed previously.

This relationship is used in FLUENT whenever the **Intensity and Hydraulic Diameter** or **Intensity and Length Scale** method is used instead of specifying explicit values for k and ϵ .

Estimating Turbulent Dissipation Rate from Turbulent Viscosity Ratio

The value of ϵ can be obtained from the turbulent viscosity ratio μ_t/μ and k using the following relationship:

$$\epsilon = \rho C_{\mu} \frac{k^2}{\mu} \left(\frac{\mu_t}{\mu} \right)^{-1} \quad (7.2-6)$$

Wall Functions in FLUENT

12.10.1 Overview

Turbulent flows are significantly affected by the presence of walls. Obviously, the mean velocity field is affected through the no-slip condition that has to be satisfied at the wall. However, the turbulence is also changed by the presence of the wall in non-trivial ways. Very close to the wall, viscous damping reduces the tangential velocity fluctuations, while kinematic blocking reduces the normal fluctuations. Toward the outer part of the near-wall region, however, the turbulence is rapidly augmented by the production of turbulence kinetic energy due to the large gradients in mean velocity.

The near-wall modeling significantly impacts the fidelity of numerical solutions, inasmuch as walls are the main source of mean vorticity and turbulence. After all, it is in the near-wall region that the solution variables have large gradients, and the momentum and other scalar transports occur most vigorously. Therefore, accurate representation of the flow in the near-wall region determines successful predictions of wall-bounded turbulent flows.

The $k-\epsilon$ models, the RSM, and the LES model are primarily valid for turbulent core flows (i.e., the flow in the regions somewhat far from walls). Consideration therefore needs to be given as to how to make these models suitable for wall-bounded flows. The Spalart-Allmaras and $k-\omega$ models were designed to be applied throughout the boundary layer, provided that the near-wall mesh resolution is sufficient.

Numerous experiments have shown that the near-wall region can be largely subdivided into three layers. In the innermost layer, called the "viscous sublayer", the flow is almost laminar, and the (molecular) viscosity plays a dominant role in momentum and heat or mass transfer. In the outer layer, called the fully-turbulent layer, turbulence plays a major role. Finally, there is an interim region between the viscous sublayer and the fully turbulent layer where the effects of molecular viscosity and turbulence are equally important. Figure 12.10.1 illustrates these subdivisions of the near-wall region, plotted in semi-log coordinates.

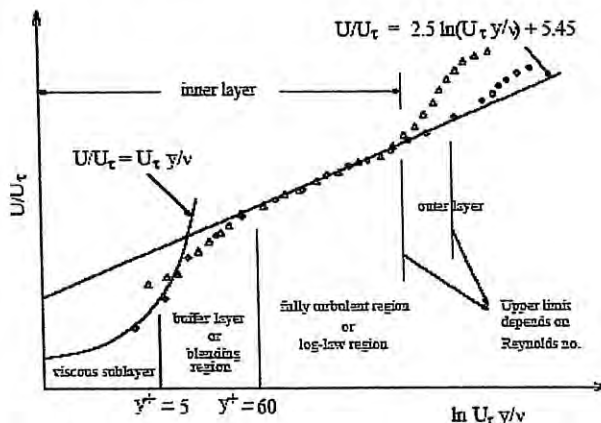


Figure 12.10.1: Subdivisions of the Near-Wall Region

In Figure 12.10.1, $y^+ \equiv \rho u_\tau y / \mu$, where u_τ is the friction velocity, defined as $\sqrt{\frac{\tau_w}{\rho}}$.

Wall Functions vs. Near-Wall Model

Traditionally, there are two approaches to modeling the near-wall region. In one approach, the viscosity-affected inner region (viscous sublayer and buffer layer) is not resolved. Instead, semi-empirical formulas called "wall functions" are used to bridge the viscosity-affected region between the wall and the fully-turbulent region. The use of wall functions obviates the need to modify the turbulence models to account for the presence of the wall.

In another approach, the turbulence models are modified to enable the viscosity-affected region to be resolved with a mesh all the way to the wall, including the viscous sublayer. For purposes of discussion, this will be termed the "near-wall modeling" approach. These two approaches are depicted schematically in Figure 12.10.2.

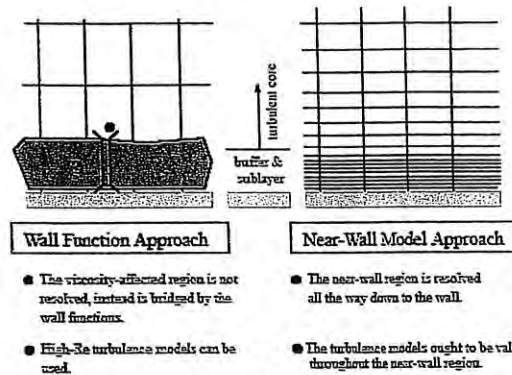


Figure 12.10.2: Near-Wall Treatments in FLUENT

In most high-Reynolds-number flows, the wall function approach substantially saves computational resources, because the viscosity-affected near-wall region, in which the solution variables change most rapidly, does not need to be resolved. The wall function approach is popular because it is economical, robust, and reasonably accurate. It is a practical option for the near-wall treatments for industrial flow simulations.

The wall function approach, however, is inadequate in situations where the low-Reynolds-number effects are pervasive in the flow domain in question, and the hypotheses underlying the wall functions cease to be valid. Such situations require near-wall models that are valid in the viscosity-affected region and accordingly integrable all the way to the wall.

FLUENT provides both the wall function approach and the near-wall modeling approach.

Wall Functions

Wall functions are a collection of semi-empirical formulas and functions that in effect "bridge" or "link" the solution variables at the near-wall cells and the corresponding quantities on the wall. The wall functions comprise

- laws-of-the-wall for mean velocity and temperature (or other scalars)
- formulas for near-wall turbulent quantities

Depending on the turbulent model you choose, FLUENT offers three to four choices of wall function approaches:

- **Standard Wall Functions**
- Non-Equilibrium Wall Functions
- Enhanced Wall Treatment
- User-Defined Wall Functions

19 35

12.10.2 Standard Wall Functions

The standard wall functions in FLUENT are based on the proposal of Launder and Spalding [197], and have been most widely used for industrial flows. They are provided as a default option in FLUENT.

Momentum

The law-of-the-wall for mean velocity yields

$$(a) \quad U^* = \frac{1}{\kappa} \ln(Ey^*) \quad (12.10-1)$$

where

$$U^* \equiv \frac{U_P C_\mu^{1/4} k_P^{1/2}}{\tau_w / \rho} \quad (12.10-2)$$

$$y^* \equiv \frac{\rho C_\mu^{1/4} k_P^{1/2} y_P}{\mu}$$

- and κ = von Kármán constant (= 0.4187)
- E = empirical constant (= 9.793)
- U_P = mean velocity of the fluid at point P
- k_P = turbulence kinetic energy at point P
- y_P = distance from point P to the wall
- μ = dynamic viscosity of the fluid

The logarithmic law for mean velocity is known to be valid for $30 < y^* < 300$. In FLUENT, the log-law is employed when $y^* > 11.225$.

When the mesh is such that $y^* < 11.225$ at the wall-adjacent cells, FLUENT applies the laminar stress-strain relationship that can be written as

$$(b) \quad U^* = y^* \quad (12.10-4)$$

It should be noted that, in FLUENT, the laws-of-the-wall for mean velocity and temperature are based on the wall unit, y^* , rather than y^+ ($\equiv \rho u_\tau y / \mu$). These quantities are approximately equal in equilibrium turbulent boundary layers.

Turbulence

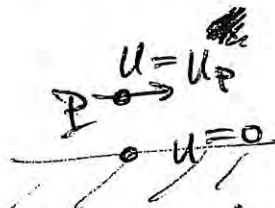
In the k - ϵ models and in the RSM (if the option to obtain wall boundary conditions from the k equation is enabled), the k equation is solved in the whole domain including the wall-adjacent cells. The boundary condition for k imposed at the wall is

$$\frac{\partial k}{\partial n} = 0$$

do not need k near wall
(12.10-9)

where n is the local coordinate normal to the wall.

$$y^* \sim k^{1/2} y \rightarrow U^*$$



1) compute k_P from below
(12.10-3)

2) for grid nearest wall, compute y^* plug into either (a) or (b) to get U^*

3) compute U_P using 12.10-2

U_P = mean velocity at P
(need τ_w)

$$\tau_w = \mu \frac{\partial u}{\partial y} = \mu \frac{U_P}{y}$$

gives closed set of wall b.c.
Code will converge
do you get correct drag?
constants set to give correct drag on flat plate

The production of kinetic energy, G_k , and its dissipation rate, ϵ , at the wall-adjacent cells, which are the source terms in the k equation, are computed on the basis of the local equilibrium hypothesis. Under this assumption, the production of k and its dissipation rate are assumed to be equal in the wall-adjacent control volume.

Thus, the production of k is computed from

$$G_k \approx \tau_w \frac{\partial U}{\partial y} = \tau_w \frac{\tau_w}{\kappa \rho C_\mu^{1/4} k_P^{1/2} y_P} \quad (12.10-10)$$

and ϵ is computed from

need ϵ on walls

$$\epsilon_P = \frac{C_\mu^{3/4} k_P^{3/2}}{\kappa y_P} \quad (12.10-11)$$

The ϵ equation is not solved at the wall-adjacent cells, but instead is computed using Equation 12.10-11. ω and Reynolds stress equations are solved as detailed in Sections 12.5.3 and 12.7.9, respectively.

Note that, as shown here, the wall boundary conditions for the solution variables, including mean velocity, temperature, species concentration, k , and ϵ , are all taken care of by the wall functions. Therefore, you do not need to be concerned about the boundary conditions at the walls.

The standard wall functions described so far are provided as a default option in FLUENT. The standard wall functions work reasonably well for a broad range of wall-bounded flows. However, they tend to become less reliable when the flow situations depart too much from the ideal conditions that are assumed in their derivation. Among others, the constant-shear and local equilibrium hypotheses are the ones that most restrict the universality of the standard wall functions. Accordingly, when the near-wall flows are subjected to severe pressure gradients, and when the flows are in strong non-equilibrium, the quality of the predictions is likely to be compromised.

Placement of The First Grid Point

- ◆ For standard or non-equilibrium wall functions, each wall-adjacent cell centroid should be located within the log-law layer $y_p^+ \approx 30 - 300$
- ◆ For enhanced wall treatment (EWT), each wall-adjacent cell centroid should be located within the viscous sublayer $y_p^+ \approx 1$
 - EWT can automatically accommodate cells placed in the log-law layer
- ◆ How to estimate the size of wall-adjacent cells before creating the grid:

$$y_p^+ = \frac{y_p u_\tau}{\nu} \Rightarrow y_p = \frac{y_p^+ \nu}{u_\tau} \quad U_\tau = \sqrt{\frac{\tau_w}{\rho}} = U_e \sqrt{\frac{\bar{C}_f}{2}}$$

- The skin friction coefficient can be estimated from empirical correlations:

$$\text{Flat plate: } \frac{\bar{C}_f}{2} \approx \frac{0.037}{\text{Re}_L^{1/5}} \quad \text{Duct: } \frac{\bar{C}_f}{2} \approx \frac{0.039}{\text{Re}_{D_h}^{1/4}}$$

- ◆ Use postprocessing tools (XY plot or contour plot) to double check the near-wall grid placement after the flow pattern has been established.

Near-Wall Modeling: Recommended Strategy

- ◆ Use standard or non-equilibrium wall functions for most high Reynolds number applications ($Re > 10^6$) for which you cannot afford to resolve the viscous sublayer.
 - There is little gain from resolving the viscous sublayer. The choice of core turbulence model is more important.
 - Use non-equilibrium wall functions for mildly separating, reattaching, or impinging flows.
- ◆ You may consider using enhanced wall treatment if:
 - The characteristic Reynolds number is low or if near wall characteristics need to be resolved.
 - The physics and near-wall mesh of the case is such that y^+ is likely to vary significantly over a wide portion of the wall region.
- ◆ Try to make the mesh either coarse or fine enough to avoid placing the wall-adjacent cells in the buffer layer ($5 < y^+ < 30$).

Inlet and Outlet Boundary Conditions

- ◆ When turbulent flow enters a domain at inlets or outlets (backflow), boundary conditions for k , ε , ω and/or $\overline{u_i u_j}$ must be specified, depending on which turbulence model has been selected
- ◆ Four methods for directly or indirectly specifying turbulence parameters:
 - *Explicitly* input k , ε , ω , or
 - This is the only method that allows for profile definition.
 - See user's guide for the correct *scaling* relationships among them.
 - Turbulence intensity and length scale
 - Length scale is related to size of large eddies that contain most of energy.
 - ◆ For boundary layer flows: $l \approx 0.4 \delta_{99}$
 - ◆ For flows downstream of grid: $l \approx$ opening size
 - Turbulence intensity and hydraulic diameter
 - Ideally suited for internal (duct and pipe) flows
 - Turbulence intensity and turbulent viscosity ratio
 - For external flows: $1 < \mu_t/\mu < 10$
- ◆ Turbulence intensity depends on upstream conditions: $I = \frac{u'}{U} \approx \frac{1}{U} \sqrt{\frac{2k}{3}} < 20\%$
- ◆ Stochastic inlet boundary conditions for LES and RANS can be generated by using spectral synthesizer or vortex method

GUI for Turbulence Models

Viscous Model

Model

- Inviscid
- Laminar
- Spalart-Allmaras (1 eqn)
- k-epsilon (2 eqn)
- k-omega (2 eqn)
- Reynolds Stress (5 eqn)

k-epsilon Model

- Standard
- RNG
- Realizable

RNG Options

- Differential Viscosity Model

Near-Wall Treatment

- Standard Wall Functions
- Non-Equilibrium Wall Functions
- Enhanced Wall Treatment
- User-Defined Wall Functions

Enhanced Wall Treatment Options

- Pressure Gradient Effects
- Thermal Effects

Options

- Viscous Heating

Model Constants

Cmu: 0.0845

C1-Epsilon: 1.42

C2-Epsilon: 1.68

Wall Prandtl Number: 0.85

User-Defined Functions

Turbulent Viscosity: none

Velocity Inlet

Zone Name: inlet

Momentum | Thermal | Radiation | Species | DPM | Multiphase | UDS

Velocity Specification Method: Components

Reference Frame: Absolute

X-Velocity (m/s): 5 constant

Y-Velocity (m/s): 1.6 constant

Turbulence

Specification Method: **K and Epsilon**

Turbulent Kinetic Energy (m2/s2): K and Epsilon

Turbulent Dissipation Rate (m2/s3): Intensity and Length Scale, Intensity and Viscosity Ratio, Intensity and Hydraulic Diameter

Navigation: Define → Models → Viscous...
 Define → Boundary Conditions...

3-91

Limitations of FLUENT - RANS - non-premixed

1.) does not separate large + small scale turbulence (LES does!)
large scale = geometry dependant, general modeling assumptions not good for complex geometries

- OK for jets, wall b.l.'s

- not OK for recirculation separation
complex corners, etc

small scale turbulence - nearly indep of geometry

so LES submodels for small scale mixing are OK

2.) not used for non-stationary turbulence $\frac{\partial \bar{u}}{\partial t} \neq 0$

- IC engines, vortex shedding from wakes, corner flow separation, acoustic instabilities, flow dynamics (valve closing)

3.) limited to purely non-premixed, cannot do lifted jet flame, highly swirled = PPC

4.) "curve fits" constants measured in jets + b.l. do not apply to complex flow - rotating turbine blade
assume isotropic turb., assume gradient diffusion
poor result for separation, swirl

5.) do not reveal new physics - not a science tool.
only an engineering curvefit that says some
conservation eqns do results look "good"

6.) complex geometries have multiple length scales

very thin sheet of fuel $\nu_T = u' L_x$
very large dia. air
vehicles have both
7.) laminar & turbulent b.l.s - difficult

these are two
 L_x values!

Advantages of RANS

1.) used in industry - "calibrate" the constants +
only consider geometries close to "calibrated"
case = interpolate between two expt. cases,
cannot extrapolate to new situations

2.) very rapid solns for complex geometries

3.) ~~easy to~~ short learning curve - people are promoted +
others come in to run code in few days

4.) always converges! bugs have been fixed

5.) many terms in eqns have been expt'ly
validated from expts (not all)

6.) get good physical understanding from simple
terms for turb. production
+ dissipation

Limitations

2. \therefore k- ϵ cannot accurately do recirculation, swirl, NO, CO
3. shape of PDF is assumed - but results are sensitive to this assumption
4. never considers physics of flame-vortex stretching of flame surface local extinction
5. cannot do partially-premixed
 - LES + G eqn. compute an interface - can put premixed or non premixed conditions on interface
6. unsteadiness affects mean properties
 - vortex shedding in bluff body wake - affects mean profiles. k- ϵ does not consider it
7. is assumed PDF shape correct for all problems? No
8. soln. depends on initial values of k, ϵ
9. still problems predicting NOx, soot CO, OK
10. small flame blowout - cannot predict
11. is formula for X_s accurate? $V_T = \text{accurate?}$

3-45

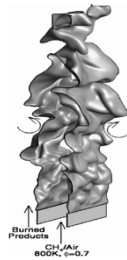
~~3-47~~
~~3-48~~
~~3-49~~

Wednesday: Non-premixed and Premixed Flames

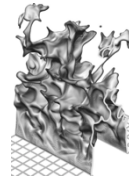
Turbulent Combustion

Experiments and Fundamental Models

J. F. Driscoll, University of Michigan



R. Sankaran,
E. Hawkes,
Jackie Chen
T. Lu, C. K. Law
premixed



Bell, Day,
Driscoll
"corrugated"
premixed



Copyright ©2016 by James F. Driscoll. This material is not to be sold, reproduced or distributed without prior written permission of the owner, James F. Driscoll



1

Outline for the week

Mon: **Physical concepts** faster mixing, faster propagation, optimize liftoff, flame surface density, reaction rate, PDF

Tues: **Kilohertz PLIF, PIV measurements of flame structure** - to assess models

Wed: **Non-Premixed and Premixed flames** - measurements, models
gas turbine example

Thurs: **Partially premixed flames** - and some examples

Fri: **Future challenges:** Combustion Instabilities (Growl) , Extinction



2

Best models of non-premixed turbulent flames

1. SSLF = steady strained laminar flamelet - Z & dissip rate (Peters, Pitsch)
2. FPV = flamelet progress variable – Z, c variables,
no dissip rate (Moin)
3. PDF = method of Pope – parcels mix, mixing time eqn, Langevin eqn
4. CMC = Conditional Moment Closure – Bilger
5. LEM = Linear Eddy Model – Kerstein, Menon



3

Non-premixed turbulent Jet Flame – closure for unstrained flamelets

See Lockwood and Naguib, Comb. Flame 24, 109

8 unknowns, 8 equations

\bar{u} from x - mom eqn

\bar{v} from continuity eqn

$\bar{Z} = \bar{f}$ from \bar{f} eqn = \bar{Z} eqn

$\tilde{g} = \overline{f'^2}$ = variance of f

k from k - eqn

ϵ from epsilon eqn

$\bar{\rho}$ from state relation

p = constant, assumed

$$\rho u \frac{\partial \bar{u}}{\partial x} + \rho v \frac{\partial \bar{u}}{\partial r} = \frac{1}{r} \frac{\partial}{\partial r} (r \mu_t \frac{\partial \bar{u}}{\partial r}) \quad \text{X - momentum}$$

$$\rho u \frac{\partial \bar{f}}{\partial x} + \rho v \frac{\partial \bar{f}}{\partial r} = \frac{1}{r} \frac{\partial}{\partial r} (r \frac{\mu_t}{\sigma_f} \frac{\partial \bar{f}}{\partial r}) \quad \text{f - eqn}$$

$$\rho u \frac{\partial k}{\partial x} + \rho v \frac{\partial k}{\partial r} = \frac{1}{r} \frac{\partial}{\partial r} \left(r \frac{\mu_t}{\sigma_k} \frac{\partial k}{\partial r} \right) + \mu_t \left(\frac{\partial \bar{u}}{\partial y} \right)^2$$

$$-C_D \frac{\rho^2 k^2}{\mu_t} + g C_\rho \frac{\mu_t}{\sigma_\rho} \frac{\partial \rho}{\partial x} \quad \text{k equation}$$



4

$$\rho u \frac{\partial \epsilon}{\partial x} + \rho v \frac{\partial \epsilon}{\partial y} = \frac{1}{r} \frac{\partial}{\partial r} \left(r \frac{\mu_t}{\sigma_\epsilon} \frac{\partial \epsilon}{\partial r} \right) + C_{\epsilon_1} C_D \rho k \left(\frac{\partial u}{\partial y} \right)^2 - \frac{C_{\epsilon_2}}{C_D} \rho \frac{\epsilon^2}{k}$$


epsilon equation

$$\rho u \frac{\partial g}{\partial x} + \rho v \frac{\partial g}{\partial r} = \frac{1}{r} \frac{\partial}{\partial r} \left(\frac{r \mu_t}{\sigma_g} \frac{\partial g}{\partial r} \right) + C_{g_1} \mu_t \left(\frac{\partial \bar{f}}{\partial y} \right)^2 - \frac{C_{g_2}}{C_D} \rho \epsilon g$$

g – equation

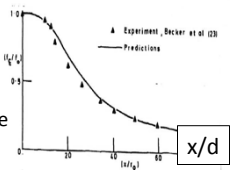
$$\mu_t = C_D \rho \frac{k^2}{\epsilon}$$

Turbulent viscosity

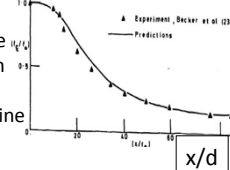

5

FLUENT –type of RANS solutions – Lockwood and Naguib, Comb Flame 24, 109

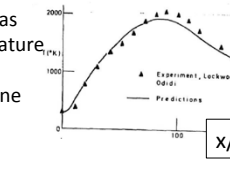
Mean Velocity On jet centerline



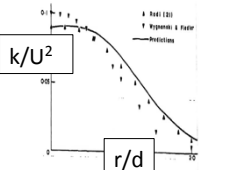
Mixture fraction On jet centerline




Mean gas temperature On jet centerline



k/U² vs r/d



Problem – need to add **strained** flamelets = scalar dissipation rate
To correctly predict temperature, NOx, CO

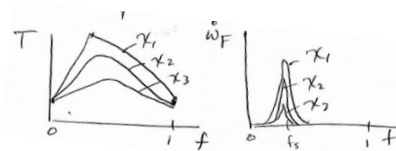

6

Non-premixed flames - add strained flamelets - Peters

Flamelet lookup tables –
solve strained
counterflow flame

Scalar
Dissipation rate

$$\chi = 2 D \left[\overline{\left(\frac{\partial Z}{\partial x}\right)^2} + \overline{\left(\frac{\partial Z}{\partial y}\right)^2} + \overline{\left(\frac{\partial Z}{\partial z}\right)^2} \right]$$



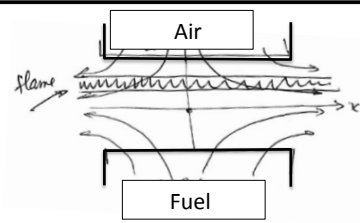
State relations =
solutions to the strained flamelet
equations with complex chemistry

Two variables are mixture fraction and
Scalar dissipation rate



7

Counter flow non-premixed flame (Peters)



$$\frac{\partial u}{\partial x} + \frac{\partial v}{\partial y} = 0 \quad \text{So: } u = \epsilon x; \quad v = -\epsilon y$$

$$\rho u \frac{dZ}{dx} + \rho v \frac{dZ}{dy} = \rho D \frac{d^2 Z}{dy^2} \quad \text{so}$$

$$(\epsilon x) [0] + (-\epsilon y) \frac{dZ}{dy} = D \frac{d^2 Z}{dy^2}$$

$$\text{so: } (-\epsilon y) \frac{dZ}{dy} = D \frac{d^2 Z}{dy^2}$$

Assume:

Laminar flow, fast chemistry
For simplicity, assume constant density
Velocity not disturbed by heat release
All species diffuse at same diffusivity D
Lewis number = 1, $D = \text{constant}$
Scalars only vary in the y (vertical) direction

$$\text{b.c.: } y = \infty, Z = 0, \quad y = -\infty, Z = 1$$



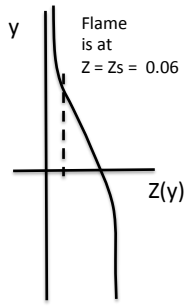
8

Solution to this equation is:

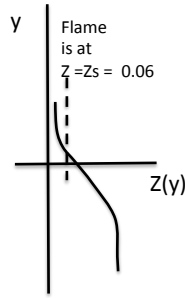
$$Z(y) = \frac{1}{2} - \frac{1}{2} \operatorname{erf} \left(\frac{y}{\sqrt{2D/\epsilon}} \right)$$

Scalar dissipation rate:

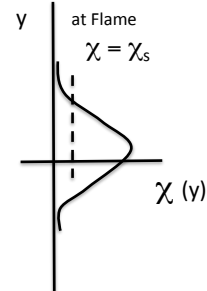
$$\chi = 2D \left[\left(\frac{\partial Z}{\partial x} \right)^2 + \left(\frac{\partial Z}{\partial y} \right)^2 + \left(\frac{\partial Z}{\partial z} \right)^2 \right]$$



For low strain rate ϵ



For high strain rate ϵ
Larger gradient



at Flame $\chi = \chi_s$
 $\chi_s = \text{constant} \cdot \epsilon$



What is flame location ($y = y_f$) ?

In solution for Z, set $Z = Z_s$ and solve for y

$$y_f = \sqrt{\frac{2D}{\epsilon}} \operatorname{erf}^{-1} (1 - 2f_s)$$

Flame location

Flame location:

Increasing $D \rightarrow y_f$ increases

Increasing ϵ or $f_s \rightarrow y_f$ decreases



Strength of a strained non-premixed counterflow flame

Strength of a non-premixed flame = mass flux of fuel at flame boundary

= J_F = mass of fuel consumed /sec per unit flame area

$$J_F = - \rho_F D \frac{\partial Y_F}{\partial y} \quad \text{Ficke's Law}$$

Use our state relation that says that Y_f is proportional to Z on the fuel side of flame

Take the derivative of the erf function formula for $Z(y)$

Plug in our formula for $y = y_f$ at the flame front to get:

$$J_F = \rho_F D^{1/2} \varepsilon^{1/2} \cdot \text{constant}$$

Stronger flame if strain rate ε is made larger



11

How is scalar dissipation rate χ_s related to strain rate ε ?

Define scalar dissipation rate

$$\chi = 2 D \left[\left(\frac{\partial Z}{\partial y} \right)^2 \right]$$

Take the derivative of our erf function for $Z(y)$ and

Plug into this formula, and plug in $y =$ our formula for y_f at flame surface, to get:

$$\chi_s = \varepsilon A \quad \text{where: } A = 4 Z_s^2 [\text{erfc}^{-1}(2 Z_s)]^2$$

So the scalar gradient is related to velocity gradient

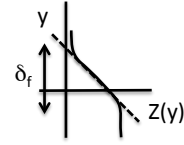


12

What is the thickness (δ_f) of a strained non-premixed flame ?

Define the thickness of a non-premixed flame to be:

$$\delta_f = \left(\frac{\partial Z}{\partial y} \right)^{-1}_{y=y_f}$$



Take the derivative of our erf function for $Z(y)$ and plug in our formula for y_f to get:

$$\delta_f = \sqrt{\frac{2D}{\chi_s}}$$

Flame gets thinner as you apply more strain

Example: if $D = 1.0 \text{ cm}^2/\text{s}$ = gas diffusivity near flame

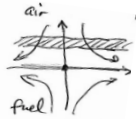
if dissipation rate $\chi_s = 100 \text{ s}^{-1}$

Then flame thickness: $\delta_f = 1.4 \text{ mm}$



13

Flamelet assumption - of Peters adds strain to allow deviations from equilibrium chemistry



instantaneous T, Y_i are related to mixture fraction and dissipation rate in a turbulent flame in the same way they are related in a laminar counterflow flame with full chemistry

Steady non-premixed strained flamelet equation:

$$\rho \frac{\partial Y_i}{\partial t} = \frac{1}{2} \rho \chi \frac{\partial^2 Y_i}{\partial f^2} + \dot{w}_i$$

$$\bar{\chi}_s = C_\chi \left(\frac{\epsilon g}{\rho} \right)$$

Solution yields state relations for all mass fractions, temperature, density as functions of Mixture fraction and Scalar dissipation rate

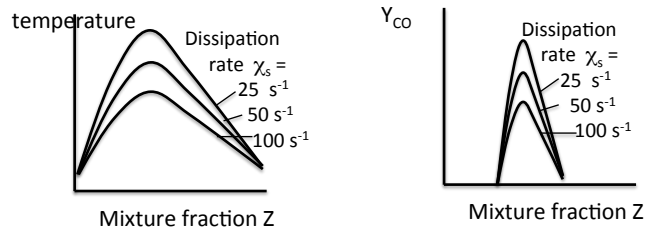
Now plug state relations into this to get mean values of temperature, density, mass fractions

$$\bar{Y}_{CO} (\bar{Z}, \bar{Z}'^2, \bar{\chi}, \bar{\chi}'^2) = \int_0^1 Y_{CO}(Z, \chi) P_1(Z, \bar{Z}, \bar{Z}'^2) P_2(\chi, \bar{\chi}, \bar{\chi}'^2) d\chi dZ$$



14

State relations - for a **strained** non-premixed counter flow laminar flamelet



Generate plots above using CHEMKIN counter flow non-premixed flame solver

Larger velocity gradient (strain rate) = larger scalar gradient (scalar dissipation rate)

Larger dissipation rate \rightarrow lowers the peak temperature,
alters the mass fractions of the species
reduces the chemical reaction rate until extinction occurs
improves prediction of CO, temperature, etc.



15

What is the goal of comparing model results to experiments ?

Many models with very different assumptions all "agree" with measurements

Is there any point in comparing output of models without assessing the basic assumptions in the model; i.e., do thin strained flamelets occur in the expt ?

If models agree to within 5%, is there any point to work for better agreement ?

Do we need to include heat losses, complex chemistry, acoustics, pressure ?

Are computations really independent of b.c.s, initial condition, grid size ?

Is the goal to identify the "best" model, or can we live with 20 models ?

How useful are models that do not solve the Navier Stokes eqns ? Some replace NS with Langevin eqn, ad-hoc mixing models, etc. ?



16

How are we doing ? How well are we making measurements and how well do models compare ?

Review of some good papers - in turbulent combustion

Barlow, R. S., Frank, J. H., A. N. Karpetis, and Chen, J.-Y., "Piloted Methane/Air Jet Flames: Scalar Structure and Transport Effects," *Combust. Flame* 143:433-449 (2005)

C. Hasse, "LES flamelet-progress variable modeling and measurements of a turbulent partially-premixed dimethyl ether jet flame" *Comb Flame* 162, 3016

Steinberg, A., Meier, W. et al., Effects of Flow Structure Dynamics on Thermoacoustic Instabilities in Swirl-Stabilized Combustion, *AIAA J.* 50, p. 952.



17

Good Models and measurements of non-premixed turbulent combustion

See TNF website <http://www.sandia.gov/TNF/>

Single point Raman/Rayleigh/LIF data for f, T, N₂, O₂, CH₄, CO₂, H₂O, H₂, CO, OH, NO and velocity

Experimental data:

Barlow, R. S., Frank, J. H., A. N. Karpetis, and Chen, J.-Y., "Piloted Methane/Air Jet Flames: Scalar Structure and Transport Effects," *Combust. Flame* 143:433-449 (2005).

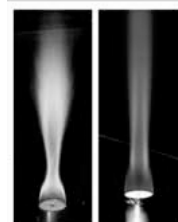
Masri, A., Dibble, R., Barlow, R., Structure of Turbulent Nonpremixed Flames Revealed by Raman-Rayleigh-LIF Measurements', *Prog. Energy Combust. Sci.*, 22:307-362 (1997).

Models

LES- FPV (flamelet progress variable) C. Hasse from Freiberg –Z and C transport eqns (mixture fraction and progress variable)

CMC model: Kronenberg, Stuttgart

PDF model: Pope, Cornell



18

Barlow: Non-premixed piloted jet flame in Comb Flame 143, 433 and

TNF website <http://www.sandia.gov/TNF/>
"Piloted methane/air jet flames: Transport effects
and aspects of scalar structure"

Single point Raman/Rayleigh/LIF measurements of
f, T, N₂, O₂, CH₄, CO₂, H₂O, H₂, CO, OH, NO, velocity,
line Raman for scalar dissipation rate:

$$\chi = 2D \left[\overline{\left(\frac{\partial Z}{\partial x}\right)^2} + \overline{\left(\frac{\partial Z}{\partial y}\right)^2} + \overline{\left(\frac{\partial Z}{\partial z}\right)^2} \right]$$

Lasers for Raman, Rayleigh: Nd:YAG at 532 nm
Lasers for LIF = Nd:YAG + dye: 282 nm for OH, 226 nm
For NO, 230 nm for CO (two photon)

Spatial resolution = 0.75 mm
Fluorescence signals were corrected for Boltzmann
fraction and collisional quenching rate



Sandia flame D
Jet diam. = 7.2 mm
Pilot dia = 18.2 mm
Jet U = 50 m/s
Coflow U = 0.9 m/s



19

Barlow: Non-premixed jet flame

in Comb Flame 143, 433

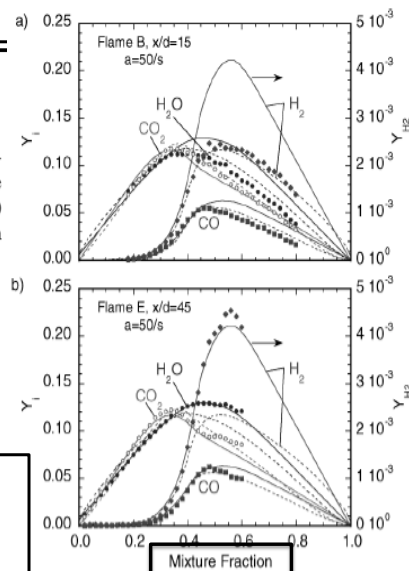
Fig. 1. Measured conditional means of species mass fractions (symbols) compared with laminar opposed-flow flame calculations including full molecular transport (dashed lines) or equal diffusivities (solid lines). Measurements are shown for (a) flame B at $x/d = 15$ and (b) flame E at $x/d = 45$.

Data points = turbulent jet flame,

Agree w steady laminar counterflow
CHEMKIN = state relations computed
for strain parameter $2 U_{oc}/R = 50 \text{ s}^{-1}$

Conclude: steady flamelet state relations

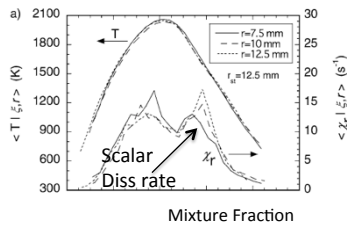
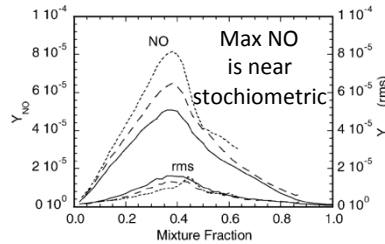
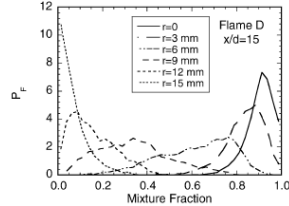
- Adequate for CO & major species
- Not adequate for H₂ or NO
- Differential diffusion is negligible



20

More Barlow measurements in turbulent non-premixed jet flames

PDF of mixture fraction is a Beta function



Barlow concludes: all important single point properties were measured in 5 piloted jet non-premixed flames, to be used to assess models



SLF = Steady laminar flamelet LES model of Sandia Flame D by Janicka

Investigation of length scales, scalar dissipation, and flame orientation in a piloted diffusion flame by LES, A. Kempf J. Janicka PROCI 30 557

Mixture fraction (Z) conservation eqn

$$\bar{\rho} \tilde{u} \frac{d\bar{Z}}{dx} + \bar{\rho} \tilde{v} \frac{d\bar{Z}}{dy} = \bar{\rho} D \frac{d^2 \bar{Z}}{dy^2}$$

State relations from solutions to steady counter flow flamelet eqn

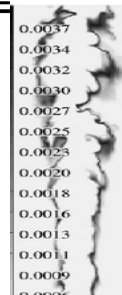
Mean mix fraction in subgrid = prop. to resolved scale gradients of Z

Variance of subgrid diss. rate = prop. to resolved scale gradients

Assume a Beta function for P(Z), log-normal for P(chi). Mean quantities from:

$$\bar{Y}_{CO}(\bar{Z}, \overline{Z'^2}, \bar{\chi}, \overline{\chi'^2}) = \int_0^1 Y_{CO}(Z, \chi) P_1(Z, \bar{Z}, \overline{Z'^2}) P_2(\chi, \bar{\chi}, \overline{\chi'^2}) d\chi dZ$$

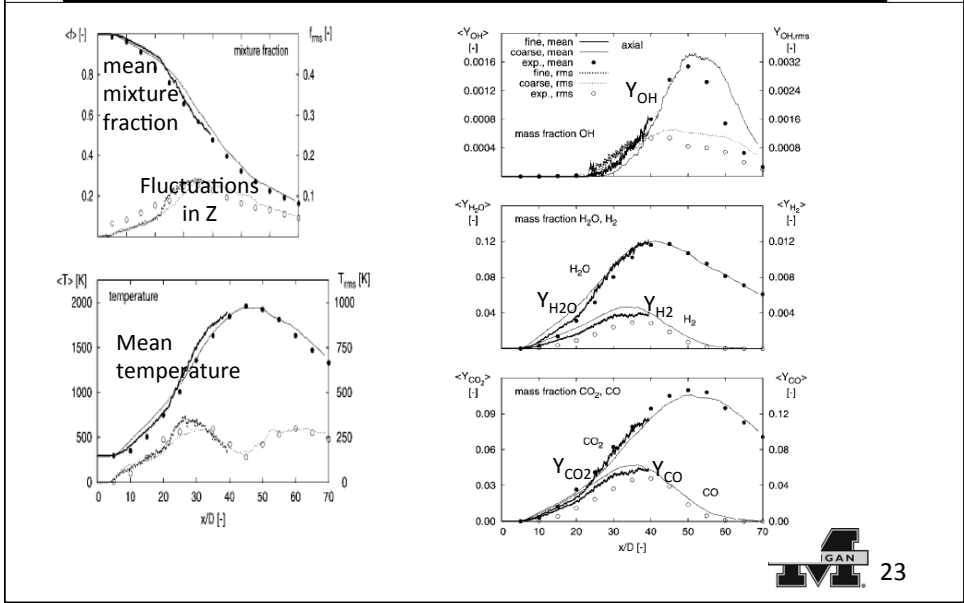
state relation PDF



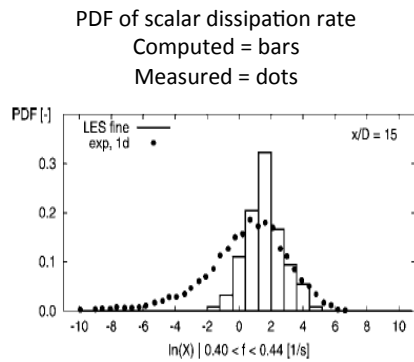
LES of Sandia flame D



Janicka - SLF steady laminar flamelet model of Sandia Jet Flame D, PROCI 30 557



Janicka SLF LES, continued



Conclude: the steady laminar flamelet LES adequately simulates

the non-premixed combustion in Sandia jet flame D

except for H2 and CO on the fuel rich side – it is a little off

Fig. 9. The PDF of the resolved scalar dissipation rate. This quantity is expected to be log-normally distributed. Comparison of LES-data (1d) to experimental 1d-data.

Flamelet progress variable (FPV-LES) model - compared to Barlow's measurements in a non-premixed jet flame

C. Hasse, "LES flamelet-progress variable modeling and measurements of a turbulent partially-premixed dimethyl ether jet flame" Comb Flame 162, 3016

$$\frac{\partial}{\partial t} (\bar{\rho} \tilde{Z}) + \nabla \cdot (\bar{\rho} \tilde{\mathbf{u}} \tilde{Z}) = \nabla \cdot \left[\left(\bar{\rho} D_z + \frac{\mu_t}{Sc_t} \right) \nabla \tilde{Z} \right]$$

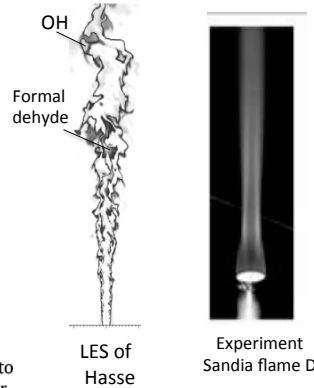
$$\tilde{Z}''^2 = C_{\tilde{Z}} \Delta^2 |\nabla \tilde{Z}|^2$$

Replace scalar dissipation rate with a new progress variable Y_c

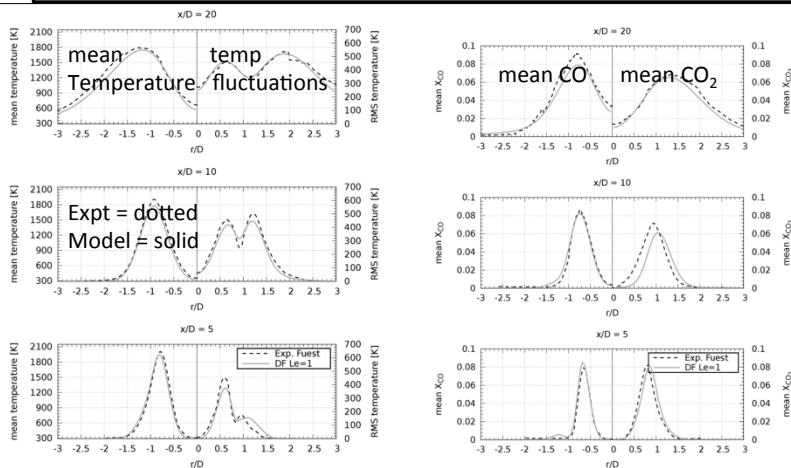
Progress variable: $Y_c = Y_{H_2} + Y_{H_2O} + Y_{CO} + Y_{CO_2}$

$$\frac{\partial}{\partial t} (\bar{\rho} \tilde{Y}_c) + \nabla \cdot (\bar{\rho} \tilde{\mathbf{u}} \tilde{Y}_c) = \nabla \cdot \left[\left(\bar{\rho} D_{Y_c} + \frac{\mu_t}{Sc_t} \right) \nabla \tilde{Y}_c \right] + \bar{\omega}_{Y_c}$$

A presumed β -shaped filtered density function (PDF) is used to integrate the mixture fraction, and a δ -PDF is applied for the normalized progress variable to account for non-resolved fluctuations. Using a δ -PDF means that no subgrid closure is employed for the normalized progress variable. For the integration process, the nor-



LES – FPV model of Hasse (Frieberg) agrees with Sandia measurements

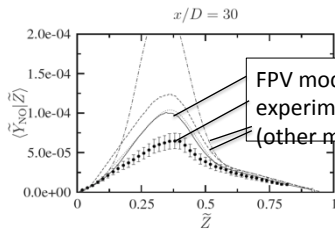


Conclude: the Flamelet Progress Variable (FPV) model gives good agreement with measurements for major species and CO. NO was not attempted



Nitric Oxide - predicted by FPV model compared to non-premixed jet experiment of Barlow

Ihme and Pitsch use FPV to predict NOx in jet flame and in a Pratt gas turbine

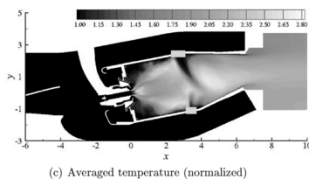


Flamelet progress variable LES overpredicts NO by 40% in a simple jet flame. Not too bad They included radiative heat loss.

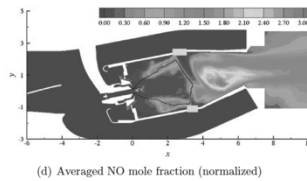
Ihme and Pitsch, Modeling of radiation and nitric oxide formation in turbulent non-pre Mixed flames using a flamelet/progress variable formulation, Phys Fluids 20, 055110



NO can be predicted with post-processing (easy)



(c) Averaged temperature (normalized)

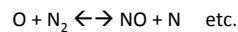


(d) Averaged NO mole fraction (normalized)

LES to compute temperature, Y_{N_2} and Y_{O_2} fields (means and variances)

NO is formed on long time scale so

$$\rho \tilde{D}_t Y_{NO} = \nabla \cdot (\rho \alpha \nabla Y_{NO}) + \rho \dot{\omega}_{NO}$$



State relation for ω_{NO} obtained from laminar flamelet eqn

$$\bar{\rho} \tilde{D}_t \tilde{Y}_{NO} = \nabla \cdot (\bar{\rho} \tilde{\alpha} \nabla \tilde{Y}_{NO}) + \nabla \cdot \tilde{\tau}_{NO}^{res} + \bar{\rho} \tilde{\omega}_{NO}$$

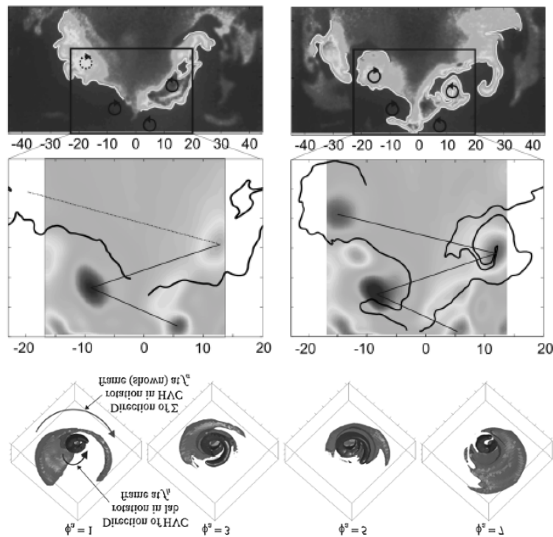
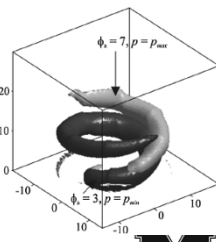
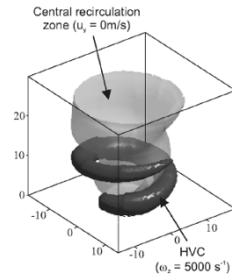
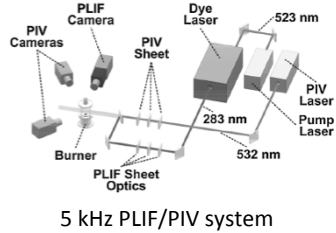
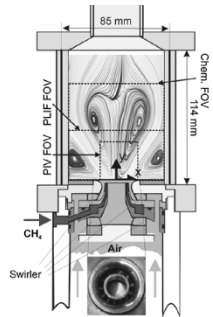
We already know T, Y_{O_2}, Y_{N_2} from resolved scale LES

Ihme and Pitsch, Modeling of radiation and nitric oxide formation in turbulent non-pre Mixed flames using a flamelet/progress variable formulation, Phys Fluids 20, 055110



A more complex problem: gas turbine-like swirl flame undergoing unsteady oscillations

Steinberg, A, Meier, W. et al., Effects of Flow Structure Dynamics on Thermoacoustic Instabilities in Swirl-Stabilized Combustion, AIAA J. 50, p. 952.



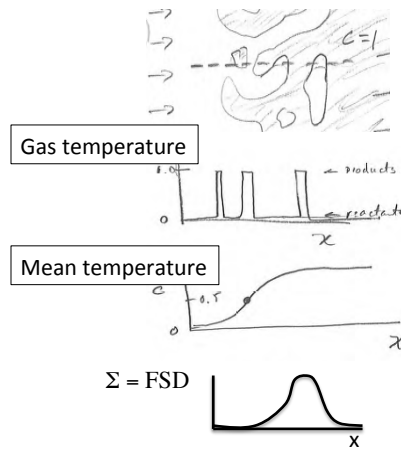
How well can we model premixed turbulent flames ?

Bray / FSD model

Assume thin or thickened wrinkled flamelets

fully premixed or stratified premixed, FSD model is being modified to handle partially-premixed

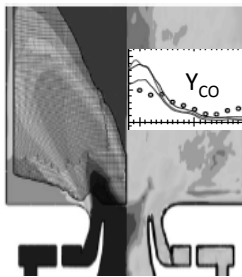
considers corrugated (pockets) flamelet merging stretch rate increases area



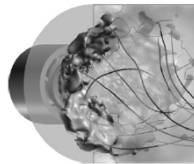
Masuya, Bray, Comb Sci Tech 25, 127



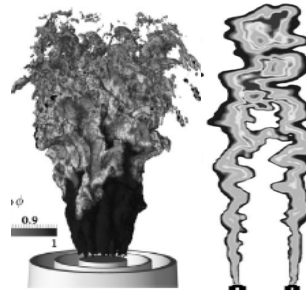
Who is using the Bray / FSD LES method ?



M. Ihme, Stanford U., Gas turbine combustor PROCI 35, 1225



Fureby, Sweden Gas Turbine Comb. PROCI 31, 3107



Veynante, Ecole C. Paris PROCI 35, 1259

Called F-TacLES = Flamelet tabulated chemistry LES



Reactedness = c is the fundamental parameter in premixed turbulent flames

$$C = \frac{T - T_R}{T_P - T_R} = 0 \text{ in reactants, } = 1 \text{ in products}$$

Since $\rho = p/RT$, it follows that inserting the above in for T yields:

$$\rho(c) = \rho_R (c \tau + 1)^{-1} \quad \text{where } \tau = (T_P/T_R - 1) = \text{approx. } 6 \text{ for typical flame}$$

This is called a state relation for gas density as a function of c : $\rho(c)$



33

Probability density function - used to define a mean value

$P(c) dc$ = probability that c lies in the range between $c - dc/2$ and $c + dc/2$

$$\bar{\rho}(\bar{c}, \overline{c'^2}) = \int_0^1 \rho(c) P(c, \bar{c}, \overline{c'^2}) dc$$

State relation:

$$\rho(c) = \rho_R (c \tau + 1)^{-1}$$

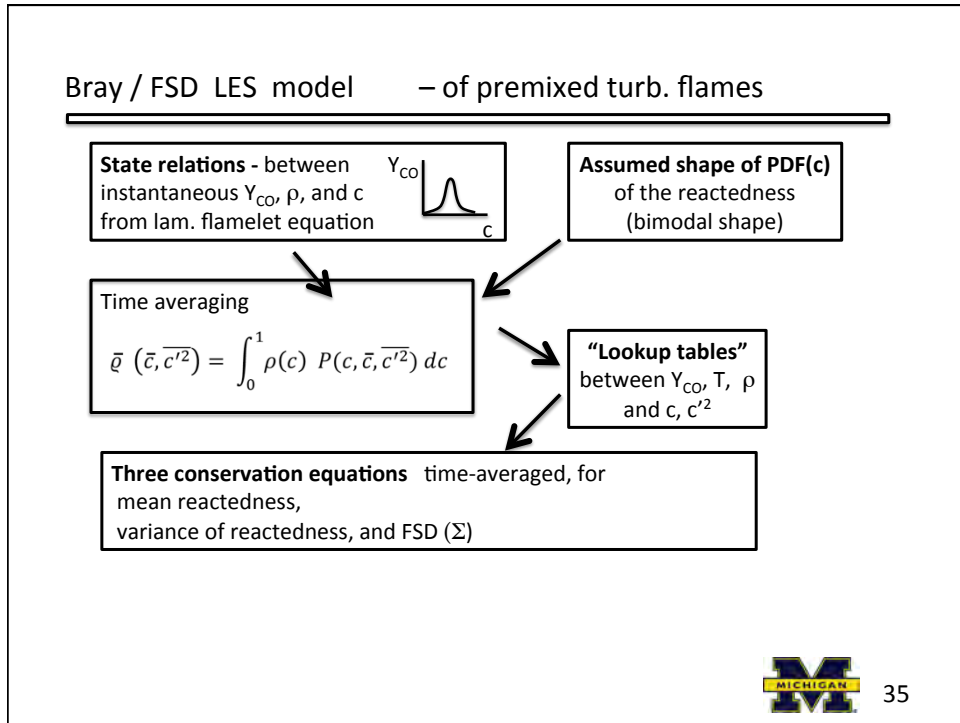


At each point in the flame, we solve conservation equations to get the mean \bar{c} , and variance $\overline{c'^2}$ and plug into above eqn to get mean density

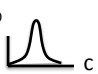
Idea: you only have to solve conservation equations for \bar{c} , and $\overline{c'^2}$ and use above integral to get other mean values; you avoid solving more conservation equations for each variable



34



State relations - between instantaneous Y_{CO} , ρ , etc. and c from lam. flamelet equation



c = reactedness
 Y_p = mass fraction products

Consider a 1-D, unstretched laminar premixed flame (see text by Law or Kuo, or solve using CHEMKIN)

$$\rho S_L \frac{dc}{dx} = \rho \alpha \frac{d^2 c}{dx^2} + \dot{\omega}_p$$

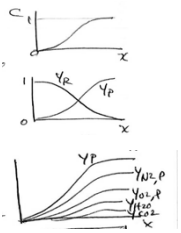
$$\rho S_L \frac{dY_p}{dx} = \rho \alpha \frac{d^2 Y_p}{dx^2} + \dot{\omega}_p$$

thus $c = \frac{T - T_R}{T_P - T_R} = Y_p$

and $Y_R = 1 - Y_p = 1 - c$


for $CH_4 + 2 O_2 + 2(79)/21 N_2 \rightarrow 2 H_2O + CO_2 + 2(79)/21 N_2$

show that $Y_{CH_4} = 0.062 Y_R = 0.062 (1-c)$ and $Y_{H_2O} = 0.12 Y_p = 0.12 c$

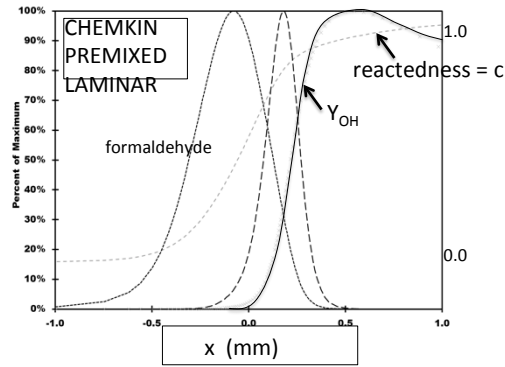


→ We only have to solve ONE equation (the top one) for $c(x)$ after we represent reaction rate of products $\dot{\omega}_p$ in terms of c and Y_R

→ From $c(x)$ we get $T(x)$, $\rho(x)$, $Y_R(x)$, $Y_p(x)$, $Y_{CH_4}(x)$, $Y_{H_2O}(x)$, etc.

 36

State relations: between Y_i, ρ, T and reactedness c



$$\bar{\rho}(\bar{c}, \bar{c}'^2) = \int_0^1 \rho(c) P(c, \bar{c}, \bar{c}'^2) dc$$



Conservation of mean reactedness

$$\frac{d}{dx} (\bar{\rho} \bar{u} \bar{c} + \overline{\rho u'' c''}) = \bar{w} = \rho_R (1-c) S_L \sum \text{reaction rate/area}$$

$\frac{d}{dx} (\bar{\rho} \bar{u} \bar{c} + \overline{\rho u'' c''})$: rate of temperature rise in x direction
 $\overline{\rho u'' c''}$: turbulent flux of temperature fluctuations
 \bar{w} : volumetric reaction rate kg/s of products /m³
 $\rho_R (1-c) S_L \sum$: reaction rate/area

Conservation of scalar flux

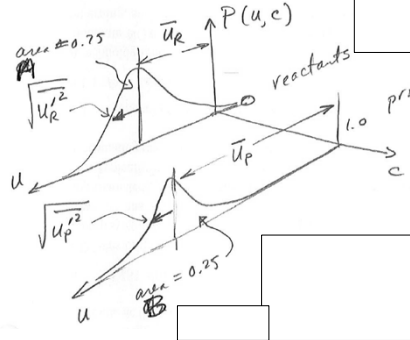
$$\frac{d}{dx} \left(\bar{\rho} \bar{u} \frac{\overline{\rho u'' c''}}{\bar{\rho}} + \overline{\rho u''^2 c''} \right) + \overline{\rho u'' c''} \frac{d\bar{u}}{dx} + \overline{\rho u''^2} \frac{d\bar{c}}{dx} = -\bar{c}'' \frac{d\bar{p}}{dx} + \overline{u'' w} - \bar{\chi}_{uc}$$

Goal: Two ODEs for the unknowns \tilde{c} and $\overline{\rho u'' c''}$



Bi - Modal PDF for a premixed flame (Bray)

$$P(u,c) = A(u) \delta(c) + B(u) \delta(1-c)$$



$\delta(c)$ is delta fcn centered at $c = 0$
 $\delta(1-c)$ is delta fcn centered at $c = 1$

A(u) and B(u) are Gaussian dist. of velocity

Areas under Gaussians $A + B = 1$

Mean of A(u) is mean velocity of reactants
 Variance of A(u) is variance of reactants

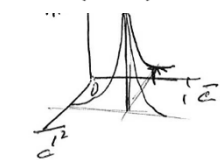
Mean of B(u) is mean velocity of products
 Variance of B(u) is variance of products



"Lookup tables"
 between Y_{H_2O}, T, ρ
 and
 $(\bar{c}, \overline{c'^2})$

$$\overline{Y_{CO_2}}(\bar{c}, \overline{c'^2}) = \int_0^1 Y_{CO_2}(c) P(c, \bar{c}, \overline{c'^2}) dc$$

$\overline{Y_{CO_2}}(\bar{c}, \overline{c'^2})$



Mean CO2 mass fraction depends only on two quantities that are computed at each (x,y,z) location using conservation equations for these two quantities

State relation
 Y_{CO_2} is a known fraction of Y_p which equals c



Relate all quantities in the two conservation equations to the two unknowns

Bimodal PDF: $P(c) = A \delta(c-0) + B \delta(c-1)$

\tilde{c} and $\overline{\rho u'' c''}$

example

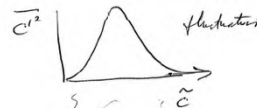
$$\overline{c'^2} = \overline{(c - \tilde{c})^2} = \int_0^1 (c - \tilde{c})^2 P(c) dc = (c - \tilde{c})^2 A \Big|_{c=0} + (c - \tilde{c})^2 B \Big|_{c=1}$$

$$= \tilde{c}^2 A + (1 - \tilde{c})^2 B \rightarrow \text{plug in } \tilde{c}, A, B \text{ formulas which are in terms of } \tilde{c}$$

$$= \frac{\tilde{c}^2 (\tau+1)^2 (1 - \tilde{c})}{(\tilde{c} \tau+1)^2 (\tilde{c} \tau+1)} + \frac{(\tilde{c})(\tau+1)}{(\tilde{c} \tau+1)} \frac{(1 - \tilde{c})^2}{(\tilde{c} \tau+1)^2}$$

$$\overline{c'^2} = \frac{\tilde{c} (1 - \tilde{c}) (\tau+1)}{(\tilde{c} \tau+1)^2}$$

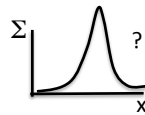
where $\tilde{c}=0$ pure reactants, $\overline{c'^2}=0$
 $\tilde{c}=1$ pure products, $\overline{c'^2}=0$



There are no fluctuations in reactivity or temperature in the pure reactants or in the pure products



Bray model closure – still have flame surface density Σ (x) in conservation eqn



Σ is proportional to turbulent reaction rate

Third conservation equation must be solved for FSD = Σ

$$\frac{d(\tilde{u} \Sigma)}{dx} - \frac{d}{dx} \left(\nu_T \frac{d\Sigma}{dx} \right) = K \Sigma - A \Sigma^2$$

Flame Surface Density Conservation Equation

mean stretch rate $K = (u' / L) \Gamma$ causes flame area to increase
 flamelet merging term $A \Sigma^2$ causes flame area to decrease

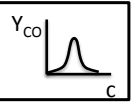
Final step:

specify correct boundary conditions and solve for $\tilde{u} = S_T$
 = turbulent burning velocity



Bray / FSD LES model – of premixed turb. flames

State relations - between instantaneous Y_{CO} , ρ , and c from lam. flamelet equation



Assumed shape of PDF(c) of the reactedness (bimodal shape)

Time averaging

$$\bar{\rho}(\bar{c}, \bar{c}'^2) = \int_0^1 \rho(c) P(c, \bar{c}, \bar{c}'^2) dc$$

“Lookup tables” between Y_{CO} , T , ρ and c , c'^2

Conservation equations time-averaged, for mean reactedness, turbulent flux of reactedness, flame surface density (Σ), is prop. to mean reaction rate

Bray / FSD model applied to premixed jet flame

Prasad and Gore Comb Flame 116,1

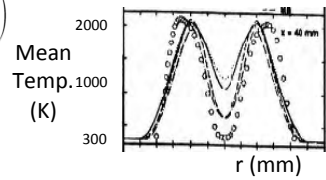
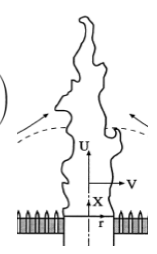
Mean Reactedness \bar{c} $\frac{\partial \bar{\rho} \bar{c}}{\partial t} + \frac{\partial \bar{\rho} \bar{u}_k \bar{c}}{\partial x_k} = \bar{w} + \frac{\partial}{\partial x_k} \left(\frac{\mu_t}{\sigma_r} \frac{\partial \bar{c}}{\partial x_k} \right)$

Flame Surface Density for Σ $\frac{\partial \Sigma}{\partial t} + \frac{\partial \bar{U}_i \Sigma}{\partial x_i} = S_1 + S_2 - D + \frac{\partial}{\partial x_i} \left(\frac{v_t}{\sigma_\Sigma} \frac{\partial \Sigma}{\partial x_i} \right)$

Axial mom. For \bar{u} $\frac{\partial \bar{\rho} \bar{u}^2 r}{\partial x} + \frac{\partial \bar{\rho} \bar{u} \bar{v} r}{\partial r} = r g (\rho_\infty - \bar{\rho}) + \frac{\partial}{\partial r} \left(r \mu_t \frac{\partial \bar{u}}{\partial r} \right)$

Continuity For \bar{v} $\frac{\partial \bar{\rho} \bar{u} r}{\partial x} + \frac{\partial \bar{\rho} \bar{v} r}{\partial r} = 0$

TKE for k, ϵ $\frac{\partial \bar{\rho} \bar{u} \bar{\varphi} r}{\partial x} + \frac{\partial \bar{\rho} \bar{v} \bar{\varphi} r}{\partial r} = r S_\varphi + \frac{\partial}{\partial r} \left(r \frac{\mu_t}{\sigma_\varphi} \frac{\partial \bar{\varphi}}{\partial r} \right)$



Conclude: model predicts correct flame height and turbulent burning velocity (if appropriate constants are selected !)

F-TacLES is Multi-variable approach - for stratified premixed

Filtered TABulated Chemistry for LES (F-TACLES)

Consider a “stratified” premixed flame - equivalence ratio varies in the reactants

Define Z = mixture fraction = mass fraction of H atoms at a point

Ex. If mixture is $\text{CH}_4 + \frac{1}{2} \text{H}_2\text{O}$ then $Z = 5 / (16 + 9) = 0.2$

$$\begin{aligned} & \bar{Y}_{CO}(\bar{c}, \overline{c'^2}, \bar{Z}, \overline{Z'^2}) \\ &= \int_0^1 Y_{CO}(c, Z) P_1(c, \bar{c}, \overline{c'^2}) P_2(Z, \bar{Z}, \overline{Z'^2}) dc dZ \end{aligned}$$



45

Premixed F-TACLES LES model

“The influence of combustion SGS submodels on the resolved flame propagation. application to the LES of the Cambridge stratified flames”

R. Mercier, T. Schmitt, D. Veynante, B. Fiorina, PROCI 35, 1259

Filtered TABulated Chemistry for LES (F-TACLES)

model propagates resolved flame at the subgrid scale turbulent flame speed $S_{T,\Delta}$

$$\rho_0 S_{T,\Delta} = \Xi_{\Delta} \gamma \int_0^1 \rho_0 S_i^{ad}(z') P(z') dz' \quad \Xi = \text{new flame surface density parameter}$$

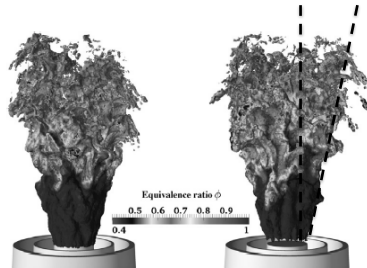
Solves for mean progress variable \widetilde{Y}_c

$$\begin{aligned} \frac{\partial \rho \widetilde{Y}_c}{\partial t} + \nabla \cdot (\rho \widetilde{\mathbf{u}} \widetilde{Y}_c) &= \nabla \cdot \left(\Xi_{\Delta} \gamma \alpha_{Y_c}^{Tab} \rho_0 D_0 \nabla \widetilde{Y}_c \right) \\ &\quad - \Xi_{\Delta} \gamma \left(\Omega_{Y_c}^{Tab} + \bar{\rho} \tilde{\omega}_{Y_c}^{Tab} \right) \end{aligned}$$

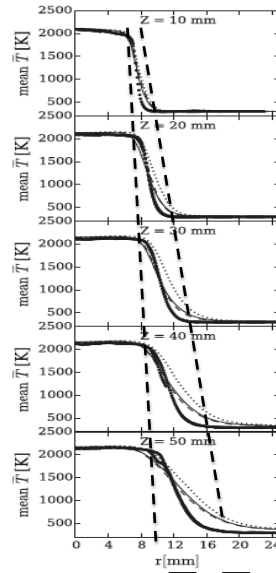


46

Thickness of flame brush computed and agrees with experiment at Cambridge – S. Hochgreb



Flame brush gets wider
As you go upward
Up is plotted down here



Large Eddy Simulation (LES) of turbulent non-premixed combustion AE 633

Kuo, K.K. Fund. Of Turbulent and Multiphase Combustion,
 Riley, J.J. Review of LES, J. Fluids Engr. ASME, 128, p. 209
 Pitsch, H., LES of Turbulent Combustion, Annual Rev. of Fluid Mech 38, p. 453.
 Kempf, A. LES of a bluff body stabilized nonpremixed flame, Combust. Flame 144, p. 170.

LES separates the fuel mass fraction (Y_{H_2} , and other variables) into their resolved scale (unsteady) component and their subgrid component. The subgrid component has to be modeled.

Resolved (large) scale component = has a hat on top: \hat{Y}_{H_2}

We solve the conservation equation for \hat{Y}_{H_2} to get a value of \hat{Y}_{H_2} at each point on the grid, at each time. Thus the solution for \hat{Y}_{H_2} looks like an unsteady DNS movie, but in LES the small scales are included in new terms in the conservation equation that are modeled.

Subgrid (small) scale component – does not have a hat on top, has the subscript sgs = subgrid scale

There are two major terms in the conservation equations that are determined mostly by subgrid motions, and the are:

- $\nu_{T,sgs}$ = turbulent kinematic viscosity, also called turbulent diffusivity; only occurs at subgrid scale
- $\dot{\omega}_{H_2,sgs}$ = reaction rate of H2 (and other species), only occurs at subgrid scale

Closure: these two unknowns appear in the conservation equations for resolved quantities, so model equations are needed to relate these two quantities to resolved scale \hat{u} , \hat{v} , \hat{Y}_{H_2} etc.

We think of the resolved scale quantities (\hat{Y}_{H_2} , etc.) to be located at each of the grid points, while the sub quantity is located at the center of the grid box; i.e., the subgrid $\nu_{T,sgs}$ and $\dot{\omega}_{H_2,sgs}$ are averaged over all the small scale motions inside the grid box (which we never can see, they are unresolved).

a) **How to model turbulent diffusivity** $\nu_{T,sgs}$ which is a subgrid quantity

See Kuo, page 272 of the CANVAS handout: he applies a spatial filter to the momentum equation:

$$\frac{\partial}{\partial t} (\overline{\rho \hat{u}_i}) + \frac{\partial}{\partial x_j} (\overline{\rho \hat{u}_i \hat{u}_j}) = -\frac{\partial \hat{p}}{\partial x_i} + \mu \frac{\partial}{\partial x_j} \left(\frac{\partial \hat{u}_i}{\partial x_j} + \frac{\partial \hat{u}_j}{\partial x_i} \right) - \frac{\partial (\tau_{ij})_{sgs}}{\partial x_j} \quad (4.236)$$

This looks like the unsteady momentum equation except that the unknown is the resolved scale velocity \hat{u}_i . The molecular viscosity μ is a known function of temperature only. The last term is the gradient of the subgrid scale stress tensor, which must be modeled. Kuo on p. 274 says:

$$(\tau_{ij})_{sgs} = 2\hat{\rho} \nu_{sgs} S_{ij} \quad \text{where}$$

$$S_{ij} = \frac{1}{2} \left(\frac{\partial \hat{u}_i}{\partial x_j} + \frac{\partial \hat{u}_j}{\partial x_i} \right) \quad \text{and} \quad \nu_{sgs} = (C_s \Delta)^2 |\overline{S}| \quad \text{and} \quad |\overline{S}| = \sqrt{2S_{ij}S_{ij}}$$

These formulas relate the new unknown $(\tau_{ij})_{sgs}$ to the resolved scale velocities \hat{u}_i . $C_s = 0.17$.

b) **How to model the chemical reaction rate** $\dot{\omega}_{H_2,sgs}$ which is a subgrid quantity

Riley's paper, p. 210 says that the unsteady conservation of fuel mass fraction, after spatial filtering, has a subgrid reaction rate term:

$$\frac{\partial \hat{Y}_f}{\partial t} + \hat{v}_i \frac{\partial \hat{Y}_f}{\partial x_i} = \frac{1}{Pe} \frac{\partial^2 \hat{Y}_f}{\partial x_i^2} + \dot{\omega}_f$$

To model the last term in this conservation equation, Riley and Pitsch use the flamelet approach:

$$\dot{\omega}_{H_2,sgs} = \iint \dot{\omega}_{H_2}(Z, \chi_s) P_1(Z) P_2(\chi_s) dZ d\chi_s$$

Integrating over all Z and all χ_s means the result for $\dot{\omega}_{H_2,sgs}$ does not depend on Z and χ_s

$\dot{\omega}_{H_2}(Z, \chi_s)$ is the state relation we get from solving the flamelet equation with full chemistry

P_1 is a Beta function. P_2 is a delta function, which has a variance of zero width.

Papers by Riley and Pitsch on CANVAS say:

The mean of the Beta PDF (P_1) is \hat{Z} for each grid box, at each time. So we choose the upper left corner of the grid box and use the value computed by the conservation equations for \hat{Z} , mean of P_1

The variance of P_1 is (Riley, p. 213, Pitsch p. 459):

$$\tilde{Z}^2 = c_V \Delta^2 (\nabla \hat{Z})^2$$

We use a central difference formula to get the gradient of \hat{Z} , knowing values of \hat{Z} at many grid points.

The mean of P_2 is (Riley, p. 213, Pitsch p. 459):

$$\tilde{\chi} = 2D_t (\nabla \tilde{Z})^2 \quad \text{where} \quad D_t = (c_Z \Delta)^2 \tilde{S} \quad \text{and} \quad \tilde{S} = |2\tilde{S}_{ij}\tilde{S}_{ij}|^{1/2}$$

(Pitsch uses tildas on top to mean hats = resolved scale quantities)

The variance of P_2 is zero, since it is a delta function.

So now the problem is mathematically closed. We have enough equations to solve the conservation equations, including the two new subgrid terms (turbulent diffusivity and turbulent reaction rate).

Kuo, K.K.,

Fundamentals of Turbulent and Multiphase Combustion

4.7 LARGE EDDY SIMULATION

The large eddy simulation (LES) technique has been developed to address the anisotropic turbulence behavior of the flow by resolving intermediate spatial and temporal scales, which are small enough to simulate dynamics of large eddies explicitly while the smaller eddies are treated by homogeneous isotropic turbulence modeling. By using proper low-pass filtering, scales lower than a selected Δx (or simply Δ) are eliminated and suitable equations for large scales are developed for solving the flow property variations in both time and spatial variables. LES is more accurate and reliable than RANS models for flows involving unsteadiness at large scales (e.g., flow over bluff bodies, which involves unsteady separation and vortex shedding). Strictly speaking, there are two different filtering processes in the LES approach: filter dimension and grid spacing. The turbulence processes occurring at scales smaller than the grid spacing (also known as grid

cut-off filter) cannot be resolved in any case, and they are always modeled. These scales are called subgrid scales (SGS). For scales smaller than the resolved scales (i.e., Δx), SGS models are used. The second scale is associated with the scale used by the LES filter (δ), to be discussed, which can be different from the grid cut-off filter (Δ). In practice, a filter scale is chosen to coincide with the grid spacing. Subgrid scales are same as subfilter scales (SFS; i.e., $\Delta = \delta$), so there is no need to define separate SFS and SGS models. The concept behind the LES method is demonstrated in Figure 4.15 in both physical and spectral space. In Figure 4.15a, the subgrid scales are shown in physical space. In Figure 4.15b, two cut-off wave numbers are shown in Fourier space; one is the desirable cut-off wavenumber, which would cover a majority of the energy spectrum, and, therefore, only the dissipation is required to be modeled. However, in practice, this wavenumber could demand very fine resolutions and therefore computationally be more expensive. The actual cut-off wavenumber also is shown in this figure; it usually is significantly lower than the desirable cut-off wavenumber.

A filtering operation is performed, to decompose the major variables into the sum of the resolved component (\widehat{U}) and the residual (or subgrid scale, SGS) component (u') or fluctuation.

$$U(\mathbf{x}, t) = \widehat{U}(\mathbf{x}, t) + u'(\mathbf{x}, t) \tag{4.216}$$

This decomposition is known as Leonard’s decomposition.

The governing equations are derived for evolution of resolved major variables (density, temperature, velocity, etc.), and these equations contain residual components (e.g., the residual stress tensor [called the SGS stress tensor in the

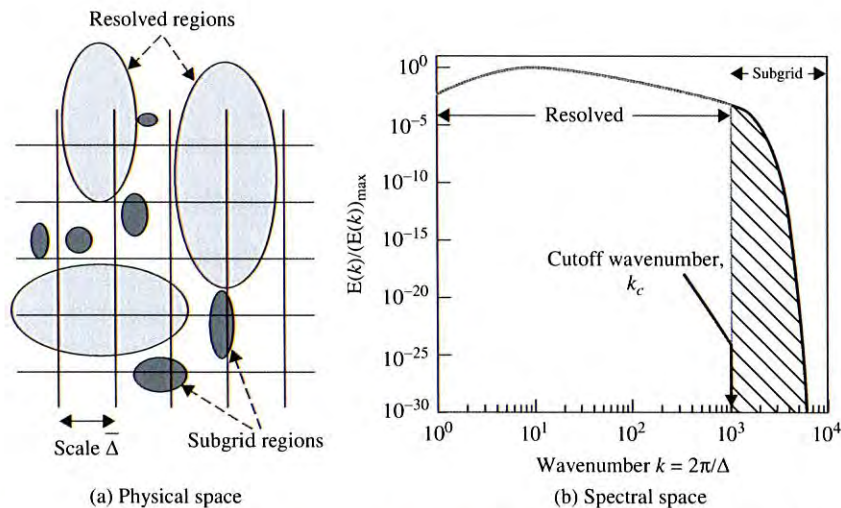


Figure 4.15 Description of large eddy simulation methodology (the actual cut-off wavenumber represents current state-of-the-art simulations) (part a from Sagaut, 1998).

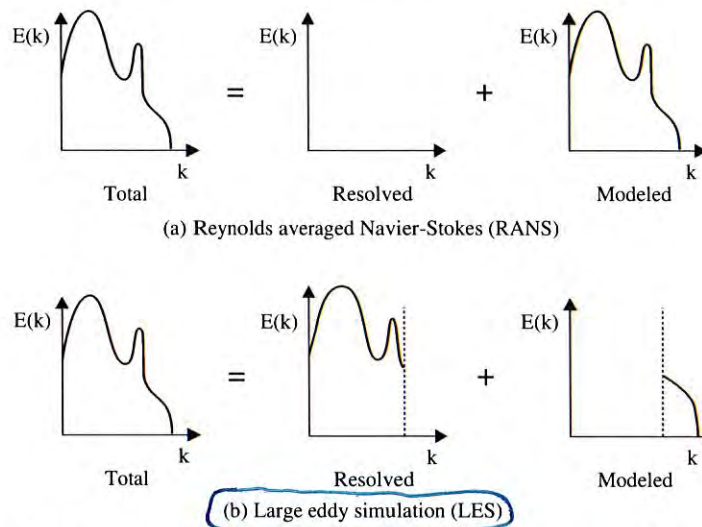


Figure 4.16 Decomposition of energy spectrum in solution associated with (a) RANS and (b) LES (symbolic representation) (modified from P. Sagaut, 1998).

momentum equation]. These residual components must be modeled to achieve closure (e.g., the residual stress tensor is modeled by the eddy-viscosity model). The modeled filtered equations are solved numerically for the resolved flow properties.

Major differences between RANS and LES can be demonstrated by comparing the two sets of plots shown in Figure 4.16.

4.7.1 Filtering

In signal processing, a filter is a function or procedure that removes unwanted parts of a signal. The concept of filtering and filter functions is very important in large eddy simulations. One particularly elegant method of filtering is by taking the Fourier transform of a signal into spectral space, performing the filtering operation in the spectral space, and finally transforming the filtered signal back into the physical space by taking the inverse Fourier transform. The Fourier transform of a function is given by

$$F(\kappa) = \int_{-\infty}^{\infty} f(x) e^{-2\pi i \kappa x} dx \tag{4.217}$$

The inverse Fourier transform can return the function in the frequency space back to the physical space—that is:

$$f(x) = \int_{-\infty}^{\infty} F(\kappa) e^{2\pi i \kappa x} d\kappa \tag{4.218}$$

Let us discuss the mathematical operation called convolution. A convolution is an integral that expresses the amount of overlap of one function g as it is shifted over another function f . It therefore “blends” one function with another. The convolution is sometimes also known by its German name, *faltung* (folding). Convolution of two functions f and g over a finite range $[0, \zeta]$ is given by Equation 4.219:

$$[f * g](\zeta) \equiv \int_0^{\zeta} f(\xi) g(\zeta - \xi) d\xi \quad (4.219)$$

A filtering operation is a convolution of a variable (e.g., a flow field variable ϕ_i) with the filter function (e.g., G); therefore, it is an important step in order to develop an understanding of a large eddy simulation. The convolution integral of ϕ_i in the next equation was proposed by Leonard in 1974:

$$\widehat{\phi}_i(\mathbf{x}, t) = \int_0^t \left[\iiint_V \phi_i(\mathbf{x}', t) G(\mathbf{x} - \mathbf{x}', t - \tau; \Delta, \delta\tau) d\mathbf{x}' \right] d\tau \quad (4.220)$$

where \mathbf{x} and \mathbf{x}' are three-dimensional position vectors of common origin, with $0 < \tau < t$ and V representing the total system volume associated with the fluid. The filter function G quantifies the influence of subgrid scale (sgs) dynamics at remote points (\mathbf{x}', τ) on filtered values at (\mathbf{x}, t) . The filter function G must satisfy the next normalization condition:

$$\int_0^t \left[\iiint_V G(\mathbf{x} - \mathbf{x}', t - \tau; \Delta, \delta\tau) d\mathbf{x}' \right] d\tau = 1 \quad (4.221)$$

For a one-dimensional case with only spatial filtering, the filtering operation introduced by Leonard in 1974 can be written as:

$$\widehat{U}(x) = \int_{-\infty}^{\infty} G(r) U(x - r, t) dr \quad (4.222)$$

In this case, the normalization condition becomes:

$$\int_{-\infty}^{\infty} G(r, x) dr = 1 \quad (4.223)$$

Let us define Favre filtering for a variable density flow as:

$$\overline{\rho \widehat{\phi}_i}(\mathbf{x}, t) = \int_0^t \left[\iiint_V \rho \phi_i(\mathbf{x}', t) G(\mathbf{x} - \mathbf{x}', t - \tau; \Delta, \delta\tau) d\mathbf{x}' \right] d\tau \quad (4.224)$$

By this definition,

$$\overline{\rho \widehat{\phi}_i} = \widehat{\rho \phi_i} \quad \text{or} \quad \widehat{\phi}_i = \frac{\widehat{\rho \phi_i}}{\overline{\rho}} \quad (4.225)$$

TABLE 4.1. Several Filter Functions in Physical Space and Spectral Space

Type	Physical Space	Spectral Space
Gaussian filter	$\left(\frac{6}{\pi \Delta^2}\right)^{1/2} \exp\left(-\frac{6r^2}{\Delta^2}\right)$	$\exp\left(-\frac{\kappa^2 \Delta^2}{24}\right)$
Sharp cut-off filter	$\frac{\sin(\pi r/\Delta)}{\pi r}$	$H(\kappa_c - \kappa)$ where $\kappa_c \equiv \pi/\Delta$
Box filter (or grid filter)	$\frac{1}{\Delta} H\left(\frac{1}{2}\Delta - r \right)$	$\sin\left(\frac{1}{2}\kappa\Delta\right)/\left(\frac{1}{2}\kappa\Delta\right)$

Then a variable can be decomposed as:

$$\phi_i(\mathbf{x}, t) = \widehat{\phi}_i(\mathbf{x}, t) + \phi_i''(\mathbf{x}, t) \quad (4.226)$$

resolved (large) scale
small subgrid scale

In a large-eddy simulation, three major filter functions often are employed: the Gaussian filter, the sharp cut-off filter, and the box filter. Their equations in both physical and spectral spaces are shown in Table 4.1.

The advantage of performing the filtering operation in the spectral space comes from the fact that the Fourier transform turns convolution into a multiplication operation.

$$F(f(x) * g(x)) = F(f(x)) F(g(x)) \quad (4.227)$$

Similarly, the Fourier transform turns a multiplication into a convolution—that is:

$$F(f(x) g(x)) = F(f(x)) * F(g(x)) \quad (4.228)$$

The symbol $[f * g](y)$ denotes convolution of f and g . Convolution is more often taken over an infinite range,

$$[f * g](y) \equiv \int_{-\infty}^{\infty} f(\xi) g(y - \xi) d\xi = \int_{-\infty}^{\infty} g(\xi) f(y - \xi) d\xi \quad (4.229)$$

The application of these three filters on the energy spectrum is shown in Figure 4.17.

4.7.2 Filtered Momentum Equations and Subgrid Scale Stresses

The momentum equation in the x_i direction for a compressible fluid can be written as:

$$\frac{\partial}{\partial t}(\rho u_i) + \frac{\partial}{\partial x_j}(\rho u_i u_j) = -\frac{\partial p}{\partial x_i} + \mu \frac{\partial}{\partial x_j} \left(\frac{\partial u_i}{\partial x_j} + \frac{\partial u_j}{\partial x_i} \right) + \frac{\partial}{\partial x_j} \left(\mu' - \frac{2}{3}\mu \right) \frac{\partial u_k}{\partial x_k} \delta_{ij} \quad (4.230)$$

Dilatation ≈ 0

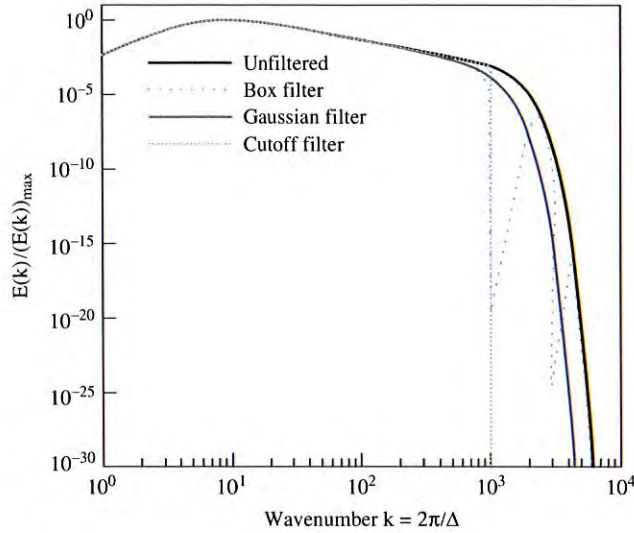


Figure 4.17 Application of various filters on the energy spectrum.

After applying the filtering operator on this equation, we get:

$$\frac{\partial}{\partial t} (\widehat{\rho u_i}) + \frac{\partial}{\partial x_j} (\widehat{\rho u_i u_j}) = -\frac{\partial \widehat{p}}{\partial x_i} + \mu \frac{\partial}{\partial x_j} \left(\frac{\partial \widehat{u}_i}{\partial x_j} + \frac{\partial \widehat{u}_j}{\partial x_i} \right) \quad (4.231)$$

The filtered momentum equation contains a nonlinear term, $\widehat{\rho u_i u_j}$. In order for Equation 4.231 to be useful, it should be expressed in terms of a filtered quantity \widehat{u}_i and subgrid scale quantity u'_i . Since we have density as a variable in these equations, we will use Favre-filtered quantities instead of regular filtered quantities. In general, a nonlinear term in the governing equations due to any random variable ϕ_i and velocity component u_j can be decomposed as:

$$\widehat{\rho \phi_i u_j} \equiv \widehat{\rho (\widehat{\phi}_i + \phi'_i) (\widehat{u}_j + u'_j)} = \widehat{\rho \widehat{\phi}_i \widehat{u}_j} + \widehat{\rho u'_j \widehat{\phi}_i} + \widehat{\rho \phi'_i \widehat{u}_j} + \widehat{\rho \phi'_i u'_j} \quad (4.232)$$

If the random variable ϕ_i is substituted by velocity component u_i in Equation 4.232, we have:

$$\widehat{\rho u_i u_j} \equiv \widehat{\rho (\widehat{u}_i + u'_i) (\widehat{u}_j + u'_j)} = \widehat{\rho \widehat{u}_i \widehat{u}_j} + \widehat{\rho u'_j \widehat{u}_i} + \widehat{\rho u'_i \widehat{u}_j} + \widehat{\rho u'_i u'_j} \quad (4.233)$$

Adding/subtracting the term $\widehat{\rho u'_i \widehat{u}_j}$ on the right-hand side of this equation, we have

$$\widehat{\rho u_i u_j} = \widehat{\rho \widehat{u}_i \widehat{u}_j} + \widehat{\rho \widehat{u}_i \widehat{u}_j} - \widehat{\rho \widehat{u}_i \widehat{u}_j} + \widehat{\rho u'_j \widehat{u}_i} + \widehat{\rho u'_i \widehat{u}_j} + \widehat{\rho u'_i u'_j} \quad (4.234)$$

Substituting this expression in Equation 4.231, we have the filtered momentum equation as:

$$\frac{\partial}{\partial t} (\overline{\rho u_i}) + \frac{\partial}{\partial x_j} (\overline{\rho \widehat{u}_i \widehat{u}_j}) = -\frac{\partial \widehat{p}}{\partial x_i} + \mu \frac{\partial}{\partial x_j} \left(\frac{\partial \widehat{u}_i}{\partial x_j} + \frac{\partial \widehat{u}_j}{\partial x_i} \right) - \frac{\partial (\tau_{ij})_{\text{sgs}}}{\partial x_j} \quad (4.235)$$

By using Equation 4.225, we can write the filtered momentum equation as:

$$\frac{\partial}{\partial t} (\overline{\rho \widehat{u}_i}) + \frac{\partial}{\partial x_j} (\overline{\rho \widehat{u}_i \widehat{u}_j}) = -\frac{\partial \widehat{p}}{\partial x_i} + \mu \frac{\partial}{\partial x_j} \left(\frac{\partial \widehat{u}_i}{\partial x_j} + \frac{\partial \widehat{u}_j}{\partial x_i} \right) - \frac{\partial (\tau_{ij})_{\text{sgs}}}{\partial x_j} \quad (4.236)$$

The subgrid scale tensor $(\tau_{ij})_{\text{sgs}}$ is:

$$\begin{aligned} (\tau_{ij})_{\text{sgs}} &= \overline{\rho u_i u_j} - \overline{\rho \widehat{u}_i \widehat{u}_j} = L_{ij} + C_{ij} + R_{ij} \\ &= \left(\overline{\rho \widehat{u}_i \widehat{u}_j} - \overline{\rho \widehat{u}_i \widehat{u}_j} \right) + \left(\overline{\rho u_j'' \widehat{u}_i} + \overline{\rho u_i'' \widehat{u}_j} \right) + \overline{\rho u_i'' u_j''} \end{aligned} \quad (4.237)$$

$$\text{Leonard stresses: } L_{ij} \equiv \left(\overline{\rho \widehat{u}_i \widehat{u}_j} - \overline{\rho \widehat{u}_i \widehat{u}_j} \right) = \overline{\rho} \left(\overline{\widehat{u}_i \widehat{u}_j} - \widehat{u}_i \widehat{u}_j \right) \quad (4.238)$$

$$\text{Cross-term stresses: } C_{ij} \equiv \left(\overline{\rho u_j'' \widehat{u}_i} + \overline{\rho u_i'' \widehat{u}_j} \right) = \overline{\rho} \left(\overline{u_j'' \widehat{u}_i} + \overline{u_i'' \widehat{u}_j} \right) \quad (4.239)$$

$$\text{Reynold's stresses: } R_{ij} \equiv \overline{\rho u_i'' u_j''} = \overline{\rho u_i'' u_j''} \quad (4.240)$$

In Equations 4.238–4.240, the next relationships were used based on the definition of Favre filtered quantities from Equation 4.225:

$$\overline{u_i'' u_j''} = \overline{\rho u_i'' u_j''} / \overline{\rho} \quad \text{or} \quad \overline{\rho u_i'' u_j''} = \overline{\rho} \overline{u_i'' u_j''} \quad (4.241)$$

Similarly,

$$\overline{\rho u_j'' \widehat{u}_i} = \overline{\rho} \overline{u_j'' \widehat{u}_i}; \quad \overline{\rho u_i'' \widehat{u}_j} = \overline{\rho} \overline{u_i'' \widehat{u}_j} \quad (4.242)$$

Also,

$$\overline{\rho \widehat{u}_i \widehat{u}_j} = \overline{\rho} \overline{\widehat{u}_i \widehat{u}_j} \quad (4.243)$$

Let ω and ψ be two random variables. If an operator $\langle \rangle$ satisfies the next properties, it is called a Reynolds operator:

$$\begin{aligned} \langle \omega + \psi \rangle &= \langle \omega \rangle + \langle \psi \rangle \\ \langle a\omega \rangle &= a \langle \omega \rangle \quad \text{where } a \text{ is a constant} \\ \langle \langle \omega \rangle \psi \rangle &= \langle \omega \rangle \langle \psi \rangle \\ \left\langle \frac{\partial \omega}{\partial s} \right\rangle &= \frac{\partial \langle \omega \rangle}{\partial s} \quad \text{where } s \text{ could be } x_i \text{ or } t \\ \left\langle \int \omega(x_i, t) dx_1 dx_2 dx_3 dt \right\rangle &= \int \langle \omega(x_i, t) \rangle dx_1 dx_2 dx_3 dt \end{aligned} \quad (4.244)$$

4.7.3 Modeling of Subgrid-Scale Stress Tensors

The subgrid-scale stress tensors have been modeled by using the eddy viscosity concept and the Boussinesq approximation based on the analogy between the interaction of small eddies and the perfectly elastic collision of molecules (i.e., molecular viscosity). Eddy viscosity models work for small scales. The most commonly known eddy viscosity model for the term $(\tau_{ij})_{\text{sgs}}$ in LES is the Smagorinsky model (1963), after Joseph Smagorinsky, who used this model for geophysical flow calculations. The first major result in LES was given by Lilly (1992), who showed that the constant used in the Smagorinsky model should have a universal value, not a tuning constant. For this reason, the model also is called Smagorinsky-Lilly model.

The subgrid scale stress is given by Equation 4.249.

$$(\tau_{ij})_{\text{sgs}} = \widehat{\rho u_i u_j} - \widehat{\rho} \widehat{u_i} \widehat{u_j} = \mu_{\text{sgs}} \left(\frac{\partial \widehat{u}_i}{\partial x_j} + \frac{\partial \widehat{u}_j}{\partial x_i} \right) \approx 2 \widehat{\rho} \nu_{\text{sgs}} S_{ij}$$

where $S_{ij} = \frac{1}{2} \left(\frac{\partial \widehat{u}_i}{\partial x_j} + \frac{\partial \widehat{u}_j}{\partial x_i} \right)$

(4.249)

The eddy viscosity ν_i is modeled by the next formula:

$$\nu_{\text{sgs}} = (C_s \Delta)^2 |\overline{S}| \quad \text{where } \Delta = (\text{Volume})^{\frac{1}{3}} \quad \text{and} \quad |\overline{S}| = \sqrt{2 S_{ij} S_{ij}} \quad (4.250)$$

where the term Δ represents the grid size and volume refers to the grid volume.

Lilly showed that the value of C_s should have a universal value of 0.17 under certain assumptions. However, the value of this constant varies between 0.1 and 0.3 depending on the problem. For a case of isotropic homogeneous turbulence, Clark et al. (1979) used $C_s = 0.2$ whereas Deardorff (1973) used $C_s = 0.1$ for a two-dimensional planar channel flow. Numerical simulations of shear flow have used a value of $C_s \sim 0.1$ to 0.12 (Meneveau, Lund, and Cabot, 1996; O'Neil, Driscoll, and Malmberg, 1997). The Smagorinsky model is very simple to implement; however, its major drawback is the inability to have a universal constant value for C_s and thus represent correctly different turbulent fields in rotating or sheared flows, near-solid walls, or transitional regimes with one eddy viscosity equation.

To overcome this deficiency, dynamic subgrid scale models were proposed by Germano and co-workers (1991). In this model, known as the Germano model, the model coefficient C_s is computed dynamically as the calculation progresses rather than being an a priori input. The model is based on an algebraic identity between the subgrid-scale stresses at two different filtered levels and the resolved turbulent stresses. The subgrid-scale stresses obtained using the Germano model vanish in laminar flow and at a solid boundary and have the correct asymptotic behavior in the near-wall region of a turbulent boundary layer. The results of large-eddy simulations of transitional and turbulent channel flow using the Germano model are in good agreement with the direct simulation data.

Review of Large-Eddy Simulation of Non-Premixed Turbulent Combustion

James J. Riley

e-mail: rileyj@u.washington.edu
Department of Mechanical Engineering,
University of Washington,

J of Fluids Engr.

Introduction

With the continuing reliance on fossil fuels as the predominant source for energy, and economic and environmental concerns emphasizing the efficient production of energy with minimal pollutants, the understanding and prediction of turbulent combustion remains a topic of considerable importance in mechanical engineering. And in the past decade, with the continuing increases in the speed, memory and storage of computers, with improvements in numerical methods, and, most importantly, with developments in subgrid-scale modeling, large-eddy simulation (LES) has begun to play a significant role in understanding and predicting turbulent reacting flows.

Early work on large-eddy simulation of turbulent, reacting flows has emphasized non-premixed reactions utilizing both mixture-fraction-based and Monte Carlo approaches. In the latter case, models based upon the filtered density function (PDF) equation (Colucci et al. [1], Jaber et al. [2], Gicquel et al. [3], James and Jaber [4]) and upon the linear eddy model (LEM, e.g., Menon and Calhoun [5]) have been developed and tested. In the PDF approach, Monte Carlo methods are introduced to solve for the moments of the modeled PDF equation, while in the LEM approach mechanistic, stochastic models are introduced to model the turbulence advection and mixing processes. Another LES approach has been to employ scale similarity arguments to close the reaction term directly (e.g., DesJardin and Frankel [6]). More recently, work has begun on the more difficult problem of premixed reactions. Several approaches have been employed, including methods to thicken the flame, either with an artificially large diffusivity (e.g., Colin et al. [7]) or larger-scale filtering (Boger et al. [8]), methods to track the flame using a progress-type (G) variable (e.g., Chakravarthy and Menon [9], Peters [10]), and also methods using models for flame-wrinkling density (Fureby [11], Knikker et al. [12]).

In this paper, recent developments in the methodology of large-eddy simulation of reacting, turbulent flows will be reviewed, with emphasis on mixture-fraction-based approaches to non-premixed reactions in single-phase, low Mach number gases. The mixture-fraction-based approaches in large-eddy simulation have, in particular, been developed to the point where they can be used with confidence in both research and applications for certain classes of problems.

In the next section the approach of large-eddy simulation will be reviewed, along with the principal issues in its application to turbulent, reacting flows. In the third section, approaches which

rely on the mixture fraction will be presented and, in the final section, some key remaining issues and the outlook for the future will be discussed.

Large-Eddy Simulation

The technique of large-eddy simulation stems from the research of meteorologists in the 1960s (e.g., Smagorinsky [13], Lilly [14], Deardorff [15]). In large-eddy simulation, Reynolds (usually time) averaging is avoided and the three-dimensional, time-dependent, detailed structure of the flow is directly simulated. In meteorological flows, however, as in most technological flows, it is impossible to numerically simulate all of the scales of motion, due to the vast range of length and time scales involved and to the limitations in computer speed and memory. Therefore, in large-eddy simulation, prior to performing the simulations, the governing equations are spatially filtered to remove motions at length (and time) scales not resolvable on the computational mesh. Thus only the "larger eddies" are simulated. For example, consider the velocity field $\mathbf{v}(\mathbf{x}, t)$; it can be spatially filtered as

$$\hat{\mathbf{v}}(\mathbf{x}, t) = \int G(\mathbf{x} - \mathbf{x}'; \hat{\Delta}) \mathbf{v}(\mathbf{x}', t) d\mathbf{x}', \quad (1)$$

where the integral is over the entire computational domain, G is a filter function, usually a top-hat or a Gaussian function, or sometimes a spectral truncation, and $\hat{\Delta}$ is the filtering scale. (Favre, or density-weighted, filtering is often used for large-eddy simulation of reacting flows. For simplicity of presentation in most of this review, however, only non-weighted filtering is considered.)

To understand the effect of this filtering operation, consider filtering the momentum equation for constant density flows:

$$\frac{\partial}{\partial t} \hat{v}_i + \hat{v}_j \frac{\partial}{\partial x_j} \hat{v}_i = - \frac{1}{\rho} \frac{\partial}{\partial x_i} \hat{p} + \nu \frac{\partial^2}{\partial x_k^2} \hat{v}_i + \frac{1}{\rho} \frac{\partial}{\partial x_k} \hat{\tau}_{ik}, \quad (2)$$

The equation, now for the corresponding filtered quantities, is identical to the momentum equation prior to filtering, except for the addition of the final term on the right-hand side. The quantity $\hat{\tau}_{ik}$, defined as

$$\hat{\tau}_{ik} = -\rho(\widehat{v_i v_k} - \hat{v}_i \hat{v}_k), \quad (3)$$

is called the subgrid-scale, or residual, stress tensor, and represents the effects of the subgrid-scale motions (which have been filtered out) on the grid-scale motions (computed in the simulations). This stress tensor requires modeling. Present models estimate the effect of the subgrid scales using information about the motions close to the scale of the computational cutoff. For example, in one modeling approach, the subgrid-scale stress tensor is modeled analogous to the Reynolds stress in mixing length

Contributed by the Fluids Engineering Division of ASME for publication in the JOURNAL OF FLUIDS ENGINEERING. Manuscript received May 14, 2004; final manuscript received December 29, 2004. Assoc. Editor: Ugo Piomelli.

theory [13], with the coefficient chosen by a “dynamic” method (e.g., Germano et al. [16]) which takes into account the behavior of the velocity field at the smaller resolvable length scales.

The approach of LES has distinct advantages and disadvantages when compared to approaches utilizing the Reynolds-averaged Navier Stokes equations (RANS). LES has the disadvantage of being a very large calculation, being three-dimensional and time-dependent, and with as many length scales resolved as possible. It has the advantages, however, that the large-scale motions are treated directly, so that only the small-scale motions require modeling. For turbulent flows the large-scale motions tend to control the overall behavior of the flow, so their direct computation is a distinct advantage. Furthermore, the small, filtered scales of motion contain little energy, so that the computed results are expected to be somewhat insensitive to the model used. Finally, the small scale-motions of a turbulent flow tend to be more universal, especially when compared to the larger-scale motions, so that a proven model should have broader applicability.

The advantage of directly computing the larger-scale motions can be very important for simulating reacting flows, especially if the flows are inherently unsteady, e.g., combustion instabilities, or if motions difficult to model in RANS control the flow, e.g., in bluff-body stabilized flames.

At the present time the approach of LES is very useful as a research tool, and is being used in a limited number of applications. There is some optimism that, as computers continue to develop, and subgrid-scale modeling continues to improve, this approach will prove more and more useful in applications in the future.

In order to understand the potential problems involved in large-eddy simulations of turbulent, reacting flows, consider for simplicity the idealization of a constant density, single-step, Arrhenius, irreversible chemical reaction occurring on a turbulent flow field. Filtering the conservation equation for fuel for this case gives, in nondimensional form,

$$\frac{\partial \hat{Y}_f}{\partial t} + \hat{v}_i \frac{\partial \hat{Y}_f}{\partial x_i} = \frac{1}{Pe} \frac{\partial^2 \hat{Y}_f}{\partial x_i^2} + \hat{\omega}_f + \frac{\partial}{\partial x_i} \hat{\sigma}_i \quad (4)$$

Here Y_f is the mass fraction of fuel and Pe is the Peclet number; $\hat{\sigma}_i = -(v_i \hat{Y}_f - \hat{v}_i \hat{Y}_f)$, representing the flux of \hat{Y}_f due to the subgrid-scale motions, is analogous to the subgrid-scale stresses, and can be treated, e.g., by Smagorinsky's model with a dynamically computed coefficient. The filtered reaction rate term is given by

$$\hat{\omega}_f = -Da \cdot \text{filter}\{Y_f Y_o \exp[-E_a/R_u T]\}, \quad (5)$$

where “filter{.}” represents the spatial filtering operation (Eq. (1)), Y_o is the mass fraction of oxidant, T the absolute temperature, R_u the universal gas constant, E_a the activation energy, and Da is the Damköhler number, the latter defined here as an estimate of the ratio of the turbulent time scale to the chemical-reaction time scale. The principal new issue is how to model this term, especially for more complex, temperature-dependent reactions.

For moderate to large Damköhler numbers and also for high activation energies, the flame will be very thin, and the chemical reaction will occur almost entirely at the subgrid scale. This behavior is very different from that of other quantities such as velocity and density, the bulk of whose dynamics is resolvable on the computational mesh, and it appears to have discouraging implications, and indicates that modeling procedures for this term must be very different from those for the flux term $\hat{\sigma}_i$. Of course, any models must be based upon grid-scale quantities. What gives hope that a reasonable model exists is that the overall reaction rate depends on the mixing rate, and the mixing rate depends on the behavior of the larger-scale eddies.

Mixture-Fraction-Based Approach

Consider the problem where the reactive species are nonpremixed, e.g., a fuel jet into air. (Figure 1 shows a slice through a



Fig. 1 Slice through the a turbulent region. Nonpremixed turbulent combustion occurs at the interface of the fuel (black) and oxidant (white).

nonpremixed turbulent region, where a reactant (colored black) is diffusing into and reacting with an oxidant (white). The chemical reaction occurs at the interface between the two. The figure was made from direct numerical simulation results employing a 512^3 -point computational grid, and reported in de Bruyn Kops et al. [17]. The chemical reaction was a one-step, irreversible, Arrhenius-type, with moderate values for the Damköhler number and activation energy. The simulated velocity field was decaying, homogeneous turbulence with an initial Reynolds number, based upon the Taylor microscale, of about 70.) For the sake of simplicity, we consider the case where a fuel stream of mass fraction Y_{fj} issues into an oxidant of mass fraction Y_{oe} in a one-step, Arrhenius reaction at low Mach number, although the following arguments can be easily generalized to realistic chemistry [18].

A major assumption in the mixture-fraction-based approaches is that the molecular diffusivities of all chemical species are equal, and furthermore their diffusivities equal the molecular diffusivity of heat. This assumption is justified for certain species, e.g., for atomic and molecular oxygen. Furthermore, for high Reynolds number turbulent flows, it is expected that the overall reaction rates become independent of these diffusivities, a fact that has some experimental, theoretical, and numerical support [19]. It must be realized, however, that the molecular diffusivities of some species are much different from those of others, e.g., the diffusivity of molecular hydrogen is much greater than that of oxygen. In addition, this assumption may break down in regions of gaseous flows where the temperature is high, and hence the viscosity is high and the Reynolds number is lower. Finally, it is important to note that recent theoretical work has suggested methods of relaxing this assumption (e.g., Nilsen and Kosály [20], Nilsen [21], Pitsch [22], Peters [10]).

The concept of a mixture fraction is based upon conserved scalars, examples of which are elementary mass fractions, e.g., those for oxygen and hydrogen, Z_O and Z_H . But, more generally, in considering the conservation equations for the fuel and oxidant, assuming equal diffusivities, the mixture fraction can be defined for this case by [23]

$$Z = \frac{rY_f - Y_o + Y_{oe}}{rY_{fj} + Y_{oe}}, \quad (6)$$

with the properties that it is conserved, and satisfies the limiting conditions:

$$Z \rightarrow \begin{cases} 1 & \text{in the fuel stream} \\ 0 & \text{in the oxidant stream.} \end{cases} \quad (7)$$

Here r is the mass of oxidant required to react with a unit mass of fuel. An interpretation of Z is that it is the local mass fraction of material originating in the fuel stream, while $(1-Z)$ is the local mass fraction of material originating in the oxidant stream; values of Z between 0 and 1 indicate the amount of mixing that has occurred.

Equilibrium Chemistry. For the case of equilibrium chemistry, the mass fractions of the various chemical species and the temperature can be written as known functions of the mixture fraction, e.g., $Y_f = Y_f^e(Z)$. Define $\hat{p}(Z)$ to be the frequency distribution of Z within a subgrid-scale volume element, where \hat{p} is known as the subgrid-scale pdf [24] or the filtered-density function [1,25]. Then

$$\hat{Y}_f = \int_0^1 Y_f^e(Z) \hat{p}(Z) dZ. \quad (8)$$

Therefore, if \hat{p} can be determined, then so can \hat{Y}_f and the other filtered mass fractions and filtered temperature.

In analogy with the approach involving the assumed pdf for the Reynolds-averaged equations (see, e.g., Bilger [23]), one model involves assuming a functional form for \hat{p} , in particular that of a β -function (Frankel et al. [26]; Cook and Riley [27]). Then \hat{p} can be obtained from the first two filtered moments of Z , i.e., \hat{Z} and the variance squared, or residual, $Z_v^2 = \hat{Z}^2 - \hat{Z}^2$. (Note that care has to be taken in the definition of the variance, since in general $\hat{Z} \neq \hat{\hat{Z}}$.) The problem then reduces to developing accurate procedures to predict both \hat{Z} and Z_v .

This approach can be readily tested in an a priori fashion using data for Z from either high-resolution direct numerical simulations (DNS) or highly-resolved scalar fields measured in laboratory experiments. (Direct numerical simulations involve solving the governing equations for *all* the dynamically relevant scales of motion, so that no subgrid-scale modeling is required.) Given the values of the mixture fraction, assuming chemical equilibrium, the values of temperature and of the mass fractions for each of the chemical species are also known at each point on the high-resolution grid. These fields can then be filtered to obtain "exact" values for the filtered temperature and species mass fraction fields. Furthermore, the first two moments of Z can be filtered, and used along with the assumed form for \hat{p} to produce models for the filtered fields. This allows one to easily compare the "exact" and modeled fields.

Such a procedure was carried out for constant density flows by Cook and Riley [27], assuming a β -distribution for \hat{p} , and using both results from high resolution direct numerical simulations [28] and laboratory data for a jet [29]. In both cases good agreement was obtained when comparing the "exact" to modeled values, validating the estimation of the filtered mass fractions for equilibrium chemistry based upon an assumed form for \hat{p} . This testing was extended by Wall et al. [30] to the variable density case, testing β -distribution models for both the subgrid-scale pdf and the density-weighted (Favre) subgrid-scale pdf. The β -distribution model was successful in both cases, although slightly better for the subgrid-scale (non-Favre) pdf.

Several authors have taken advantage of this model for use in large-eddy simulations of chemically-reacting, nonpremixed turbulent shear flows. For example, Jiménez et al. [31] considered a planar, nonpremixed shear layer. Such a flow has considerable intermittency, which is difficult to model with RANS. With the β -distribution assumption for \hat{p} , very good agreement was obtained with results from high resolution DNS. Reveillon and Vervisch [32] used a similar approach in studying large-eddy simulations of nonpremixed reactions with heat release. Again,

good agreement was found in comparing modeled results with results from DNS. Branley and Jones [33,34] and also Forkel and Janicka [35] used a similar approach to simulate hydrogen jet diffusion flames, and obtained good agreement with laboratory data for major species. And Pierce and Moin [36] simulated a swirling, confined, coaxial jet including heat release using the same modeling. Again comparisons of simulation results with laboratory data were impressive.

Recently Mellado et al. [37] have relaxed the assumption of a β -function for \hat{p} using a deconvolution procedure with approximate reconstruction of \hat{p} using additional moments of Z . This approach has the potential to provide overall improvement to mixture-fraction-based approaches.

Quasi-steady Chemistry. The assumption of chemical equilibrium can be relaxed for fast, but finite rate chemistry, i.e., when the Damköhler number is large, but finite. An important value of Z is its stoichiometric value, attained when the fuel and oxidant are in stoichiometric proportions. When the Damköhler number is large, it is expected that the flames are very narrow, and that they occur near the stoichiometric surfaces. Peters [38] took advantage of these facts to develop the flamelet model, wherein the Damköhler number is assumed to be large enough that the flame regions are very "thin." Here thin is taken to mean that the flame thickness δ is much smaller than either of the two local principal radii of curvature R of the flame itself. There is some argument that, in order for this inequality to hold, in addition to the assumption of large Damköhler number, the flame thickness must be small compared to the local Kolmogorov scale [39], although this requirement is in dispute.

At any point in the flow field a local orthogonal coordinate system can be set up, with one unit vector in the direction of the gradient of Z . The equations are transformed into this local system; then, since Z is locally monotonic in the direction of its gradient, Z can be used as an independent variable. Forming the equations for the species mass fractions in this local coordinate system, and neglecting higher order terms in the small parameter δ/R , results in the simplified form of the conservation equation, called the flamelet equation, here written in dimensional form for the fuel mass fraction,

$$\rho \frac{\partial Y_f}{\partial t} = \dot{\omega}_f + \rho \mathcal{D} |\nabla Z|^2 \frac{\partial^2 Y_f}{\partial Z^2}. \quad (9)$$

Here \mathcal{D} is the molecular diffusivity of fuel. For large Damköhler numbers, which implies that the chemical time scale is much smaller than the turbulence time scale, it is often argued that the reaction is quasi-steady so that the flamelet equation reduces to

$$\dot{\omega}_f = -\rho \frac{1}{2} \chi \frac{\partial^2 Y_f}{\partial Z^2}, \quad (10)$$

the quasi-steady flamelet equation. Note that this is a simplified form of the conservation equation for the fuel, and can be assumed to hold at each point in the flow. Similar equations can be derived for the other species.

Note that the scalar dissipation rate $\chi = 2\mathcal{D} |\nabla Z|^2$ enters into the theory, carrying information about the local *rate* of scalar mixing. To develop the model further, assumptions are needed regarding χ and its relationship to Z . One approach for χ is to assume that the flow in the vicinity of the diffusion flame is a local counterflow, implying both that δ is less than the Kolmogorov scale and also locally uniform strain [38]. The solution to the quasi-steady flamelet equation can then be written as, e.g.,

$$Y_f = Y_f^n(Z, \chi). \quad (11)$$

Therefore, with $\hat{p}(Z, \chi)$ representing the joint frequency distribution of Z and χ in a subgrid-scale volume element, the filtered value of Y_f in this volume element is

$$\hat{Y}_f = \int_0^{\infty} \int_0^1 Y_f^n(Z, \chi) \hat{p}(Z, \chi) dZ d\chi. \quad (12)$$

Assumptions are now required to determine $\hat{p}(Z, \chi)$. It is usually assumed that Z and χ are statistically independent inside each volume element; furthermore it can be argued that \hat{Y}_f depends mainly on $\hat{\chi}$, and only weakly on $\chi' = (\hat{\chi}^2 - \hat{\chi}^2)^{1/2}$ [40], which results in

$$\hat{Y}_f = \int_0^1 Y_f^n(Z, \hat{\chi}) \hat{p}(Z) dZ. \quad (13)$$

As in the case for equilibrium chemistry, \hat{p} can be taken to be a β distribution, determined in terms of \hat{Z} and the variance Z_v . Denoting this assumed form as $\hat{p}_a(Z; \hat{Z}, Z_v)$, then the model result for \hat{Y}_f for quasi-steady chemistry is

$$\hat{Y}_f = \int_0^1 Y_f^n(Z, \hat{\chi}) \hat{p}_a(Z; \hat{Z}, Z_v) dZ = \hat{Y}_f(\hat{Z}, Z_v, \hat{\chi}). \quad (14)$$

These results imply that the filtered mass fractions of the chemical species can be obtained by setting up tables, e.g., for $\hat{Y}_f(\hat{Z}, Z_v, \hat{\chi})$, prior to performing an LES. These tables can be constructed by first solving Eq. (10) for an appropriate range of $\hat{\chi}$, and then using the result in Eq. (14) for an appropriate range for $(\hat{Z}, Z_v, \hat{\chi})$. Once these tables are set up, then the LES is performed; in it \hat{Z} , Z_v and $\hat{\chi}$ would be needed to be computed locally on a pointwise basis; the values for \hat{Y}_f would then be obtained by table look-up. Note that, e.g., one can also determine \hat{Y}_o , \hat{Y}_p , and $\hat{\omega}_f$ in a similar manner. For example, the filtered value of the reaction rate for fuel is obtained as

$$\hat{\omega}_f = \int_0^1 \hat{\omega}_f[Y_f^n(Z, \hat{\chi}), Y_o^n(Z, \hat{\chi}), \dots] \hat{p}_a(Z; \hat{Z}, Z_v) dZ, \quad (15)$$

where, for a given problem, $\hat{\omega}_f(Y_f, Y_o, \dots, T)$ is a known function of the chemical composition and temperature.

Note that, since the chemistry and filtered species concentrations can be tabulated prior to performing the simulations, the method involves very little additional computational overhead compared to simulations for a non-reacting flow, an important attribute of this approach.

This approach can be readily extended to realistic chemistry with exothermicity and strong density variations [18]. The extension involves bringing in the temperature dependence of the various thermodynamically-related quantities, working with the density-weighted (Favre) filter, including filtered thermodynamic state equations, and employing several additional assumptions such as the neglect of the subgrid-scale fluctuations in viscosity. In doing this, the modeling of the subgrid-scale stresses and concentration fluxes, the filtered reaction rates, and the inferred filtered mass fractions and temperature are treated in the same manner as discussed above.

This approach, or variations of it, has been used in several large-eddy simulations of finite-rate, non-premixed chemical reactions. For example, Cook et al. [40], Cook and Riley [18], and de Bruyn Kops et al. [41] have compared predictions of this model with filtered results from direct numerical simulations. It was found that the model works well for moderate to high Damköhler numbers with continuous burning. Jiménez et al. [31] extended their studies to slightly out-of-equilibrium problems. Instead of the counter-flow model for $\hat{\chi}$ mentioned above, they employed a log-normal frequency distribution. Again, good agreement was obtained in comparing model predictions to results from high resolution direct numerical simulations.

More recently, de Bruyn Kops and Riley [42] have applied this

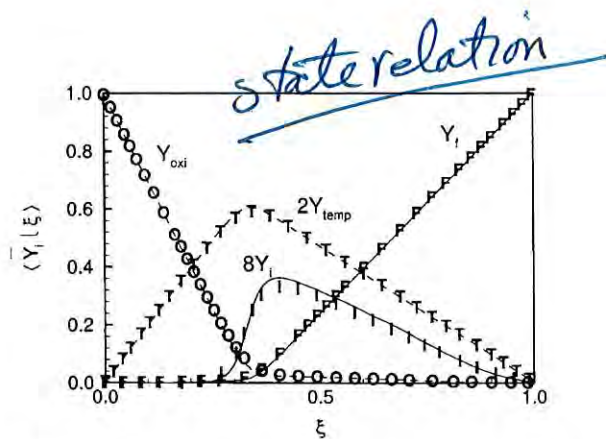


Fig. 2 Filtered mass fraction and scaled temperature for a two-step reaction on a scalar mixing layer. Lines are predictions from a 64^3 -point LES; symbols are from a 512^3 -point DNS. Notation is as in Swaminathan and Bilger [43].

modeling approach to simulate one-step, strongly temperature-dependent reactions, and a two-step methane-oxygen mechanism (Swaminathan and Bilger [43]), both on a scalar mixing layer. The large-eddy simulation results were compared to filtered results from very high resolution direct numerical simulations that had themselves been validated by comparison with laboratory experiments (de Bruyn Kops and Riley [44,45]). Models for Z_v and $\hat{\chi}$ were taken as the best models from a previous study (de Bruyn Kops and Riley [46], see below). The predictions for the mass fractions and temperature were found to be in excellent agreement with the DNS results for moderate to large values of a global Damköhler number. In addition, predictions of the filtered reaction rate were found to be very good when the frequency function for $\hat{\chi}$ is introduced in the computation, as suggested by Jiménez et al. [31]. A typical example of their results is given in Fig. 2, where the filtered mass fraction and scaled temperature for the two-step methane-oxygen mechanism are plotted for a case employing moderate values of the Damköhler number for the two reactions. Lines are predictions from a 64^3 -point LES; symbols are from a 512^3 -point DNS. Notation is as in Swaminathan and Bilger [43]. The velocity field simulated was decaying, homogeneous turbulence with an initial Reynolds number, based upon the Taylor microscale, of about 70.

Finite-Rate Chemistry. A principal limitation in the quasi-steady flamelet model is its lack of applicability to cases where reactions might be slow, e.g., for free radicals, or where extinction and possible reignition might occur. It is tempting to then treat the time-dependent flamelet equation, Eq. (9), instead of Eq. (10). It must be realized, however, that the computational overhead can then become much greater, as the chemistry in general cannot then be tabulated, and the dynamic equations for species conservation and temperature must be solved, and potentially on higher dimensional computational grids (since Z is also an independent variable).

Pitsch and Steiner [47] have relaxed the assumption of quasi-steadiness, and included the time-derivative term in Eq. (9) in simulating the spatial development of a methane/diffusion flame. The time derivative is interpreted as the time rate of change following the average velocity, conditioned on the stoichiometric value of the mixture fraction. The instantaneous values of the mixture fractions, temperature and scalar dissipation rate are assumed to be independent of the azimuthal θ and radial r coordinates, so that, for example, $Y_f(Z, r, \theta, x, t) = Y_f(Z, x, t)$ in Eq. (9), where x is the axial coordinate. These Z -dependent quantities are analogous to conditional averages discussed below, and there is experimental evidence that, at least in the Reynolds-averaged mean, they are not dependent on r and θ for the jet flame consid-

ered. These assumptions of spatial uniformity greatly simplify the simulations, eliminating the problem of increasing dimensionality mentioned above. The quantity $\chi(Z, x, t)$ is obtained by solving the integral equation,

$$\hat{\chi}(\mathbf{x}, t) = \int_0^1 \chi(Z, x, t) \hat{p}(Z, \mathbf{x}, t) dZ, \quad (16)$$

given the local filtered value of χ . In order to solve the integral equation for $\chi(Z, x, t)$, it must also be assumed that $\hat{\chi}$ is uniform over a somewhat large spatial region.

The approach is then to model $\hat{\chi}$ in a manner similar to Girimaji and Zhou [48] (see the next section), solve for $\chi(Z, x, t)$ using (16), and then with $\chi(Z, x, t)$ known to solve the unsteady laminar flamelet equation (Eq. (9)) for $Y_f(Z, x, t)$ and the other species and temperature. The filtered quantities are then obtained from the integral

$$\hat{Y}_f(\mathbf{x}, t) = \int_0^1 Y_f(Z, x, t) \hat{p}(Z, \mathbf{x}, t) dZ. \quad (17)$$

Pitsch and Steiner used a reduced form of the GRI 2.11 mechanism (Bowman, C.T., R. K. Hanson, D. F. Davidson, W. C. Gardiner, Jr., V. Lissianski, G. P. Smith, D. M. Golden, M. Frenlach, E. M. Goldenberg, Gri-mech 2.11, <http://www.me.berkeley.edu/gri-mech/>) consisting of 29 global reactions to simulate the Sandia flame D, a piloted methane/air diffusion flame; they obtained reasonably good agreement with the experimental data.

Bushe and Steiner [49] and Steiner and Bushe [50] employed a variation of the conditional moment closure (CMC) model (Bilger [51], Klimenko [52]) to close the reaction term in the filtered chemical species conservation equations (e.g., Eq. (4)). The CMC model, which produces final equations very similar to those using the flamelet model, but with seemingly different assumptions (Klimenko [53]), deals with averages of quantities, conditioned on the value of the mixture fraction Z. A principal assumption is the neglect of averages of fluctuations about the conditional average; for example, the conditional filtered reaction rate term is modeled as

$$\text{filter}\{\dot{\omega}_f(Y_f, Y_o, \dots) | Z\} = \dot{\omega}_f(\overline{Y_f | Z}, \overline{Y_o | Z}, \dots), \quad (18)$$

so that the filtered value of $\dot{\omega}_f$ can then be obtained as

$$\dot{\omega}_f = \int_0^1 \dot{\omega}_f(\overline{Y_f | Z}, \overline{Y_o | Z}, \dots) \hat{p}(Z) dZ, \quad (19)$$

similar to Eq. (15) above using the flamelet approach. As with the conditionally filtered value of χ above, the quantities $(\overline{Y_f | Z})$, etc., are obtained by solving the integral equation

$$\hat{Y}_f = \int_0^1 (\overline{Y_f | Z}) \hat{p}(Z) dZ. \quad (20)$$

The procedure is therefore to explicitly solve the equations for the filtered species mass fractions and temperature. At each point in time, the filtered reaction rate is needed and can be obtained by first solving the integral equations for the conditionally filtered species mass fractions and temperature, and then utilizing Eq. (19) to obtain the filtered reaction rates. Comparisons of model predictions with filtered results from high resolution direct numerical simulations indicates that the method works well. Furthermore, the authors suggest conditionally filtering on both Z and χ , which may be useful in treating problems with extinction and/or reignition.

Both of these methods appear to have considerable potential for addressing problems with slower chemistry, as long as the chemical reaction mechanisms can be computed efficiently, and either the problem defined has certain symmetries to reduce the dimensionality of the mathematical problem and/or the conditional mo-

ments can be treated in a quasi-homogeneous manner.

Several models have been introduced to treat partial premixing. In addition to the mixture fraction, these models usually employ some type of progress variable in order to indicate the amount of premixing. For example, Pierce and Moin [54] use a mixture fraction and a progress variable, the latter which tracks the global extent of reaction of the local mixture. They apply this approach to a methane-fueled coaxial jet combustor for which laboratory data is available for comparison. Significant premixing occurs in the near field of the combustion zone, resulting in a lifted flame. Good agreement is obtained for model predictions of the experimental data. In another approach, in addition to the mixture fraction and progress variable, Vervisch et al. [55] define a flame indicator $\chi_{F,O} = -D \nabla Y_f \cdot \nabla Y_o$ in order to determine whether the flame is locally premixed or nonpremixed. (It can be shown that $\chi_{F,O} > 0$ in nonpremixed flames, while $\chi_{F,O} < 0$ in premixed flames.) Interesting results for the dynamics of the turbulent flame base were obtained for the case of the lifted flame in a turbulent cold wake.

Recently Mitarai et al. [56] have introduced a quasi-Lagrangian version of the flamelet model, specifically developed to treat problems where extinction and reignition are important. Lagrangian particles are tracked, and their local flamelet equation (Eq. (9)) is solved in time. A simplified model, consistent with overall energy conservation, is used to transfer heat between burning and extinguished flamelets. The model gives good agreement when its predictions are compared with results of direct numerical simulations of nonpremixed reactions which include significant extinction and reignition.

Modeling $\hat{\chi}$ and Z_v

de Bruyn Kops and Riley [46] evaluated several models for $\hat{\chi}$ and Z_v with both a priori and a posteriori comparisons of modeling predictions with results from very high resolution direct numerical simulations of a scalar mixing layer. For the variance Z_v , models were considered which relate Z_v to the resolved gradient of Z, i.e., to $|\nabla Z|^2$ (Yoshizawa [57], Mathey and Chollet [58]), and to the variance near the grid-scale cut-off (the test-scale variance) (Cook and Riley [27]). In one form of both models, the coefficient in the models is computed by assuming a form for high wave number spectrum, and fitting this form to the simulation data [59]. It was found that both models worked very well when assumed spectra were used to determine the coefficients.

For the filtered dissipation rate, following Girimaji and Zhou [48] the models were directly related to $|\nabla \hat{Z}|^2$, i.e.,

$$\hat{\chi} = C |\nabla \hat{Z}|^2,$$

the only difference in the models being the method of computing the coefficient C. In one case the coefficient was related to the energy flux from the grid scales, while in the other cases it was determined by fitting an assumed high wave number spectrum. (Note that for large-eddy simulations, since the equation for \hat{Z} is directly computed, an estimate for $\hat{\chi}$ is immediately available as the flux of \hat{Z} energy from the grid scales to the subgrid scales.) As in the case with Z_v , the models which performed best relied on fitting the assumed form for the spectrum.

Typical results from the study of de Bruyn Kops and Riley are presented in Fig. 3, where the filtered scalar dissipation rate and subgrid-scale variance versus downstream distance are plotted for the case of homogeneous, isotropic, decaying turbulence at an initial Taylor Reynolds number of about 70. The DNS results are obtained using 512^3 grid points; the LES results are from 64^3 -point simulations of the same flow. The results from several different models are shown.